PhD thesis

Interglacial ice core dust from Greenland

Marius Folden Simonsen

Supervisors: Paul Vallelonga and Anders Svensson

Centre for Ice and Climate, Niels Bohr Institute
University of Copenhagen

This thesis has been submitted to the PhD School of The Faculty of Science, University of Copenhagen

March 28, 2018

Abstract

Atmospheric dust is an active component of the climate system. Paleo dust records from the early Holocene and Eemian, which were both a few degrees warmer than today, are used to constrain models of a future warmer climate. Ice core records provide a strong tie point for paleo dust models, as they have a high temporal resolution and are representative of a large geographical area. However no insoluble dust record from Greenland of the Holocene and Eemian has so far been published. This is partly due to the low dust concentration, which demands high accuracy from the instruments.

In this thesis it is shown that the discrepancy between the two most commonly used instruments for dust concentration and size distribution measurements in ice cores, the Coulter Counter and the Abakus, is due to the non-spherical shape of the particles. The Amsterdam Discrete Dipole Approximation is used to show that the Abakus is strongly influenced by Mie scattering when measuring standard polystyrene spheres, while the Mie scattering effects cancel out for real dust particles due to their variable shape. Furthermore, the Abakus assigns a larger size to the particles than the Coulter Counter, since the particles are elongated. A Single Particle Extinction and Scattering Instrument (SPES) was used to measure an aspect ratio of 0.39 ± 0.03 for local east Greenlandic dust and 0.33 ± 0.03 for remote Asian dust in the east Greenlandic RECAP ice core. The aspect ratio derived from the discrepancy between the Coulter Counter and Abakus agrees with the SPES results, and is able to discern between the local and remote dust. If the aspect ratio is known, the Abakus can be calibrated to the Coulter Counter, so it gives accurate concentrations and size distributions.

The Abakus has been used to measure the dust concentration and size distribution of the RECAP ice core, which was drilled in 2015 on the Renland ice cap by the East Greenland coast. The RECAP dust record has a high concentration of large particles during the Holocene and Eemian, but few during the glacial. On the other hand, the glacial has a much higher concentration of small particles than the interglacials. This glacial record is almost identical to the NGRIP dust record, which indicates that the RECAP glacial dust comes from Asia like the NGRIP dust. The 20 μm mode and geochemical analysis of the interglacial dust shows that it has a local origin, coming from the Scoresby Sund area. The large particle concentration fell by more than 90% from 116.6 ± 0.7 to 111.1 ± 0.5 ka b2k (before year 2000 CE) and rose again from 12.1 ± 0.1 to 9.0 ± 0.1 ka b2k. The reduction of large particles at the onset of the glacial was because the Greenland ice sheet and glaciers grew and covered the dust sources. The large particle concentration increased at the same time as surface exposure dating of rocks shows glacier retreat. The

non-zero large particle concentration shows that some ice free area persisted throughout the glacial.

As opposed to RECAP, which is dominated by local sources, the NEEM Holocene dust record from north central Greenland has a remote source, and can therefore be used as a tie point for global dust models. It has an increasing flux from 10 to 15 mg/m^2/year through the Holocene, and the same concentration during the Eemian and early Holocene. It is similar to the NGRIP2 dust record, which only covers the first millenium of the Holocene. The NEEM calcium flux, a proxy for dust, is around 1.5 mg/m^2/year with no increase through the Holocene, and is similar to the GRIP, NGRIP1 and GISP2 calcium records. A comparison of all records shows no consistent trend over the Holocene, and there is no geographical variation in flux. Modern lobal dust models predict up to 20 times more dust at NEEM than measured, and up to 10 times more dust at NEEM than in GRIP and GISP2. This inconsistency shows the need for further developing Greenland atmospheric dust models.

Resumé

Acknowledgements

First and foremost I would like to thank my supervisor Paul Vallelonga and co-supervisor Anders. There has been no limit to the time and effort they have put into advising me scientifically, and as importantly, they have also advised me on all other concerns I have had. Both their professional and personal advise have extended far beyond what a PhD student could hope for.

My thanks go to Nancy Bertler at GNS in Wellington, New Zealand, who hosted me for 2 months during the RICE campaign in 2014. Her leadership during the strenuous campaign was very inspiring, and my time in New Zealand will remain a happy memory. Similarly, I would like to thank Todd Sowers for hosting me last winter at Penn State University. I greatly appreciate his concern for both my scientific projects and personal well being. He introduced me for Richard Alley and helped me visit Meredith Kelly at Dartmouth College, both of which gave valuable input to the interpretation of the RECAP dust record. Not least, he gave me ice and lab facilities, so I could prepare RECAP samples for Alejandra Borunda's geochemical measurements at Lamont-Doherty Earth Observatory.

Warm thanks go to my scientific collaborators, especially Alejandra Borunda at Lamont-Doherty, Barbara Delmonte, Giovanni Baccolo, Marco Potenza and Llorenç Cremonesi for the great effort they have put into our common projects. Special thanks also go to Llorenç Cremonesi for his great patience and commitment while writing the instrument paper.

I would also like to thank my old office mate Troels Mikkelsen, for his participation in both my personal and work life. His support has been invaluable. In the same way I would like to thank Nicholas Rathmann and Christian Holme, for keeping up the spirit and always helping with science and writing during the last few months.

I will always be grateful to Sune Rasmussen and Inger Seierstad for how they helped me get back to normal when I was sick. Along this line I thank everyone at CIC for their great support, here among Jørgen Peder Steffensen for great discussions and taking me to Greenland, Steffen Bo Hansen for teaching me how to drill, and Dorthe Dahl-Jensen for ensuring that I had enough time to finish the thesis.

Lastly, I would like to thank Philip, Rasmus, Tobias and especially Andrea for accepting my behaviour while writing the thesis.

Marius Folden Simonsen
Centre for Ice and Climate, Niels Bohr Institute
University of Copenhagen

March 28, 2018

Contents

Chapter 1

Motivation and outline

Atmospheric mineral dust strongly impacts the climate system by changing radiative forcing and albedo, acting as cloud condensation nuclei and fertilizing the oceans. These effects have considerable uncertainty in climate models, so further research could lead to a better prediction of future climate change. Not only does dust play an important role in the climate system, it is also strongly affected by anthropogenic activities. Both deforestation and agriculture increases the area of bare soil that can act as a source of dust storms. The physics of dust entrainment, transport and deposition is complex, and model parameters are hard to estimate. Observational data therefore provide strong tie points for the model. Especially records from the past give reveals dust deposition under different climates.

The central parts of the ice sheets at Greenland and Antarctica are unique among paleo dust records, as their sources are located thousands of kilometers away. They therefore contain information about a many thousand kilometer long part of the climate system. Furthermore, ice cores have an exceptionally high temporal resolution and very precise dating. The dust record from the last glacial period in the NGRIP ice core has therefore been very valuable for climate models of the glacial. However, as temperatures were 15 °C colder than today, and the atmospheric CO_2 concentration was less than half of the present values, glacial conditions are not very representative of a future warmer climate. In that respect it would be more interesting the study the early Holocene 8,000 years ago and Eemian 120,000 years ago, which were a few degrees warmer than today. However, no dust record from interglacial periods in Greenland has been published before.

In 2015, I got the chance to measure the interglacial dust concentration with an Abakus laser sensor of the RECAP ice core from Renland, east Greenland. However, this did not produce the anticipated dust records. The Abakus cannot be used to measure absolute dust mass concentration due to its poor assessment of particle size distribution. It has to be calibrated to a Coulter Counter. The discrepancy between the two instruments was puzzling, as it was not there for standard polystyrene. Through a strong collaborative effort with my coauthors of the manuscript in **Chapter 3**, we found that the discrepancy was due to the elongated shape of the particles, and that the shape can be determined from the difference between the two instruments. This work involved an analytically derived

model, Single Particle Extinction and Scattering Instrument measurements of particle shape, numerical Amsterdom Discrete Dipole Approximation simulations and together with the Abakus and Coulter Counter measurements.

Even before the issue of poor size distributions was solved, it became clear that the RECAP interglacial dust had a local origin, and could therefore not be used as large scale climate proxy. This was evident from the very large 20 μm mode of the particle size distribution measured by Coulter Counter and geochemical analysis, and supported by satellite images showing large dust storms rising less than 50 km from Renland. It turned out that the large particles disappeared during the glacial, since the sources were covered by ice. The record could therefore be used as a proxy for ice sheet extent in the Scoresby Sund area around Renland. This is discussed in the manuscript of **Chapter 4**.

Finally, I got access to the NEEM Holocene and Eemian dust record. It is similar to other Greenlandic Holocene dust and calcium records, and together they paint a picture of constant dust flux both temporally and geographically. This disagrees with dust models, and could therefore help refine these models and their prediction of future climate. This is discussed in **Chapter 5**.

Chapter 2

Background

Mineral dust from the past atmosphere is preserved in the Greenland ice sheet and can be extracted from ice cores. The Greenland ice sheet is formed by accumulating snow. Melt events are very rare on the central ice sheet, which ensures that the stratification of the snow layers is preserved. As snow falls, the lower layers are compacted and flow out to the edges of the ice sheet, where the ice melts or is discharged as icebergs from sea terminating glaciers. The flow leads to thinning, but does in many cases not disturb the stratigraphy. Therefore, the ice sheet contains a continuous vertical record of past snow. This record includes mineral dust and other aerosols settling on the ice sheet or caught by snow in the atmosphere, as well as air bubbles formed between the compressed snow flakes. To access this record, ice cores have been drilled from surface to bedrock (Figure 2.1).

Ice cores can be dated precisely by annual layer counting down to 60 ka b2k (before year 2000 CE) (Svensson et al., 2008). The ratio of isotopes of oxygen and hydrogen in the water molecules depends on the condensation temperature in the cloud and therefore contains a strong seasonal signal. In addition, the concentration of many aerosols displays seasonal variability, including mineral dust, which is primarily deposited in spring. For annual ice layers of a few centimeters or thinner, dust is superior for counting, partly because of its high measurement resolution (Bigler et al., 2011) and partly because it does not diffuse in the ice. Ice older than 60 ka b2k has been dated by extrapolating the thinning due to ice flow and the relation between water isotopes and accumulation rate (Wolff et al., 2010). To further improve dating, volcanic eruptions can be used as stratigraphic markers, as they leave tephra and sulphate in the ice (Seierstad et al., 2014).

Greenland ice cores cover the whole Holocene, the last glacial and part of the last interglacial. While the Holocene has had a relatively stable climate, the glacial exhibits rapid temperature oscillations between stadials and interstadials. The alternating cold stadials and warm interstadials each lasted from a few hundred to some thousand years while the transition from stadial to interstadial took only a few decades (Steffensen et al., 2008). At NGRIP in central Greenland, the mean annual temperature was between -40 and 55 °C during stadials, while interstadials were 10 to 20 °C warmer (Kindler et al., 2014). By contrast, the present temperature of -30.2 °C (Steffen and Box, 2001) is only 2.5 °C

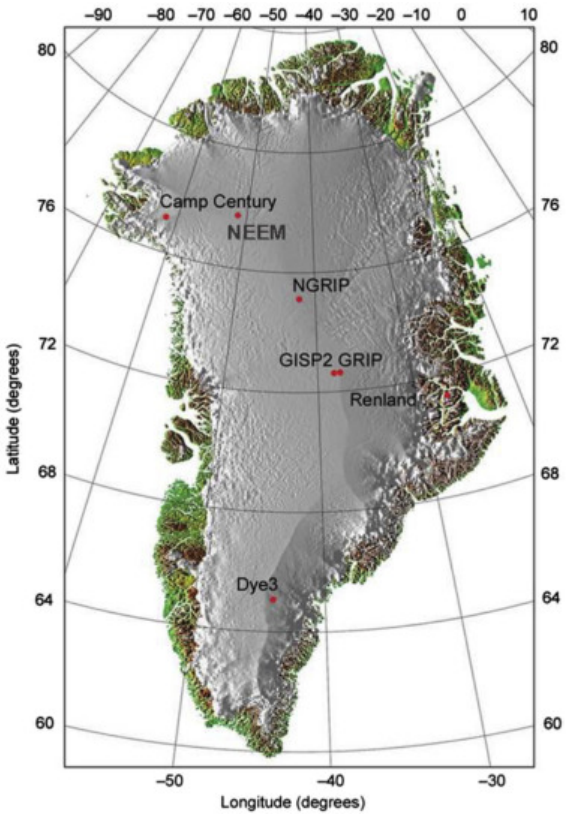

Figure 2.1: Major Greenland ice core locations. From Kang et al. (2015).

colder than during the Holocene climatic optimum 8 ka b2k (Vinther et al., 2009). During the Eemian, the last interglacial, the global average temperature was 1-2 °C warmer than today (Kaspar et al., 2005), while Greenland was 8 ± 4 degrees warmer (Dahl-Jensen et al., 2013). The atmospheric CO_2 concentration was at a preindustrial level (Barnola et al., 1987), and the global sea level was 8-10 m higher than today (Dutton and Lambeck, 2012; Kopp et al., 2009). The higher temperature makes the Eemian an important tie point for models predicting the effects of future global warming (Hansen and Sato, 2012).

2.1 Mineral dust

Mineral dust deposited on the Greenland ice sheet mainly comes from the Central Asian deserts (Svensson et al., 2000; Bory et al., 2003a). Most of the dust arrive in spring (Banta et al., 2008), so the dust record has a strong seasonal signal. At present, the annual dust flux is 10 mg/m^2 while the dust flux was up to 30 times higher during the glacial (Steffensen, 1997). The increased glacial dust flux was caused by larger sources, stronger winds and less precipitation outwash. For an overview of ice core mineral dust, see Vallelonga and Svensson (2014).

2.1.1 Dust provenance

The source of dust particles in ice is most commonly determined from the ratios of radiogenic ^{87}Sr and ^{143}Nd to ^{86}Sr and ^{144}Nd respectively. Due to the very small variability in ^{143}Nd/^{144}Nd, the derived quantity

$$\epsilon\mathrm{Nd} = \left(\frac{^{143}\mathrm{Nd}/^{144}\mathrm{Nd}}{(^{143}\mathrm{Nd}/^{144}\mathrm{Nd})_{\mathrm{CHUR}}} - 1 \right) \times 10^4 \tag{2.1}$$

is normally used instead of ^{143}Nd/^{144}Nd. Here $(^{143}\mathrm{Nd}/^{144}\mathrm{Nd})_{\mathrm{CHUR}} = 0.512636$ (Svensson et al., 2000), the present day mean chondritic uniform reservoir value, is used as a standard reference value. Mantle magma has lower ^{87}Sr/^{86}Sr and higher ϵNd now than in the past. Furthermore, the concentrations of ^{87}Sr and ^{143}Nd increase in rocks over time due to radioactive decay. Together with isotopic fractionation processes, this gives different ^{87}Sr/^{86}Sr and ϵNd values in different rocks, which can be used to determine the provenance of mineral dust. For example, young Icelandic volcanic rock has a low ^{87}Sr/^{86}Sr value of 0.704 and ϵNd between 7 and 10, (Shorttle et al., 2013), while Central Asian deserts have ^{87}Sr/^{86}Sr between 0.715 and 0.73 and ϵNd between -18 and -5 (Bory et al., 2003a).

Mineral dust in ice cores is often mixed with tephra from volcanic eruptions, which has low ^{87}Sr/^{86}Sr and high ϵNd values. The tephra interferes with the dust isotope measurements, and measured isotope ratios therefore often lie on a mixing curve in ^{87}Sr/^{86}Sr,ϵNd-space between the dust and tephra end members. [1]

For the Central Greenlandic GRIP ice core, the ^{87}Sr/^{86}Sr and ϵNd values of both the Holocene (Bory et al., 2003a; Svensson, 1998) and the last glacial period (Svensson et al., 2000; Biscaye et al., 1997) point to the Central Asian deserts as the primary dust source

[1] FiXme Note: talk to paul/anders about this

	Kaolinite/chlorite	Smectite
GRIP glacial	< 1	$< 5\%$
GISP2 glacial	< 1	$< 2\%$
NGRIP present	< 1	$< 2\%$
Asia	< 1	$< 6\%$
Sahara	> 2	$> 10\%$
North America	> 1.5	

Table 2.1: Kaolinite/chlorite ratio and smectite concentration of late glacial dust from the GRIP (Svensson et al., 2000), GISP2 (Biscaye et al., 1997) ice cores and present day dust from the NGRIP ice core (Bory et al., 2002), together with possible source areas (Svensson et al., 2000).

(Figure 2.2). Mineral dust in Central Greenlandic ice cores is predominantly deposited in spring. The dust concentration peaks in March and April, where it is 4 times higher than the minimum in September (Banta et al., 2008). During the peak season, the dust isotopes suggest the Takla Makan desert north of the Tibetan Plateau, while lower ϵNd values during fall indicate a contribution from the more easterly located Tengger and Mu Us deserts (Bory et al., 2003b).

The coastal Greenlandic ice cores from Hans Tausen and Renland ice caps have higher $^{87}Sr/^{86}Sr$ and lower ϵNd values than Central Greenlandic ice cores during the Holocene. This indicates mixing with local Greenlandic dust (Bory et al., 2003a). While Asian desert dust is created by saltation of sand grains, Greenlandic dust is made by glacial erosion. The glacial flour thereby created is washed out by melt water and deposited when melt water streams dry out. It is then uplifted by winds and brought to the ice cap. This process is also seen in Patagonia, which supplied the majority of Antarctic dust during the last glacial period (Sugden et al., 2009). In chapter 4 local Greenlandic Holocene dust will be discussed further.

The concentration of clay minerals in the dust can also reveal the provenance. This excludes Sahara and North America as significant dust sources both during the glacial and today (Table 2.1), and supports East Asia as the primary dust source in Central Greenland.

In the southern Greenlandic DYE-3 ice core, lower ϵNd values during the 18th century give evidence of Saharan dust (Lupker et al., 2010). At present day Summit, where the GRIP core was drilled, the elemental composition of the dust points to 1/3 of the dust being of Saharan origin (VanCuren et al., 2012). This contrasts the isotopic measurements of the GRIP core (Bory et al., 2003a; Svensson, 1998) that show no indication of Saharan dust during the 16th and and 17th centuries. More present day isotopic measurements would be useful for resolving this apparent discrepancy.

2.1.2 Glacial cycle dust

During the cold stadials of the glacial, the dust flux in central Greenland was up to 30 times higher than during the Holocene (Steffensen, 1997; Ruth et al., 2003; Mayewski

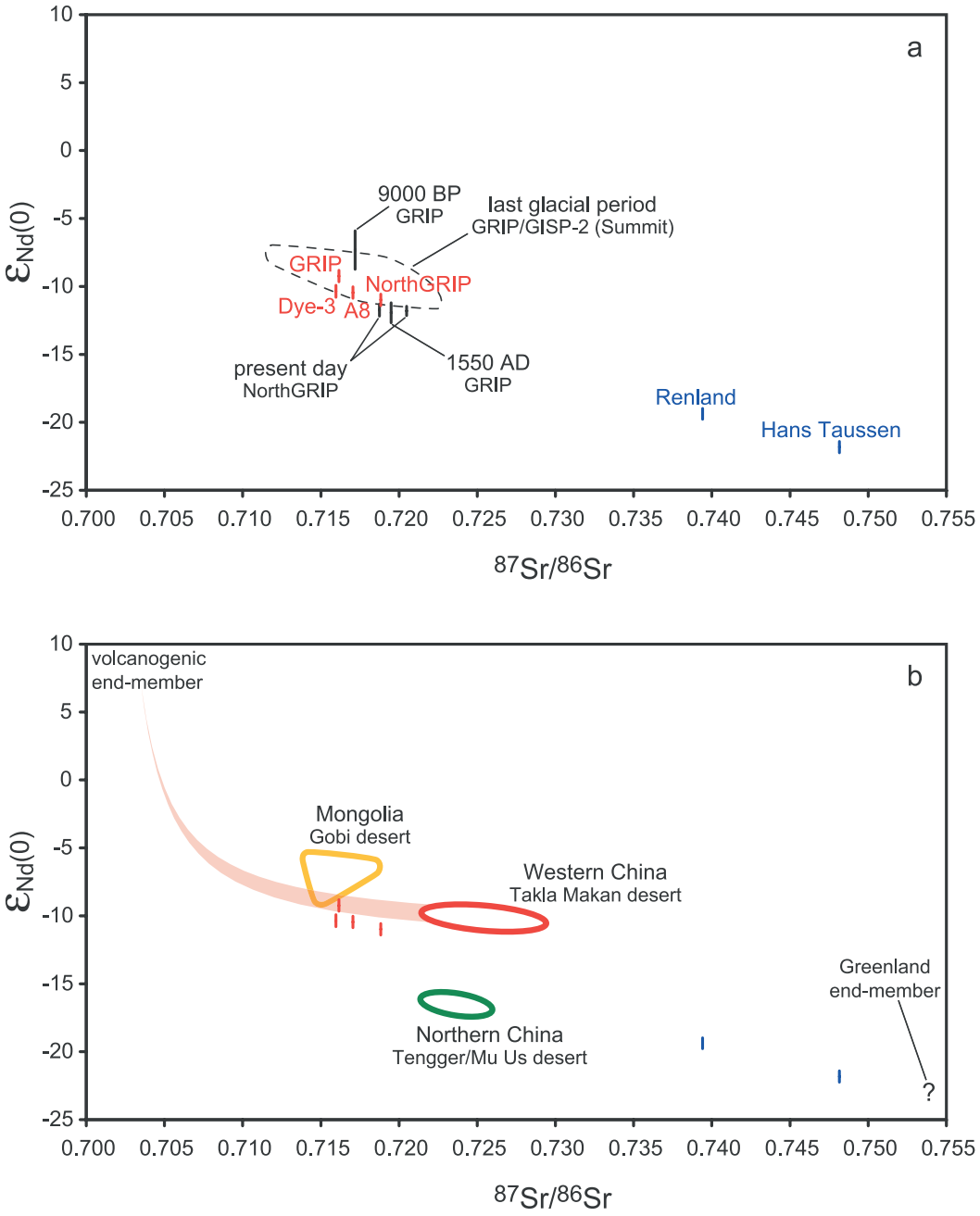

Figure 2.2: Strontium and neodymium isotope ratios for ice core dust and possible source areas. The ice core dust samples without age specification are from the 17th century, except for Hans Tausen, which is from around year 1,000 CE. From Bory et al. (2003a).

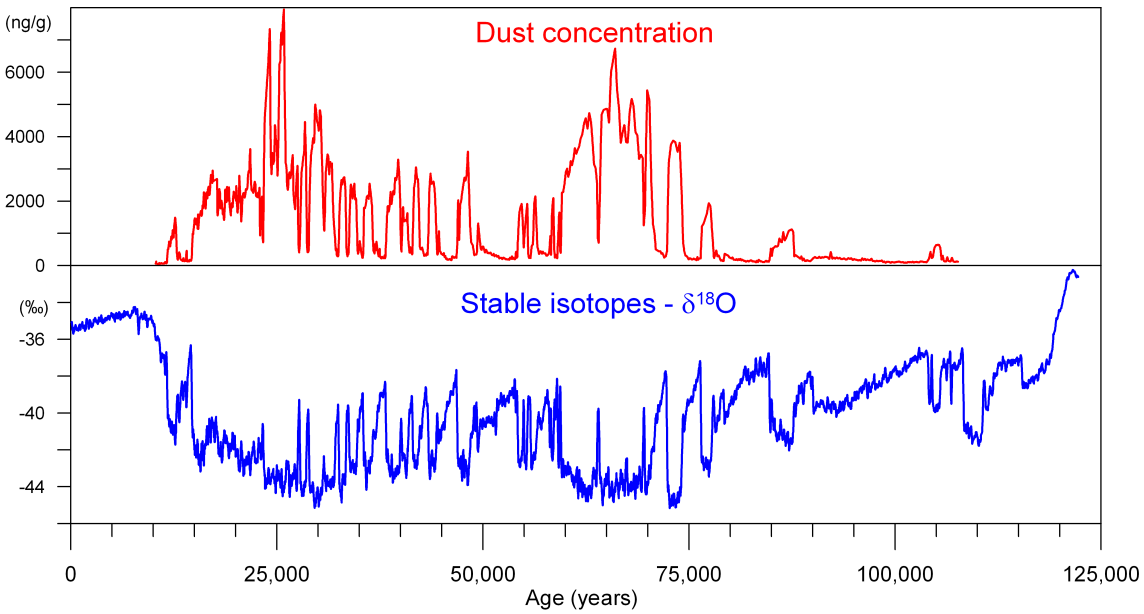

Figure 2.3: Dust and stable isotope record from NGRIP, Central Greenland. From Vallelonga and Svensson (2014).

et al., 1997). The warmer interstadials had 3 times greater dust flux than the Holocene, and the transitions from stadials to interstadials happened over 50 years (Steffensen et al., 2008) (Figure 2.3). The strong correlation with temperature and the rapid transitions indicate that the dust flux during the glacial on sub millennial time scales were dominated by changing atmospheric conditions. During the Holocene, the dust concentration has been constant compared to the large fluctuations of the glacial (Mayewski et al., 1997). The diameter mode of the particle volume size distribution is between 1.5 and 2 μm during the glacial, which is 20% larger than during the Holocene (Figure 2.4). The larger glacial particle size is consistent with stronger winds during transport.

2.1.3 Atmospheric dust processes and models

During the last glacial maximum, the global average atmospheric dust concentration was 2.5 times higher than at present, while it was 20-30 (Mahowald et al., 1999; Lambert et al., 2015) times higher over Central Greenland. Several factors contributed to the higher dust concentration during the last glacial maximum. Stronger winds caused more entrainment and faster transport from source regions to the ice sheet, and lower precipitation meant less outwash during transport. Additionally, the Asian dust sources were larger during the glacial than today. (Mahowald et al., 1999)

Mid-latitude dust sources, like the Central Asian deserts, occur due to low precipitation and easily erodible soil with little or no vegetation. In the high latitudes, an important dust source is glacial outwash plains (Bullard et al., 2016). Glaciers erode the bedrock while sliding over it, thereby producing a very fine grained material called glacial flour.

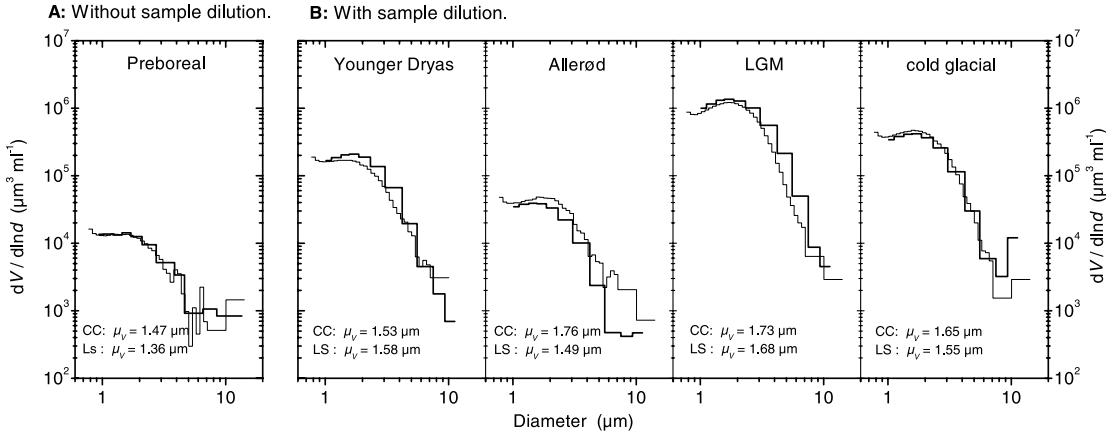

Figure 2.4: Dust size distributions for different climate periods by Coulter Counter (thin lines) and Abakus Laser sensor (thick lines). The Abakus bins have been shifted to fit the Coulter Counter distributions. From Ruth et al. (2003).

Subglacial melt water streams transport the glacial flour out to the glacial outwash plain in front of the glacier. The dust emission from glacial outwash plains can have a strong seasonal signal, as seen for the Copper River in Alaska (Crusius et al., 2011). During peak melt water season in summer, glacial flour is transported onto the outwash plain, but cannot be caught by winds while submerged in water. As the temperature drops, the melt water stream ceases, but snow cover during winter also limits atmospheric entrainment. The peak emission season is therefore autumn (Bullard et al., 2016).

Paleo dust modules (Albani et al., 2014) are used to constrain climate models to dust records and predict effects of dust on the radiation balance in the future (Mahowald et al., 2006). They are based on a general circulation climate model constrained by past climate forcings such as solar insolation, CO_2 concentration and vegetation cover. The dust model gives entrainment, transport and deposition based on winds, precipitation, soil erodibility and other factors from the climate model. Dust models overestimate the dust flux to Central Greenland by almost a factor 10 during the Holocene (Albani et al., 2015, 2016; Mahowald et al., 2006) and a factor 2.5 during the last glacial maximum (Mahowald et al., 2006) compared to the GISP2 record (Mayewski et al., 1997). Furthermore, Mahowald et al. (2006) model that the majority of the Greenland dust comes from the contiguous USA, Alaska and Siberia, and Albani et al. (2015) have to suppress Alaskan dust emission to not get too high discrepancy between model and ice core records. This disagrees with geochemical dust provenance studies (Section 2.1.1). In Chapter 5 we will compare other Greenland Holocene dust records to models, and show that the discrepancy between the GISP2 core and models is also seen in other Greenland Holocene dust records.

	Holocene	Last glacial maximum
GRIP	0.23	0.08
NGRIP	0.29	0.11
DYE-3	∼0.23	∼0.23

Table 2.2: Ca^{2+}/dust ratios during the Holocene and last glacial maximum in the GRIP (Steffensen, 1997), NGRIP (Ruth et al., 2002) and DYE-3 (Steffensen, 1997) ice cores.

2.1.4 Calcium as dust proxy

Dissolved calcium ions in the ice come from both sea salt aerosols and mineral dust. However, sea salt calcium only contributes 5% of the total soluble calcium at central Greenland during interstadials and 1% during stadials, so total Ca^{2+} concentration is a good dust proxy (De Angelis et al., 1997). The calcium to dust ratio in the GRIP and NGRIP ice core was however 3 times lower during the stadials than during the Holocene and interstadials (Table 2.2). In the more southerly and lower elevation DYE-3 core, the calcium to dust ratio was identical during both warm and cold periods to the GRIP warm period calcium to dust ratio (Steffensen, 1997). The relation between dust and calcium therefore change over climatic transitions and between geographical locations, so calcium cannot be used directly as a quantitative dust proxy. It has been hypothesised that the high dust concentration during the glacial could be due to exposure of continental shelves, from which the dust could be uplifted (Cragin et al., 1977). However, as they would be rich in $CaCO_3$ from shells of sea organisms, the dust would be enriched in calcium. As the Holocene calcium to dust ratio is higher than the glacial, it is unlikely that the glacial dust originated primarily from continental shelves.

2.1.5 Dry versus wet deposition

Dust is deposited on the ice sheet either by gravitational settling or by scavenging by snow in the atmosphere. While the lifetime of particles due to wet deposition is independent of size, dry deposition lifetime decreases sharply with size. Wet deposition lifetime is on global average around one week, while the dry deposition lifetime is around 1 day for 10 μm particles and 100 days for 1 μm particles (Tegen and Fung, 1994; Mahowald et al., 2006). With a diameter around 2 μm, ice core dust is therefore primarily wet deposited. If the atmospheric dust concentration is not depleted, the dust flux to the ice sheet is proportional to the snow accumulation rate. The concentration in the ice core is in this case proportional to the atmospheric dust concentration independent of the accumulation rate. For dry deposition, the flux is independent of accumulation rate. This means that the ice core concentration is inversely proportional to the accumulation rate for a fixed atmospheric dust concentration. If the atmospheric dust concentration is reduced during a snowfall event, the relation between atmospheric dust concentration and ice core dust concentration is somewhere between dry and wet deposition.

2.1.6 Antarctica

Central Antarctic dust originates primarily from Southern South America (Grousset et al., 1992; Delmonte et al., 2004; Basile et al., 1997) during the glacial periods, while interglacial dust has other contributing sources (Delmonte et al., 2007). Where Greenlandic ice cores only go back to the Eemian around 130 ka b2k, the Dome C dust record spans 800 ka. As in Greenland, the dust concentration correlates strongly with temperature (Lambert et al., 2008) (Figure 2.5). The coastal Talos Dome ice core contains a higher coarse particle fraction in the early Holocene than in the last glacial period (Delmonte et al., 2010). Due to their low atmospheric residence time, the coarse particles must have a local origin, suggesting the rocky surfaces of Victoria Land, which were also exposed during the glacial. The relative increase in local dust concentration was due to a strong decrease in dust flux from remote sources, and not an absolute increase in local dust flux. In Chapter 4 we will show that local dust sources emerged in Eastern Greenland after the deglaciation, leading to an absolute increase in coarse ice core dust particles.

2.2 Instruments

2.2.1 Coulter Counter

Ice core dust particle size distributions have traditionally been measured by Coulter Counter instruments. The GRIP (Steffensen, 1997) size distributions have been measured by Coulter Counter and is a key reference for Greenland ice core dust size distributions. The Coulter Counter was patented in 1953, and is widely used in medicine for counting and characterising cells. It counts each particle in the sample individually and measures its volume, by what is called the Coulter Principle. The Coulter Counter has two separate containers connected by a small orifice. The sample liquid starts in one container and is sucked through the orifice during measurement. In each container there is an electrode, creating a voltage drop over the orifice. For a melted ice core sample, salt is added to make the water more electrically conductive than the particles. While only electrolyte solution is sucked through the orifice, the electric current running from one electrode to the other is constant. When a particle enters the orifice, the path of the current is partially blocked, and the current drops. Larger particles block a larger part of the orifice and thereby create a larger current drop. In this way the size of the particle is measured.

The relative resistance increase from a particle scales with d^2/D^2, where d is the particle diameter and D is the orifice diameter. For highest accuracy, it is therefore necessary to have as small an orifice as possible. Modern Coulter Counters can measure particles down 1/50 times the orifice diameter. Particle shape also has a small influence on the measured diameter. However, the relative error on the measured diameter due to shape is for an optimized setup less than $\frac{1}{10}d^2/D^2$, which is negligible for most purposes (Coulter-Electronics-Limited, 1988).

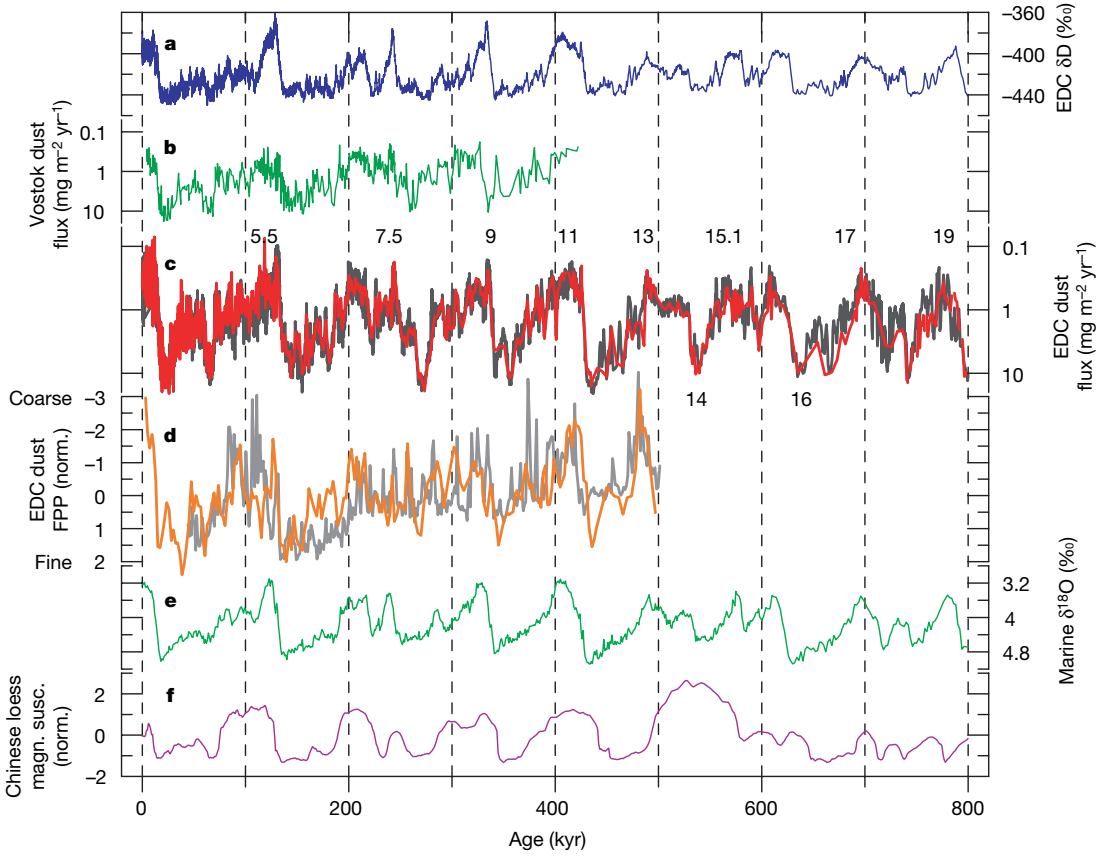

Figure 2.5: The temperature proxy δD together with dust from the EPICA Dome C ice core. The red line is Coulter Counter data, while the dark grey is Abakus. FPP is the normalized percentage of fine particles, where orange is Coulter Counter and light grey is Abakus. From Lambert et al. (2008).

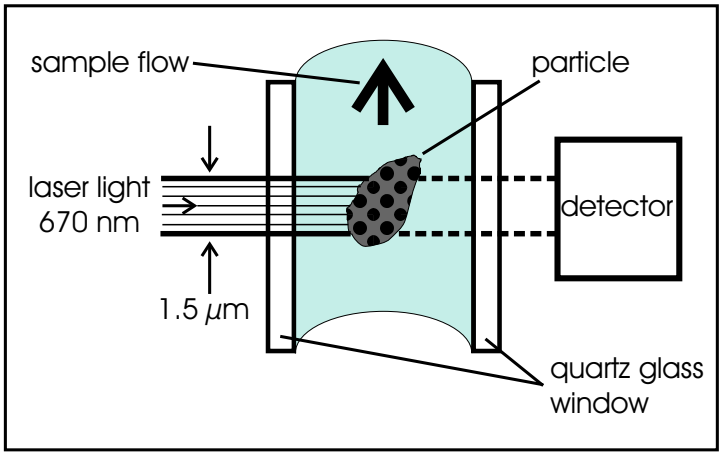

Figure 2.6: The Abakus flow cell. From Ruth (2002).

2.2.2 Abakus

The Abakus laser particle detector from Klotz GmbH, Germany, has replaced the Coulter Counter for many dust concentration and size distribution measurements since its first use by Saey (1998). Its advantages over the Coulter Counter are that it is easier to operate and it can measure smaller samples and more samples per time when connected to a continuous flow analysis system. On the other hand, its measurement of particle size is inaccurate, which leads to poor size distribution and total dust mass measurements (Ruth et al., 2008). Addressing this problem is the main subject of Chapter 3.

In the Abakus, the sample liquid flows through a flow cell of cross section 250 × 220 μm. The cell is illuminated from the side by a laser beam 1.5 μm thick covering the whole cross section. Opposite of the laser, the light intensity is detected by a photo diode. When a particle flows through and partially blocks the laser beam, the detected light is attenuated. This attenuation increases with the size of the particle (Figure 2.6). The attenuation peaks are counted and sorted into up to 32 bins according to their size (Ruth, 2002). By calibrating with polystyrene spheres of known size, a histogram of particle sizes is obtained.

Connected to a CFA system, the Abakus has an ice depth resolution of 3 mm (Bigler et al., 2011). To clean Coulter Counter samples, the surface has to be melted away in three consecutive clean MQ water baths. This limits the minimum sample size to a few centimeters. In the RECAP ice core, the high depth resolution of the Abakus enabled annual layer counting down to 4,000 years and precise depth registration of Dansgaard-Oeschger cycles in the very compressed glacial. While a CFA system is running, the Abakus requires no maintenance. This contrasts the Coulter Counter, which requires 1-2 persons for efficient operation. In addition, the Abakus only requires 2 mL of sample per minute for optimal operation. For a melt rate of 3 cm per minute, this corresponds to 0.7 cm^2 of ice core cross section.

The Abakus has higher resolution and lower sample and labour requirements than the Coulter Counter. On the other hand, it has a much lower accuracy. It is not possible to measure the total dust mass in a sample by Abakus alone, even if it is well calibrated to standard polystyrene spheres. Ruth et al. (2003) circumvented this problem by measuring the same samples with both Coulter Counter and Abakus and comparing the size distributions. They shifted the Abakus bin limits until the size distributions of Coulter Counter and Abakus were identical. The optimal binning was then used to calculate the dust mass concentration from the continuous Abakus data. This method combines the high accuracy of the Coulter Counter with the high resolution of the Abakus under the assumption that the relation between Abakus and Coulter Counter bins is the same over the whole ice core. It has proven accurate for EDC and EDML Antarctic ice over a range of 2.5 orders of magnitude. In chapter 3 we show that the relation between Abakus and Coulter Counter data depends on the shape of the particles, which depends on transport and source areas.

In other studies (Lambert et al., 2012), the size bins are not calibrated, but only the total number of particles is used. The total Abakus particle number is then calibrated to total Coulter Counter dust mass for selected samples. As noted by Lambert et al. (2012), a change in size distribution over time could change the Abakus particle number without changing the dust mass, thereby biasing the interpretation. We will show in chapter 4, that in the RECAP ice core, the volume size distribution mode increases by a factor 10 from glacial to Holocene, which using this method would lead to relative underestimation of the Holocene dust mass.

2.2.3 Continuous flow analysis

Continuous flow analysis (CFA) is widely used for analysis of water isotopes, gases and impurities in ice cores (Bigler et al., 2011; Dallmayr et al., 2016). It is an alternative to discrete sample analysis, and is less labour intensive and provides higher ice depth resolution. The Abakus dust record presented in Chapter 4 has been measured on the Copenhagen CFA system, which is similar to the system described by Bigler et al. (2011). For the Copenhagen CFA system 35×35 mm sticks are cut from the whole length of ice core to ensure that the whole stratigraphy is measured. The sticks are then placed on top of a gold coated copper melt head, which is heated to ensure a steady melt rate of 3.5 cm per minute. At the center of the melt head, the melt water is sucked out through a hole connected to a tube and sent to the instruments. A ridge separates the inner 25×25 mm of the melt head from the outer part. Only the interior melt water is sucked by the central tube, the rest is discarded. This ensures that no contamination from the surface of the stick enters the instrument. The surface therefore does not need to be cleaned, which greatly reduces processing time compared to discrete samples. The ends of the sticks still need to be cleaned, but in case of inadequate cleaning, the contaminated data can be discarded.

2.2.4 Size distributions

Dust concentration measurements by Coulter Counter or Abakus are performed by counting the particles in a known volume of melt water and measuring their size. In this way a distribution of particle number as a function of size is obtained, from which the mass total dust mass concentration can be derived by assuming a density. Normally, a density of 2.5 g/cm^3 is assumed (Delmonte et al., 2002). The mass concentration is what we normally refer to as the dust concentration. Other parameters, like mean particle size and ratio between large and small particle concentrations, can also be of interest. A log normal distribution often fits ice core dust size distributions well, except that the data often have heavier tails both for small and large particles (Steffensen, 1997). By multiplying the number size distribution by the volume of the particles, the volume size distribution is obtained. If the number distribution is lognormal, the volume distribution is also lognormal with a larger mode. Typically volume distributions and not number distributions are used for ice core dust data, as they have a mode within the Coulter Counter and Abakus measurement ranges.

2.2.5 Size distribution mathematics

The Coulter and Abakus measure dust as a histogram, counting the number of particles in size bins. As the number of particles in each bin increases with the width of the bin, it is convenient to introduce probability density functions, which keep roughly the same shape independent of the binning. For n bins, define the upper bin boundaries $\{x_1, ..., x_i, ..., x_n\}$ and the number of particles in the bins $\{N_1, ..., N_i, ..., N_n\}$. The number size distribution $\frac{\mathrm{d}N}{\mathrm{d}x}(x)$ has the values

$$\frac{\mathrm{d}N}{\mathrm{d}x}\left(\frac{x_i + x_{i-1}}{2}\right) = \frac{N_i}{x_i - x_{i-1}}. \tag{2.2}$$

For evenly distributed data, if a bin is reduced to half its size, both the numerator and the denominator will be reduced by a factor 2, so the probability density function maintains its value. The argument $\frac{x_i+x_{i-1}}{2}$ is the position of the center of the bin. $\frac{\mathrm{d}N}{\mathrm{d}x}$ can only be estimated for these x-values. However, for ice core dust distributions, $\frac{\mathrm{d}N}{\mathrm{d}x}$ normally forms a smooth function and can be interpolated reasonably between the bin positions if necessary.

Since ice core dust often follows a lognormal distribution, it is convenient to use

$$x = \ln d, \tag{2.3}$$

where d is the particle diameter. This gives

$$\frac{\mathrm{d}N}{\mathrm{d}\ln d}\left(\ln\sqrt{d_i d_{i-1}}\right) = \frac{N_i}{\ln d_i/d_{i-1}}. \tag{2.4}$$

The number of particles in the size interval $[d_1, d_2]$ is

$$N([d_1, d_2]) = \int_{d_1}^{d_2} \frac{\mathrm{d}N}{\mathrm{d}\ln d}(\ln d)\mathrm{d}\ln d, \tag{2.5}$$

so the total number of particles is

$$N_0 = \int_0^\infty \frac{\mathrm{d}N}{\mathrm{d}\ln d}(\ln d)\mathrm{d}\ln d. \tag{2.6}$$

The volume size distribution is defined as the number size distribution times the particle volume of the bin. For spherical particles, where the volume is $V = \frac{\pi}{6}d^3$,

$$\frac{\mathrm{d}V}{\mathrm{d}\ln d}(\ln d) = \frac{\pi}{6}d^3\frac{\mathrm{d}N}{\mathrm{d}\ln d}(\ln d). \tag{2.7}$$

The normalized lognormal distribution is

$$\mathrm{LN}(\ln d) = \frac{1}{\sqrt{2\pi}\ln\sigma}\exp\left(-\frac{1}{2}\left(\frac{\ln d - \ln\mu}{\ln\sigma}\right)^2\right), \tag{2.8}$$

where μ is the mode, ie. the maximum value, and σ is the lognormal standard deviation. When plotted with a logarithmic x-axis, it shows as a gaussian with a standard deviation of σ, and on double logarithmic axes it forms a parabola. Equation 2.8 is the normalized lognormal, so a number size distribution following a lognormal would need to be multiplied by the total particle number,

$$\frac{\mathrm{d}N}{\mathrm{d}\ln d}(\ln d) = N_0\mathrm{LN}(\ln d). \tag{2.9}$$

If the number size distribution is a lognormal, the volume size distribution is also lognormal, as seen in the following way, by combining equations 2.7, 2.8 and 2.9.

$$\begin{aligned}
\frac{\mathrm{d}V}{\mathrm{d}\ln d}(\ln d) =& \frac{\pi}{6}d^3 N_0\mathrm{LN}(\ln d) && (2.10)\\
=& \frac{\pi}{6}d^3\frac{N_0}{\sqrt{2\pi}\ln\sigma}\exp\left(-\frac{1}{2}\left(\frac{\ln d - \ln\mu}{\ln\sigma}\right)^2\right) && (2.11)\\
=& \frac{\pi}{6}\exp(3\ln d)\frac{N_0}{\sqrt{2\pi}\ln\sigma}\exp\left(-\frac{1}{2}\left(\frac{\ln d - \ln\mu}{\ln\sigma}\right)^2\right) && (2.12)\\
=& \frac{\pi}{6}\frac{N_0}{\sqrt{2\pi}\ln\sigma} && (2.13)\\
& \exp\left(-\frac{1}{2}\left(\frac{(\ln d)^2 + (\ln\mu)^2 - 2\ln d\ln\mu - 6(\ln\sigma)^2\ln d}{(\ln\sigma)^2}\right)\right). && (2.14)
\end{aligned}$$

By completing the square of the numerator, we obtain

$$\frac{\mathrm{d}V}{\mathrm{d}\ln d}(\ln d) = \frac{\pi}{6}\frac{N_0}{\sqrt{2\pi}\ln\sigma} \tag{2.15}$$

$$\exp\left(-\frac{1}{2}\left(\frac{(\ln d - (\ln\mu + 3(\ln\sigma)^2))^2 - (9(\ln\sigma)^4 - 6\ln\mu(\ln\sigma)^2)}{(\ln\sigma)^2}\right)\right) \tag{2.16}$$

$$= \frac{\pi}{6}\frac{N_0}{\sqrt{2\pi}\ln\sigma}\exp(4.5(\ln\sigma)^2 + 3\ln\mu) \tag{2.17}$$

$$\exp\left(-\frac{1}{2}\left(\frac{(\ln d - (\ln\mu + 3(\ln\sigma)^2))^2}{(\ln\sigma)^2}\right)\right) \tag{2.18}$$

$$= \frac{\pi N_0\mu^3\exp((\ln\sigma)^2)}{6}\frac{1}{\sqrt{2\pi}\ln\sigma} \tag{2.19}$$

$$\exp\left(-\frac{1}{2}\left(\frac{\ln d - (\ln\mu + 3(\ln\sigma)^2)}{\ln\sigma}\right)^2\right) \tag{2.20}$$

$$= \frac{V_0}{\sqrt{2\pi}\ln\sigma}\exp\left(-\frac{1}{2}\left(\frac{\ln d - \ln(\mu_{\mathrm{vol}})}{\ln\sigma}\right)^2\right), \tag{2.21}$$

where

$$V_0 = \frac{\pi N_0\mu^3\exp((\ln\sigma)^2)}{6} \quad \text{and} \tag{2.22}$$

$$\mu_{\mathrm{vol}} = \mu\exp(3(\ln\sigma)^2). \tag{2.23}$$

V_0 is the total dust volume and μ_{vol} is the mode of the volume distribution. The volume distribution is therefore lognormal if the number distribution is lognormal.

2.3 Renland

Renland is located in the Scoresby Sund area of Greenland, the world's largest fjord system. Today the area is dominated by steep mountains several kilometers high and deep fjords. Mountains and high altitude areas are covered by glaciers and ice caps, and the Greenland Ice Sheet is less than 100 km from Renland. Outlet glaciers from the Greenland Ice Sheet and local ice caps have large outwash plains, where eroded glacial flour is deposited. This provides material for local dust storms. The present day mountains were created during the Caledonian orogeny, when Greenland and Europe collided around 500 - 400 Ma ago. The rocks of Renland and neighbouring areas to the north and south are around 1,000 Ma old, but were partly reactivated during the Caledonian orogeny. Jameson Land to the east is composed of Jurassic sediments, while the area south of Scoresby Sund is composed of basaltic rocks formed 58-54 Ma ago (GEUS, 2018a) (Figure 2.7).

Renland is a peninsula of 88 times 62 km at the northwestern end of the Scoresby Sund system. It has mountains more than 2 km high that surround a plateau containing the Renland ice cap. At the summit of the ice cap, the surface elevation is 2340 m, and the ice is up to 600 m thick. However, the bedrock below the ice has valleys and peaks

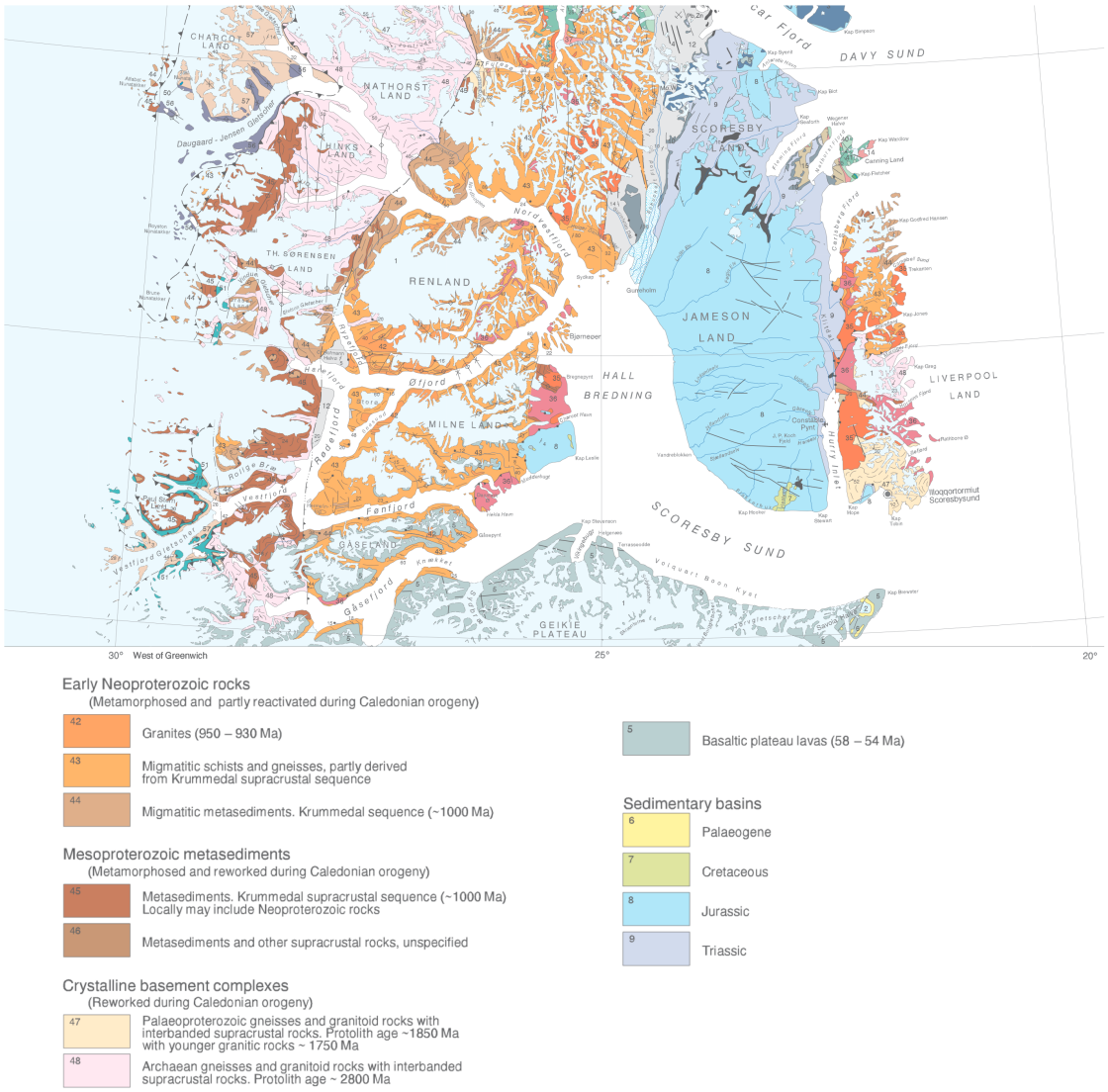

Figure 2.7: Geology of the Scoresby Sund area. Adapted from GEUS (2018b).

with steep slopes, so the thickness of the ice sheet is variable. At the RECAP drill site, the ice is 584 m thick (RECAP, 2018), while it is only 325 m at the Renland ice core site (Johnsen et al., 1992) 1.5 km from RECAP.

2.3.1 Glaciation history

The glaciation history of the Scoresby Sund area has been mapped from the Saalian to today by Funder et al. (2011). During the Saalian (ca. 300-130 ka b2k), the Greenland ice sheet covered Jameson land and the coastal mountains and filled the fjord. In the Eemian, (135-115 ka b2k), the ice sheet retreated, and temperatures were at least 5°C warmer than today (Johnsen et al., 1992). Eemian ice in the old Renland ice core shows that the Renland ice cap did not melt away completely during the Eemian. After the Eemian, in the last glacial period, ice filled the fjord again, and covered most of the Scoresby Sund area. Local glaciers advanced and retreated several times in the early glacial, but the area was almost completely ice covered from the onset of MIS4 (around 71 ka ago) to the end of the glacial (Funder et al., 1998). Only Jameson Land was possibly ice free, as there is no evidence of glacial erosion after the Saalian. Whether it was completely ice free or covered by a non-erosive ice cap is however still disputed (Håkansson et al., 2009; Funder et al., 2011). In chapter 4 we show that there has to be some ice free area in the vicinity of Renland to produce the constant large particle dust flux seen throughout the glacial part of RECAP, which suppports an ice free Jameson Land.

Chapter 3

Particle shape accounts for instrumental discrepancy in ice core dust size distributions

Ice core dust particle concentrations and size distributions have traditionally been measured by Coulter Counter (Steffensen, 1997). Coulter Counter measurements are accurate but relatively labour intensive, requiring at least one person working continuously for measuring a few tens of samples per hour. When the Abakus laser sensor (Klotz GmbH, Germany) was applied to ice cores (Saey, 1998), it quickly became popular, since it requires almost no labour and has sub centimeter measurement resolution when connected to a continuous flow analysis system (Bigler et al., 2011). However, calibrating the Abakus was not straight forward. Even though the relation between measured light intensity and size was chosen to give the right diameter for standard polystyrene spheres, the size distributions had a larger mode than Coulter Counter measurements of the same samples (Ruth et al., 2002).

In this chapter, we show that the discrepancy between Coulter Counter and Abakus is due to the non-spherical shape of the dust particles. The Abakus measures the optical extinction cross section, from which it derives the diameter under the assumption that the particles are spherical. Since the diameter of most dust particles is only a few times larger than the laser wavelength (670 nm), the optical extinction cross section oscillates strongly as a function of diameter due to Mie scattering. The diameters of maximum and minimum extinction cross section depend on the shape and orientation of the particles, so on average, for ice core dust with a wide distribution of shapes, the oscillations cancel out. The strong Mie oscillations that appear when spherical standard latex spheres are measured should therefore be subtracted when the calibration is applied to ice core dust.

The optical extinction cross section depends on the orientation of the particles, and is on average larger for non-spherical than for spherical particles. For particles of a known apsect ratio, the distribution of extinction diameters measured by the Abakus can be derived from the distribution of volumetric diameters measured by the Coulter Counter. This relation can be inverted, within some uncertainty, so the volumetric diameter distri-

bution can be calculated from the Abakus data. With a Single Particle Extinction and Scattering instrument (SPES) (Villa et al., 2016; Potenza et al., 2016), the average aspect ratio of dust in the RECAP ice core was measured to be 0.39 ± 0.03 in the Holocene and 0.33 ± 0.03 in the glacial. The difference between Holocene and glacial dust will be further discussed in chapter 4. While the extinction diameter distribution measured by Abakus differs from the Coulter Counter by up to a factor 10 for some bins, the volumetric diameter distribution calculated from the Abakus and SPES only differ by at maximum a factor 2, which is within the uncertainty.

Instead of determining the volumetric diameter distribution from the Abakus and SPES data, the aspect ratio can also be derived from comparing the Coulter Counter and Abakus data. A more extreme aspect ratio requires a larger shift of the Abakus bins. By shifting the bins to fit the Coulter Counter distribution, the aspect ratio can therefore be determined. For the RECAP data this gives the right aspect ratio for both the Holocene and glacial, and the uncertainty is low enough to give a significantly larger aspect ratio for the Holocene than for the glacial.

This is further expanded in the following manuscript, which is under review in Climate of the Past (Simonsen et al., 2017).

Particle shape accounts for instrumental discrepancy in ice core dust size distributions

Marius Folden Simonsen[1], Llorenç Cremonesi[2], Giovanni Baccolo[4], Samuel Bosch[1], Barbara Delmonte[4], Tobias Erhardt[3], Helle Astrid Kjær[1], Marco Potenza[2], Anders Svensson[1], and Paul Vallelonga[1]

[1]Centre for Ice and Climate, Niels Bohr Institute, University of Copenhagen, Copenhagen, Denmark
[2]Department of Physics, University of Milan and National Institute for Nuclear Physics (INFN), Via Celoria 16, I20133 Milan, Italy
[3]Climate and Environmental Physics, Physics Institute & Oeschger Centre for Climate Change Research, University of Bern, Sidlerstrasse 5, 3012 Bern, Switzerland
[4]Department of Earth and Environmental Sciences, University Milano-Bicocca, Piazza della Scienza 1, I20126 Milan, Italy

Correspondence to: Marius Folden Simonsen (msimonse@fys.ku.dk)

Abstract. The Klotz Abakus laser sensor and the Coulter Counter are both used for measuring the size distribution of insoluble mineral dust particles in ice cores. While the Coulter Counter measures particle volume accurately, the equivalent Abakus instrument measurement deviates substantially from the Coulter Counter. We show that the difference between the Abakus and the Coulter Counter measurements is mainly caused by the irregular shape of dust particles in ice core samples. The irregular shape means that a new calibration routine based on standard spheres is necessary for obtaining fully comparable data. This new calibration routine gives an increased accuracy on Abakus measurements, which may improve future ice core record intercomparisons. We derived an analytical model for extracting the aspect ratio of dust particles from the difference between Abakus and Coulter Counter data. For verification, we measured the aspect ratio of the same samples directly using a Single Particle Extinction and Scattering Instrument. The results demonstrate that the model is accurate enough to discern between samples of aspect ratio 0.3 and 0.4 using only the comparison of Abakus and Coulter Counter data.

1 Introduction

Ice cores from Greenland contain a record of climate proxies over the last 120,000 years. One of those proxies is mineral dust in the size range 0.5-100 μm. The dust has several properties that provide useful information of the past: concentration, size distribution, morphology and chemical and isotopic composition. These measurements have revealed that the dust in ice cores come from central Asia during both the Holocene and the last glacial period (Biscaye et al., 1997). The observed 100-fold decrease in dust concentration from glacial to Holocene (Ruth et al., 2003; Steffensen, 1997) has constrained the aridity, windiness and insolation forcing of glacial climate models (Mahowald et al., 1999; Lambert et al., 2015).

Traditionally, the Coulter Counter technique has been used to measure concentration and size distribution. It works by measuring the electrical impedance over an orifice, through which a sample flows. For ice cores, this sample is melted ice core water, with pure NaCl added to stabilise the electrical conductivity. When a particle flows through and displaces the conductive

liquid, the impedance rises. This signal increases with the particle volume. The Coulter Counter has the disadvantage that it applies only to discrete samples and has not been combined with continuous flow analysis (CFA) systems.

CFA systems (Röthlisberger et al., 2000; Kaufmann et al., 2008) on the other hand are a common technique for analysing impurities in ice core samples, offering faster measurement speed and often higher resolution. On the Copenhagen CFA system, $35\times35\times550$ mm sticks are cut from the ice core and melted upon a gold coated melt head (Bigler et al., 2011). The melt water from the outer 5 mm of the ice core surface is discarded, while the inner uncontaminated water is transported by a peristaltic pump to the connected instruments. One of these instruments is the Abakus laser sensor (LDS23/25bs, Klotz GmbH, Germany) for measuring insoluble particle concentration and size distribution.

The Abakus instrument measures the intensity of laser light through a flow cell filled with the sample liquid. When a particle passes, the light is attenuated. The Abakus therefore measures the optical extinction cross section of the particle, and can measure particles in the range 1-15 µm. Since it measures optical transmissivity rather than electrical impedance, it is much less sensitive to electrical noise than the Coulter Counter. The Abakus on a CFA system can have a measurement depth resolution of 3 mm (Bigler et al., 2011), and requires almost no maintenance when the CFA system is running. The Coulter Counter on the other hand typically integrates a thicker depth interval, and requires work from the operator all the time during measurements (Delmonte et al., 2004; Lambert et al., 2012).

The aspect ratio of ice core dust particles was measured using the novel Single Particle Extinction and Scattering (SPES) instrument (Villa et al., 2016; Potenza et al., 2016). The SPES measures both the extinction cross section, which is also measured by the Abakus, and the optical thickness of the particles (Potenza et al., 2016).

The optical thickness depends on the geometrical thickness of the particle and its refractive index. If the refractive index is known, the aspect ratio can be derived from the combination of extinction cross section and geometrical thickness. The SPES is able to discern between oblate and prolate particles.

The extinction and scattering cross sections of irregularly shaped particles can be accurately calculated with the discrete dipole approximation (DDA) (Draine and Flatau, 1994). In the present work, we have used the Amsterdam Discrete Dipole Approximation (ADDA) code (Yurkin and Hoekstra, 2011). The ADDA simulations were used to simulate the SPES measurements and thereby extract the aspect ratio from the SPES data. Furthermore the ADDA simulations were used to show that the Mie scattering effects on the optical extinction cross-section for spherical particles do not affect ice core dust due to its irregular shape (Chỳlek and Klett, 1991).

The measured samples are from the Renland Ice Cap Project (RECAP) ice core drilled during the summer of 2015 on the Renland ice cap in Eastern Greenland only 2 km away from the old Renland ice core (Hansson, 1994). This ice core covers the last glacial cycle, and samples were taken from both the Holocene and the last glacial period (supplement A). As found for the central Greenlandic ice cores, the glacial RECAP dust comes from central Asia (Biscaye et al., 1997). The Holocene dust, similar to the old Renland core (Bory et al., 2003), is dominated by a local East Greenlandic source. The volume mode of the glacial dust is 2 µm, versus 20 µm for the Holocene dust, due to the increased transport size fractionation for the glacial dust (Ruth et al., 2003).

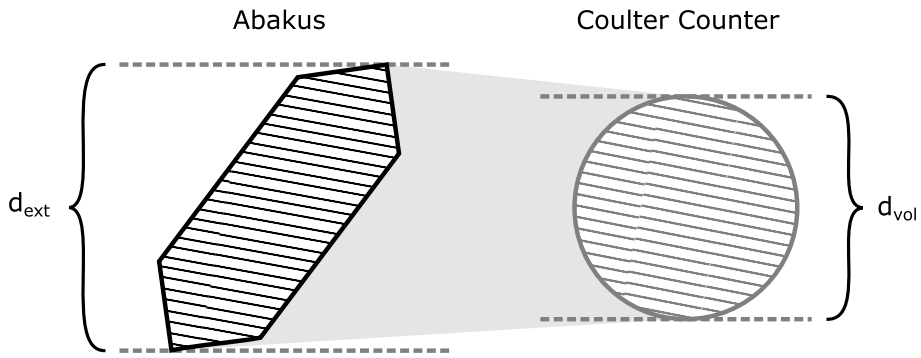

Figure 1. The Abakus measures the extinction cross section of the particles, while the Coulter Counter measures their volume. Both instruments convert this to an equivalent diameter, d_{ext} and d_{vol} respectively.

Although both instruments are typically calibrated using standard spheres of known diameter, they produce substantially different size distribution results when ice core samples are measured (Ruth et al., 2003; Lambert et al., 2008, 2012; Koffman et al., 2014). It has been proposed that this difference is because ice core dust is generally non-spherical (Lambert et al., 2012; Potenza et al., 2016). We show here that the non-spherical shape of the particles does quantitatively account for the main discrepancy between the two instruments (Figure 1). One important shape effect arises from the aspect ratio, defined as the ratio between the length of its shortest and the longest side. We have found that Greenland ice core dust is dominated by oblate particles of aspect ratio $0.3-0.4$, which is significantly different from the aspect ratio of 1 of the polystyrene standard spheres used for calibration.

2 Materials and Methods

2.1 Abakus

For the Abakus measurements, square sticks of $35\times35\times550\ \mathrm{mm}$ were cut from the center of the RECAP ice core, These sticks were melted on the RECAP CFA system. This CFA system is an enlargement of the one described by Bigler et al. (2011), with higher melt rate, more analytical channels and pressure decoupling after the debubbler. The Abakus was connected to the CFA system with a flow rate of $2\ \mathrm{mL/min}$. The attached tubes and the Abakus were cleaned with MQ water (Millipore Advantage, 18.2 MOhm/cm) after each 5.5 m of ice measured. Occasionally the Abakus was clogged by a large particle and required flushing with a syringe while the system was running. The depth resolution is 5 mm due to mixing in the tubes from the melt head to the Abakus. For high dust concentrations, two particles may pass through the detector at the same time and show up as one larger particle. We found that this effect was negligible (see Supplement F for details). The Abakus was originally calibrated to give the correct diameter for polystyrene beads of 2, 5, and 10 $\mu\mathrm{m}$.

Polystyrene standard spheres 1.5, 2, 4, 5 and 10 μm diameter from BS-Partikel GmbH, Wiesbaden, Germany (supplement B), were measured by the Abakus. They were diluted to concentrations between 15000 and 90000 particles/mL. To avoid coagulation, the standards were sonicated for 30 seconds before measurements. Each of the standards was measured for 6 minutes.

2.2 Coulter Counter

The Coulter Counter measured discrete samples 55 cm in length. The measured ice consisted of an outer triangular piece 3×1 cm in cross section cut to 10 cm long pieces. The samples were decontaminated by rinsing in three consecutive jars of MQ water. In each jar the outer layer of ice was melted away and removed, leaving only the cleaner inner part to be analyzed. This treatment reduced the sample size by 50%. The samples were measured in two Beckman Coulter Counters, one with a 100 μm aperture and one with a $30\,\mu$m aperture. The samples were shaken prior to measurement in the $100\,\mu$m Coulter Counter. Afterwards the samples were measured by the 30 μm Coulter Counter. The 30 μm aperture data were used for particles smaller than 4 μm and the 100 μm aperture data were used for particles larger than 4 μm. Selected samples representative of Holocene and glacial climates, were measured by the Coulter Counter for this study. For the Holocene, selected samples from 356 to 4008 years b2k (before AD 2000) were used, while for the glacial, the whole period from 17760 to 33885 years b2k was measured (supplement A). The same samples were used for the Abakus.

2.3 SPES

After the Coulter Counter measurements, the samples were measured by SPES (section 3.3). The sample flows through a 200 μm flow cell, and is illuminated by a laser. The light is measured by two detectors, which in combination gives the extinction cross section and the optical thickness. There is no focusing of the particle stream in the cell, so only a small fraction of the particles passing through the cell is measured by the laser. Therefore the sample is circulated through the cell several hundred to thousand times. This gives an accurate measure of the shape distribution of the particles, but it does not allow concentration measurements.

The narrow cell ensures high shear, forcing the particles to attain a preferential direction along one direction. Oblate particles in a shear flow orient themselves with the flat side along the flow lines, and are randomly oriented in the shear direction. Prolates lie in a plane of constant velocity, and are free to rotate within it (Jeffery, 1922).

3 Results

3.1 ADDA simulations

Using the Amsterdam Discrete Dipole Approximation software (ADDA) (Yurkin and Hoekstra, 2011), we have calculated the extinction diameter for different particles. The extinction diameter is based on the optical extinction cross section. The optical extinction cross section is defined for a plane light wave interacting with a particle as the difference between the incoming and transmitted light intensity divided by the incoming light intensity and multiplied by the area of the plane incoming wave.

For spherical particles much larger than the wavelength of the light, the relation between diameter and optical extinction cross section is $\sigma_{\mathrm{ext}} = \frac{\pi}{2} d^2$. For smaller particles of size comparable to the light wavelength, the relation differs due to optical effects (Figure 2) (van de Hulst, 1957). However, we define the extinction diameter as $d_{\mathrm{ext}} = \sqrt{\frac{2}{\pi}\sigma_{\mathrm{ext}}}$ for all particles. We associate each particle with its volumetric diameter: A sphere with volume V has the diameter $d_{\mathrm{vol}} = \sqrt[3]{\frac{6V}{\pi}}$. For any particle of known volume, the volumetric diameter is given by this relation.

Specifically, we have used ellipsoids and oblate prisms with an aspect ratio of 0.3 in the volumetric diameter range 1 to 8 µm (Figure 3). While spheres have a unique extinction diameter for each volumetric diameter, the extinction diameter of other particles depends on their orientation. For each volumetric diameter, there will therefore be several possible Abakus measurements of the extinction diameter, described by a probability density function. This is described in more detail in Section 3.4, where it is called $\frac{dP(d_{\mathrm{ext}}|d_{\mathrm{vol}})}{d\ln d_{\mathrm{ext}}}$. The broadness of the probability density function for non-spherical particles results in a smoothing of the relationship between the extinction and volumetric diameters (Figure 3). Furthermore, the extinction diameter oscillation maxima are not located at the same d_{vol} for different particle shapes. Since ice core dust has a variable shape (supplement C), it is sampled from a sum of the ellipsoid, prismatic and many more distributions. In this sum of distributions the oscillation pattern averages out.

The average extinction diameter is higher than the volumetric diameter since the measured dust particles are elongated (discussed further in section 3.4). For particles larger than 1.7 µm, the average extinction diameter is approximately proportional to the volumetric diameter. For much smaller particles, the extinction diameter is independent of the particle shape. The Abakus after calibration (section 3.2) does however not measure particles smaller than 1.8 µm, so the measured Abakus data is within the range of proportionality: $d_{\mathrm{ext}} \propto d_{\mathrm{vol}}$.

3.2 Extinction calibration using particle size standards

We have measured the diameters of five different particle size standards (supplement B, section 2.1) with the Abakus (Figure 2). The 2, 5, and 10 µm standards were measured twice with a one year delay, without significantly different results. This shows that the Abakus calibration is stable over the time scale of a typical measurement campaign.

Since d_{ext} is proportional to d_{vol} for ice core dust (section 3.1), and the proportionality constant depends on particle shape and is unknown, we would like to calibrate the Abakus such that it gives the extinction diameter d_{ext} and not the true diameter for the standard spheres (using the term true for the certified diameter given by the manufacturer). Therefore we define a calibration function such that the measured diameter divided by the calibration function is the extinction diameter. To avoid artifacts in the calibrated distribution, the calibration function has to be a continuous function of the measured diameter with a continuous first derivative. Since we want the relative error on each standard to have the same weight, the function is fitted to the logarithm of the ratio between the measured and extinction diameter. The function $y = a(x - x_0)^2$, where $y = \frac{\ln(d_{\mathrm{meas}})}{\ln(d_{\mathrm{ext}})}$ and $x = \ln(d_{\mathrm{meas}})$, is fitted to the data as calibration function (Figure 4). The fit parameters found are $(a, x_0) = (-0.086, 2.60)$. This particular calibration function is chosen because it is simple, fits the data well and satisfies the conditions described above. $x_0 = 2.60$ corresponds to $d_{\mathrm{meas}} = 13.5$ µm. As the calibration function is equal to 1 for $d_{\mathrm{meas}} = 13.5$ µm and standards larger than 13.5 µm were not tested, no calibration is applied for diameters larger than 13.5 µm.

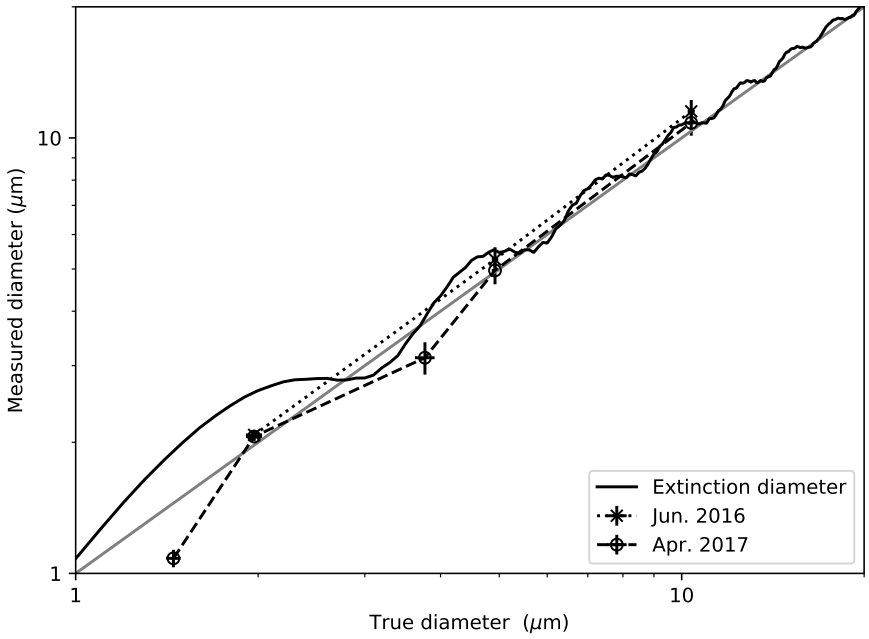

Figure 2. The diameter of standard polystyrene spheres measured by the Abakus as a function of the true diameter certified by the manufacturer (circles and dashed line), together with three of the same standards measured a year earlier (crosses and dotted line) and the optical extinction diameter of a sphere as a function of diameter (solid black curve). The grey line is where the measured and the true diameter are equal, to which the extinction diameter converges for large true diameters.

The particle size standard calibration has been applied to ice core dust data (Figure 5). Since the calibration function is less than 1 for diameters smaller than 13.5 μm, the effect of applying the calibration function is that the small diameter data is shifted towards larger diameters. This is most pronounced for the smallest diameters, since the calibration values are smallest for small diameters. The positive slope of the calibration function means that the calibrated bin positions are squeezed more tightly together than the uncalibrated bins. Since the probability density function is defined as the number of counts in a bin divided by its size, the calibrated probability density function has higher values than the uncalibrated one. This effect decreases with diameter, as the slope decreases.

3.3 SPES

We have measured optical thickness (ρ) and extinction cross section (σ_{ext}) with SPES for both Holocene and glacial samples (Figure 6), using the method of Villa et al. (2016), and compared the results to ADDA simulations. The distribution of particles in $\rho, \sigma_{\mathrm{ext}}$ space can be simulated using ADDA for a given particle shape and size distribution. We have done this for oblate right square prisms of aspect ratios 0.2, 0.25, 0.3, 0.4 and 0.5. A total of 20,000 particles with a volumetric diameter ranging from

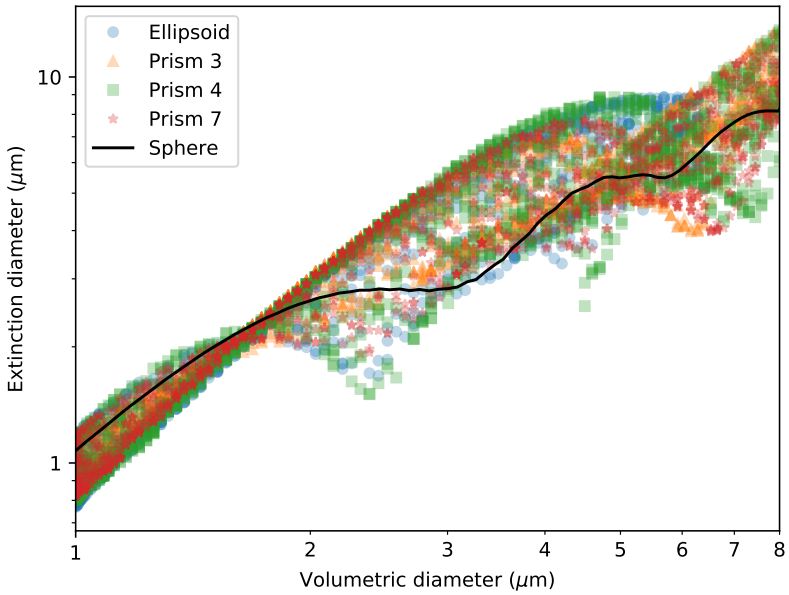

Figure 3. ADDA simulations of particles with a refractive index of 1.586 and, except for the spheres, an aspect ratio of 0.3. The prisms are oblate and their cross sections are equilateral polygons with 3, 4 and 7 sides.

100 nm to 2 µm and different refractive indexes and orientations were simulated. This size range covers the SPES measurement range.

The refractive index, n, of atmospheric dust is on average between 1.52 and 1.55 (Shettle and Fenn, 1979; Sokolik et al., 1993; Grams et al., 1974). At Dome C, Antarctica, the refractive index of Holocene and glacial ice core dust is 1.53 and 1.56 (Royer et al., 1983). We have run the simulations using the refractive indices 1.52 and 1.55 and found only a small effect of the refractive index on the modelled aspect ratio.

By comparing to SPES measurements of oblate and prolate particles in Villa et al. (2016) and Potenza et al. (2016), it was found that the samples are dominated by oblates. Prolates have a much narrower distribution of optical thickness than oblates, since their orientation is fixed by the flow. The absence of a superimposed prolate distribution indicates that no more than than 15% prolates are compatible with the measured SPES results. The following analysis therefore only focuses on oblates. For a similar analysis of prolates, see supplement G.

To compare the simulations and the data, the average of the logarithm of the simulated optical thickness as a function of extinction cross section was calculated. This average was then used as a least squares fit to the measured data, where the aspect ratio is the variable parameter. For values of σ_{ext} approaching the lower and upper bound of the extinction cross section range, the SPES is not sensitive in the full optical thickness range. To avoid bias, only experimental data between the 0.25 and 0.75 quantile of the extinction cross section was used in the fit.

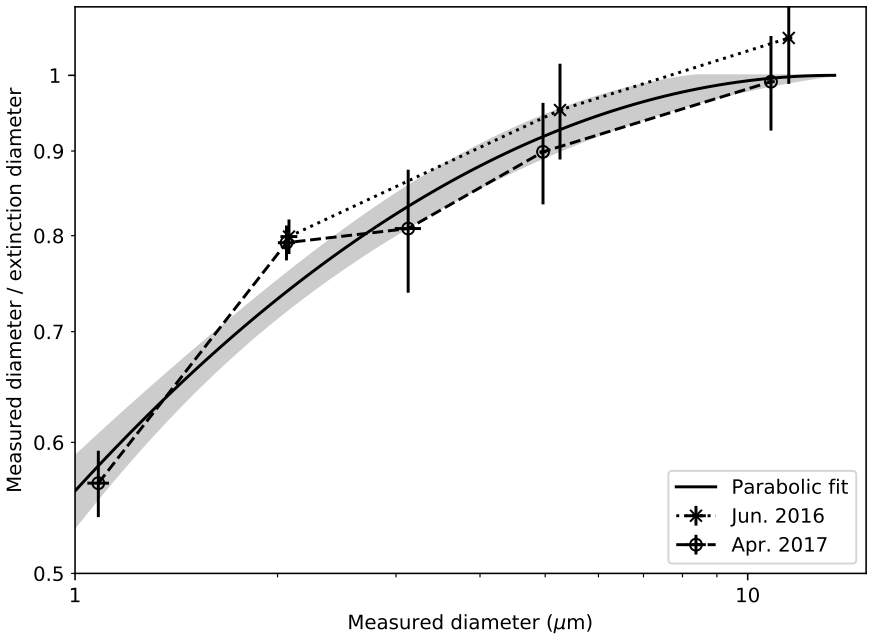

Figure 4. The ratio between the diameter of spheres measured by the Abakus in April 2017 and their extinction diameter (Figure 2) (circles and dashed line), together with three of the same standards measured a year earlier (crosses and dotted line) and a fit to the logarithm of the April 2017 data (solid line). The fitted parameters are $(a, x_0) = (-0.086, 2.60)$ of the function $a(x - x_0)^2$ where x is the logarithm of the diameter in µm. The uncertainty on the fit (shading) is based on the uncertainty on the data points.

For $n = 1.52$ the Holocene aspect ratio is 0.42 ± 0.03 and the glacial is 0.38 ± 0.02, while for $n = 1.55$ the Holocene is 0.36 ± 0.01 and the glacial is 0.29 ± 0.01. This is independent of the volumetric diameter size distribution used in the simulation. The average in the refractive index range of ice core dust is therefore 0.39 ± 0.03 for the Holocene and 0.33 ± 0.04 for the glacial.

3.4 Aspect ratio effect

Spheres have the lowest geometrical cross section to volume of all particles, when averaged over all rotation angles of the particles (Brazitikos et al., 2014). We define the geometric cross section diameter of a particle as $d_{\mathrm{geom}} = \sqrt{\frac{2}{\pi}\sigma_{\mathrm{geom}}}$, where σ_{geom} is the geometric cross section of the particle. However, since ice core dust is non-spherical, (section 3.3), $d_{\mathrm{geom}} > d_{\mathrm{vol}}$ and $d_{\mathrm{ext}} = d_{\mathrm{geom}}$ (section 3.2). We can therefore calculate the distribution of d_{ext} based on the aspect ratio c and the distribution of d_{vol}. The distribution of d_{vol}, $\frac{dP(d_{\mathrm{vol}})}{d\ln d_{\mathrm{vol}}}$, can be determined by the Coulter Counter.

Since oblates dominate the measured samples, we will focus our model on those, instead of also considering prolates (section 3.3). As previously mentioned (section 2.3), oblate particles in a shear flow orient themselves with the flat side along the flow lines, while they are randomly oriented in the shear direction (Jeffery, 1922). Since they are free to rotate along an axis

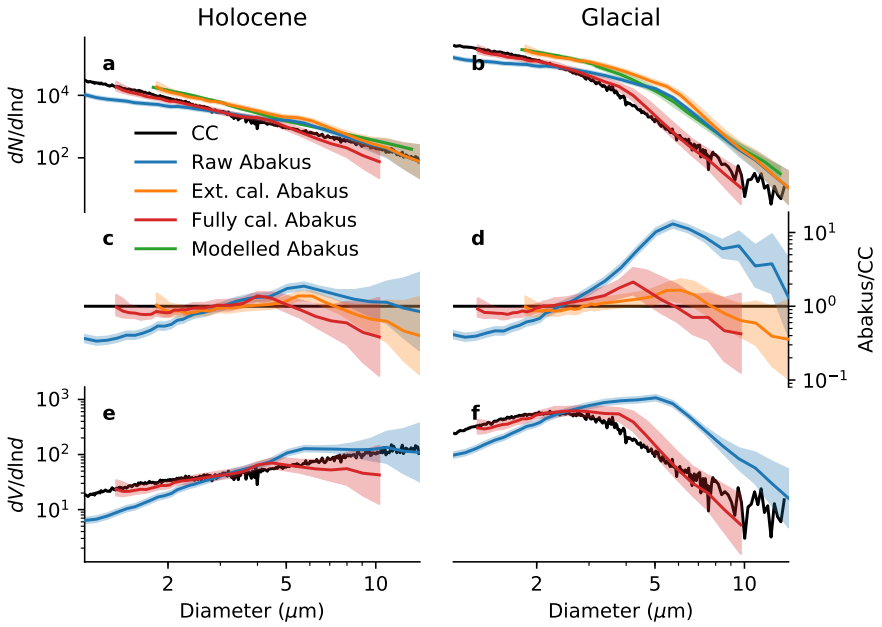

Figure 5. Size distributions of the dust particles in the RECAP ice core for both Holocene and last glacial period measured by Abakus and Coulter Counter. **a**,**b**: Probability density functions of the number of particles as function of volumetric diameter, measured diameter or extinction diameter for Coulter Counter (black, volumetric diameter), raw Abakus (blue, measured diameter), extinction calibrated Abakus (Section 3.2) (orange, extinction diameter), modelled Abakus data based on Coulter Counter data and the aspect ratio measured by SPES (Section 3.4) (green, extinction diameter) and Abakus data fully calibrated to Coulter Counter data using both the extinction calibration and aspect ratio (Section 3.5) (red, volumetric diameter). The uncertainty (shaded area) on the raw Abakus data is measurement uncertainty (Supplement E), while the remaining uncertainties are linearly propagated from the Abakus and aspect ratio uncertainties. **c**,**d**: Raw Abakus data divided by Coulter Counter (blue, from blue and black in a, b), extinction calibrated Abakus data divided by modelled Abakus data (orange, from orange and green in a, b) and fully calibrated Abakus data divided by Coulter Counter (red, from red and black in a,b). **e**,**f**: Probability density functions of particle volume derived from the number density functions of figure a,b for Coulter Counter (black), raw Abakus (blue) and fully calibrated Abakus data (red).

orthogonal to the light beam direction, we can model them as rectangles embedded in 2 dimensions for which all orientation angles are equally likely (supplement D). The light and detector also lie in the plane. In this 2 D model, d_{vol} is the square root of the area of the rectangle, and d_{ext} is the cross section of the rectangle.

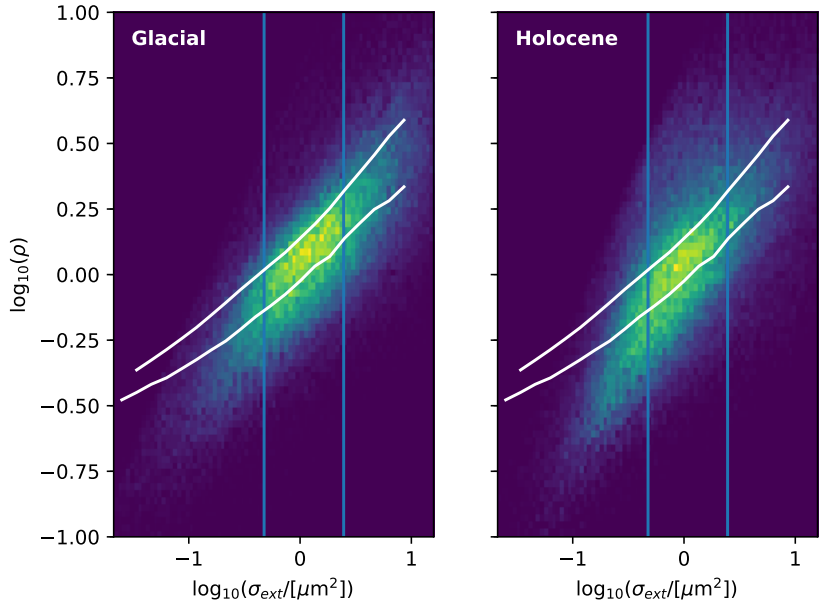

Figure 6. Glacial and Holocene samples measured by SPES. The brighter colors have a higher number of measured particles in a bin. The blue lines mark the 0.25 and 0.75 quantiles of σ_{ext}. The white curves are the mean optical thickness as a function of σ_{ext} for ADDA simulations with a refractive index of 1.55. The upper is for an aspect ratio of 0.5, the lower for 0.2.

Denoting the length of the short side b, the length the long side a, and the aspect ratio $c = b/a$, the probability of d_{ext} given a certain d_{vol} is

$$\frac{dP(d_{\mathrm{ext}}|d_{\mathrm{vol}})}{d\ln d_{\mathrm{ext}}} = \begin{cases} 0 & \text{for } d_{\mathrm{ext}} < b \\ z & \text{for } b < d_{\mathrm{ext}} < a \\ 2z & \text{for } a < d_{\mathrm{ext}} < \sqrt{a^2+b^2} \end{cases}, \tag{1}$$

for

$$z = \frac{2}{\pi}\frac{1}{\sqrt{\frac{a^2+b^2}{d_{\mathrm{ext}}^2}-1}}. \tag{2}$$

The distribution of d_{ext} for all d_{vol} can then be found as

$$\frac{dP(d_{\mathrm{ext}})}{d\ln d_{\mathrm{ext}}} = \int \frac{dP(d_{\mathrm{ext}}|d_{\mathrm{vol}})}{d\ln d_{\mathrm{ext}}}\frac{dP(d_{\mathrm{vol}})}{d\ln d_{\mathrm{vol}}} d\ln d_{\mathrm{vol}}. \tag{3}$$

In section 3.2 we calibrated the Abakus such that $d_{\mathrm{meas}} = d_{\mathrm{ext}}$. Therefore $\frac{dP(d_{\mathrm{ext}})}{d\ln d_{\mathrm{ext}}}$ calculated here simulates Abakus measurements.

This can be used to find the aspect ratio of the particles just from the Coulter Counter-Abakus discrepancy. To do this, the sum of the square of the logarithm of the ratio between $\frac{dP(d_{\mathrm{ext}})}{d\ln d_{\mathrm{ext}}}$ calculated from the Coulter Counter data and the Abakus data was minimized with respect to the aspect ratio. This gives the aspect ratio where $\frac{dP(d_{\mathrm{ext}})}{d\ln d_{\mathrm{ext}}}$ is most consistent with the Abakus data, which is the most likely aspect ratio given the data. For the Holocene data this gave $c = 0.41 \pm 0.09$, while for the glacial $c = 0.31 \pm 0.04$. The errors are propagated from the total errors on the calibrated Abakus data. There is however a large correlation between the errors on the Holocene and glacial data, so the error on the difference is only around 0.02, confirming a significant difference in aspect ratio between glacial and Holocene dust particles.

3.5 Calibration of Abakus

Equation 3 gives the extinction diameter size distribution (Abakus) given a measured volumetric size distribution (Coulter Counter) and a known aspect ratio. However, often a measurement of the volumetric size distribution is desired, while only Abakus measurements are available. To derive a volumetric size distribution from Abakus data, the Abakus data first have to be extinction calibrated (Section 3.2) so it gives extinction diameter instead of measured diameter (Section 3.2). Then an inverted Equation 3 has to be applied to account for the aspect ratio effect. The inversion cannot be done exactly with $\frac{dP(d_{\mathrm{ext}}|d_{\mathrm{vol}})}{d\ln d_{\mathrm{ext}}}$ (Equation 1) in its current form. It therefore has to be done semi empirically. Since the modelled Abakus data fits the extinction calibrated Abakus data (Figure 5), the discrepancy between the Abakus and Coulter Counter can be explained by wrong binning, and not by missing counts. For the aspect ratio inversion, it is therefore only necessary to shift the bins, and not change the counts in each bin. We propose to multiply the Abakus bins by $\sqrt[3]{c} = (0.73, 0.69)$ for the Holocene and glacial respectively, where c is the aspect ratio. The result is the fully calibrated Abakus data seen in Figure 5. The multiplication factor is chosen to make the fully calibrated Abakus data consistent with the the Coulter Counter data. For the glacial volumetric distributions, the mode of the Coulter Counter, the uncalibrated Abakus and the fully calibrated Abakus data are respectively 2.3, 5.0 and 2.7 $\mu\mathrm{m}$.

4 Discussion

When the Abakus is calibrated using the true diameter of polystyrene spheres, it gives up to 10 times as many counts as the Coulter Counter for some particle sizes, when ice core samples are measured (Figure 5). This result is consistent with the findings of Ruth et al. (2008, Figure 1a) who demonstrated that the data produced by the two instruments are proportional over four orders of magnitude, even if the absolute concentration results do not agree. The discrepancy between the two instruments is systematic, because they measure two different properties of the particles: volumetric and extinction cross section. It is therefore not possible in general to calibrate the Abakus such that it yields the same distribution as the Coulter Counter for all ice core samples. However, by combining Coulter Counter and Abakus data, additional information is gained about the aspect ratio that was not available from the two instruments individually.

It has previously been suggested that it is impossible to calibrate the Abakus using polystyrene beads due to the strong Mie oscillations (Ruth, 2002, p. 20). It was argued that since for spheres the measured extinction cross section is a non-monotonous

function of the true diameter, it cannot be inverted. However, this is based on the criterion that d_{meas} of the Abakus should be identical to d_{true} when measuring spheres. Since spheres have strong Mie oscillations but ice core dust does not, this criterion is invalid. Therefore the Abakus should be calibrated such that d_{meas} is equal to d_{ext} instead of d_{true} (section 3.2).

With the SPES instrument we found that the average aspect ratio of our ice core dust samples is 0.39 ± 0.03 for the Holocene and 0.33 ± 0.04 for the glacial, so the particles are significantly elongated (section 3.3). Using our simple model for the relation between d_{meas} and d_{vol}, we have calculated the aspect ratio independently from the Abakus and Coulter Counter data. This gave an aspect ratio of 0.41 ± 0.09 for the Holocene and 0.31 ± 0.04 for the glacial in accordance with SPES. The SPES aspect ratio was calculated for particles less than 2 μm volumetric diameter, and the Abakus for particles between 1.2 and 9 μm, so the measurements are not directly comparable. However, as we only investigate the leading order effect of the aspect ratio, and atmospheric studies find no size dependence of the aspect ratio (Knippertz and Stuut, 2014, page 28), it is assumed that any possible size dependence of the aspect ratio is not large enough to significantly change the results. In addition to giving the same aspect ratio as SPES, the model also gives a consistent size distribution within the Abakus uncertainties (Figure 5).

In the Dome C ice core from the East Antarctic plateau the aspect ratios of oblate and prolate particles have been determined to be 0.2 ± 0.1 and 3.5 ± 1.3, respectively (Potenza et al., 2016). The ranges refer to the variability in the aspect ratio among different particles and not the uncertainty of the mean. In the RECAP ice core studied here, we found a similar but slightly less extreme aspect ratio both in the Holocene and in the glacial ice. For the RECAP core, we speculate that the Holocene dust originates from local Eastern Greenlandic sources, while the glacial dust is from central Asia (Bory et al., 2003). Measurements of dust particles in dust storms generally show an aspect ratio above 0.5. However, during transport, the dust fractionates towards more extreme aspect ratios (Knippertz and Stuut, 2014, p. 28-30). Since large ice sheets are located far from typical dust sources, the dust extracted from ice cores would be subject to more fractionation. Therefore we do expect more extreme aspect ratios to be found in ice core dust than in the atmospheric dust storm measurements. The greater aspect ratio of the local Greenlandic Holocene dust compared to the Asian glacial dust agrees well with the observed aspect ratio fractionation observed in the atmosphere.

5 Conclusions

The Abakus laser sensor and the Coulter Coulter give different size distributions when measuring the same ice core dust sample. This is because ice core dust particles are not spherical, so the particle volume measurements of the Coulter Counter are different from the cross section measurements of the Abakus. When spherical particles are measured by the Abakus, the measured extinction diameter oscillates strongly as a function of particle size due to Mie scattering oscillations. The extinction diameter of ice core dust does not show this oscillation pattern, but is proportional to the volumetric diameter. When the Abakus is calibrated using spherical particles, it should therefore be calibrated to the extinction diameter and not to the true diameter.

We derived a model for extracting the aspect ratio of the dust particles from the differences between Abakus and Coulter Counter measurements of the same ice core dust samples. This process suggests an aspect ratio of 0.41 ± 0.01 for Holocene and 0.32 ± 0.01 for glacial dust samples from the RECAP ice core, consistent with direct aspect ratio measurements from a

Single Particle Extinction and Scattering instrument. This shows that not only is the discrepancy between the two instruments explained by the non-spherical shape of the particles, it can also be used to obtain the aspect ratio. As the Holocene dust has Greenlandic origin while the glacial dust is Asian, the aspect ratio could potentially aid in provenance determination and in understanding atmospheric transport processes. Moreover, by determining the aspect ratio, a better size distribution can be obtained from the Abakus data.

6 Data availability

The data for all plots will be made available on www.iceandclimate.dk/data upon acceptance.

Appendix A: Bags measured by the Coulter Counter

Holocene				
Bag	Top depth (m)	Bottom depth (m)	Top age (years b2k)	Bottom age (years b2k)
300	164.45	165.00	356	358
304	166.65	167.20	363	365
305	167.20	167.75	365	367
321	176.00	176.55	395	397
335	183.70	184.25	423	425
714	392.15	392.70	1980	1989
716	393.25	393.80	1998	2006
746	409.75	410.30	2282	2293
747	410.30	410.85	2293	2303
755	414.70	415.25	2379	2390
759	416.90	417.45	2423	2434
760	417.45	418.00	2434	2446
762	418.55	419.10	2457	2469
788	432.85	433.40	2785	2799
795	436.70	437.25	2884	2899
797	437.80	438.35	2914	2928
799	438.90	439.45	2943	2958
800	439.45	440.00	2958	2974
836	459.25	459.80	3588	3608
837	459.80	460.35	3608	3629
838	460.35	460.90	3629	3650
840	461.45	462.00	3671	3692
842	462.55	463.10	3713	3734
847	465.30	465.85	3822	3845
848	465.85	466.40	3845	3868
850	466.95	467.50	3890	3914
851	467.50	468.05	3914	3937
852	468.05	468.60	3937	3961
854	469.15	469.70	3984	4008

Glacial				
Bag	Top depth (m)	Bottom depth (m)	Top age (years b2k)	Bottom age (years b2k)
972	534.05	534.60	17760	21170
973	534.60	535.15	21170	24745
974	535.15	535.70	24745	28783
975	535.70	536.25	28783	33885

Appendix B: Polystyrene sphere standards

The polystyrene sphere standards were produced by BS-Partikel GmbH, Wiesbaden, Germany. d_{true} is the certified diameter given by the manufacturer, d_{meas} is the diameter measured by the Abakus, and σ_{true} and σ_{meas} are their uncertainties.

Nominal diameter (µm)	d_{true} (µm)	d_{meas} (µm)	σ_{true} (µm)	σ_{meas} (µm)	Lot No.	Catalog No.
1.5	1.45	1.08	0.04	0.05	LS0248.161	LS0150-05
2	1.97	2.06	0.06	0.05	LS239.111	LS0200-05
4	3.77	3.12	0.14	0.27	LS237.161	LS0400-05
5	4.92	4.96	0.06	0.35	LS122.111	LS0500-05
10	10.37	10.83	0.14	0.71	LS108.509	LS1000-05

Appendix C: Microscope photographs

Photographs of both glacial and Holocene dust were taken through a microscope (Figures 7 and 8). The highly non-spherical shape is clearly seen. As the particles orient themselves with as low center of mass as possible on the substrate, they will typically lie on their flattest side. The aspect ratio is therefore not directly visible.

Appendix D: Extinction diameter calculation in the 2D model

The particles in the Abakus are modelled as 2D rectangles, for which all rotation angles are equally likely (Figure 9). The cross section of the particle is equal to d_{ext} in the 2D model.

D1 Rod

For calculating the cross section of a rectangle, the cross section of a rod is needed. We define a rod with length l and zero width. For an angle of rotation ϕ, the cross section is $d_{\text{ext}} = l \sin\phi$. From symmetry, the ϕ values are confined to $\phi \in [0, \frac{\pi}{2}]$ Assuming a uniform probability distribution for the angle, the probability of measuring the particle in the interval $[\phi, \phi + d\phi]$ is $dP(\phi; d\phi) = \frac{2}{\pi} d\phi$, which is normally written $\frac{dP(\phi)}{d\phi} = \frac{2}{\pi}$.

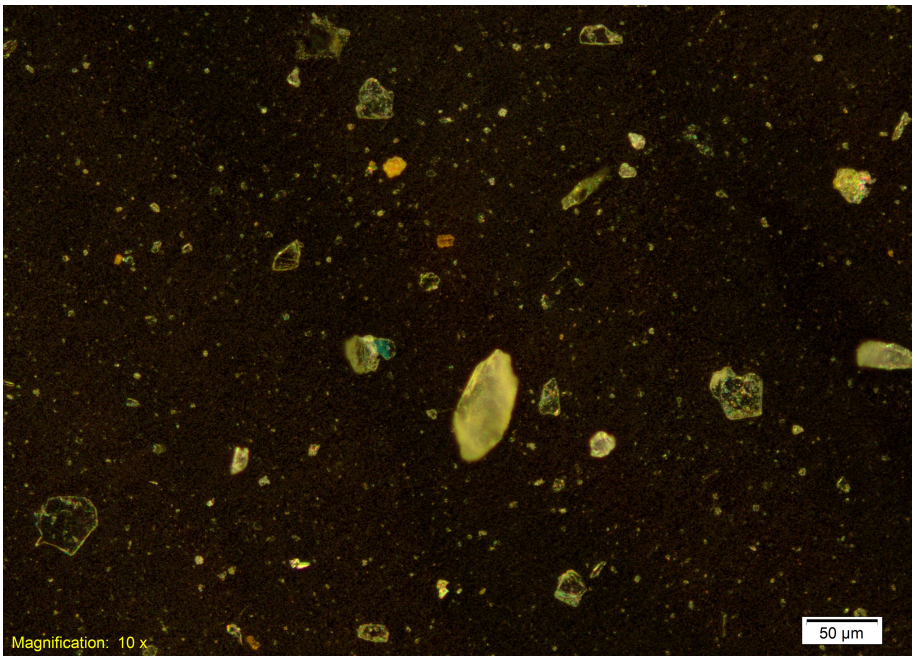

Figure 7. Microscope photograph of RECAP Holocene dust from bag 837.

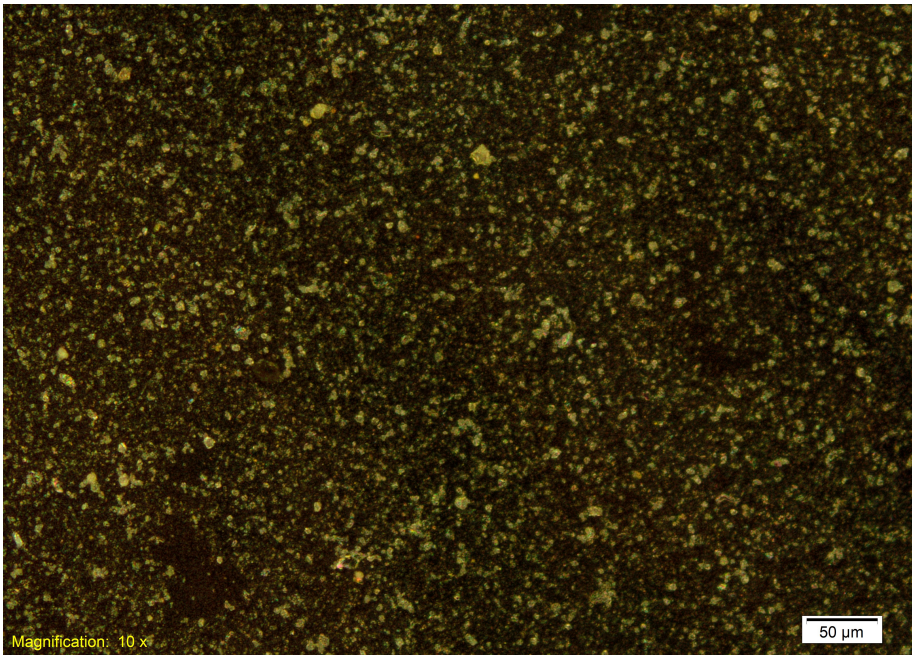

Figure 8. Microscope photograph of RECAP glacial dust from bag 975.

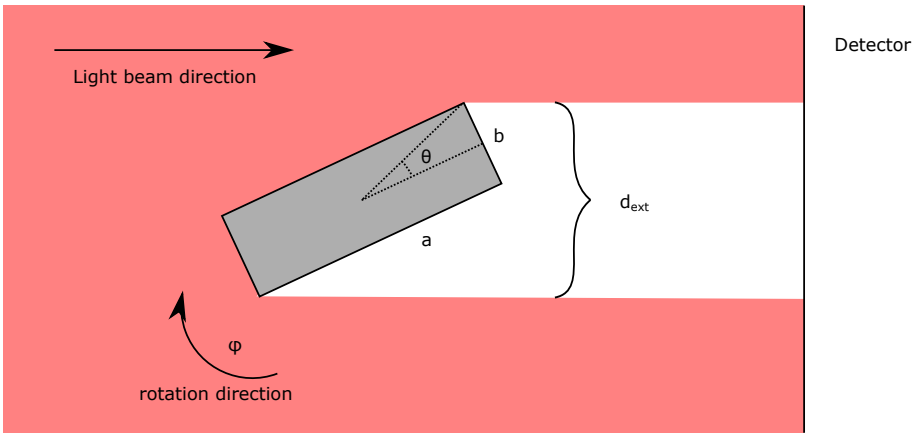

Figure 9. 2D model of the particle orientation in the Abakus.

For converting this to d_{ext} space, $d\phi$ needs to be expressed in terms of dd_{ext}:

$$d_{\text{ext}} = l \sin\phi \tag{D1}$$

$$\Rightarrow dd_{\text{ext}} = l \cos\phi d\phi \tag{D2}$$

$$\Rightarrow d\phi = \frac{1}{\sqrt{l^2 - d_{\text{ext}}^2}} dd_{\text{ext}} \tag{D3}$$

Therefore

$$\frac{dP(d_{\text{ext}})}{dd_{\text{ext}}} = \frac{2}{\pi} \frac{1}{\sqrt{l^2 - d_{\text{ext}}^2}} \tag{D4}$$

$$\Rightarrow \frac{dP(d_{\text{ext}})}{d \ln d_{\text{ext}}} = z, \tag{D5}$$

where

$$z = \frac{2}{\pi} \frac{1}{\sqrt{\left(\frac{l}{d_{\text{ext}}}\right)^2 - 1}}. \tag{D6}$$

It is seen that it diverges for $d_{\text{ext}} \to l$, because d_{ext} is almost constant as a function of angle when the rod is close to being perpendicular to the light source.

D2 Rectangle

Consider a rectangle with side lengths a and b. As for the rod, by symmetry, it is only necessary to consider the angles $\phi \in [0, \frac{\pi}{2}]$. In this case the cross section is given by the cross section of the diagonal. This is just the cross section of a rod rotated by

$$\phi_+ = \phi + \theta \tag{D7}$$

$$\Rightarrow \phi_+ \in [\theta, \frac{\pi}{2} + \theta], \tag{D8}$$

where θ is the angle between the side a and the diagonal. If ϕ is uniformly distributed in $[0, \frac{\pi}{2}]$, so is ϕ_+ in $[\theta, \frac{\pi}{2} + \theta]$. The derivation for the rod is only valid when d_{ext} is a monotonous function of ϕ. This means that it can only be directly applied for $\phi_+ < \frac{\pi}{2}$. However, due to symmetry, the cross section is the same for $\phi_+ = \frac{\pi}{2} + \Delta\phi$ and $\phi_+ = \frac{\pi}{2} - \Delta\phi$, for any $\Delta\phi$. Therefore, the probability of measuring a cross section corresponding to $\phi \in [\frac{\pi}{2} - \theta, \frac{\pi}{2}]$ is twice as high as the probability of measuring the cross section of a rod in this interval. The cross section of $\frac{\pi}{2} - \theta$ is a. This means that the probability distribution is

$$\frac{dP(d_{\mathrm{ext}})}{d\ln d_{\mathrm{ext}}} = \begin{cases} 0 & \text{for } d_{\mathrm{ext}} < b \\ z & \text{for } b < d_{\mathrm{ext}} < a \\ 2z & \text{for } a < d_{\mathrm{ext}} < \sqrt{a^2 + b^2} \end{cases}, \tag{D9}$$

for

$$z = \frac{2}{\pi} \frac{1}{\sqrt{\frac{a^2+b^2}{d_{\mathrm{ext}}^2} - 1}}. \tag{D10}$$

Appendix E: Replicate ice core measurements

The upper 93 m of the RECAP ice core has been measured twice (Figure 10). This means that two parallel sticks have been cut from the core, each of which has been measured on the Copenhagen CFA system. The CFA system was modified slightly between the two measurement campaigns, including changes in the pump and tubing setup, as well as general wear and roughening of the tubing walls. Therefore, the difference between the two measurements most likely reflects the error introduced by the CFA system. For the smaller particles, the replicate values are 12 $\%$ larger than the main. In comparison, for the large particles the replicate measurement has up to 3 times lower values than the main measurement. This is probably because the transport of the large particles from the melt head to the instrument depends more on the specific system setup than the small particle transport.

The difference between the two measurements is used as uncertainty for the Abakus measurements. However, a mininum uncertainty of 12 $\%$ is used, since the crossing of the two curves gives an artificially low differerence.

Appendix F: Coincidence

There is no indication of coincidence in the Abakus. If two small particles coincide in the Abakus detector, their combined shadow will make them look like a larger particle. This effect might skew the Abakus distribution towards showing more large particles. It has previously been shown that the coincidence effect is negligible for concentrations below 240,000 particles/mL (Saey, 1998). The highest dust concentrations measured in the RECAP core were around 220,000 particles/mL. We will therefore test whether there is a coincidence bias in the following way. If the concentration of small particles is C, the concentration of coincidences is proportional to C^2. In an ice core dust sample, we would expect the ratio between small and large particles to be more or less independent of the concentration. We can therefore check for coincidence by comparing the ratio

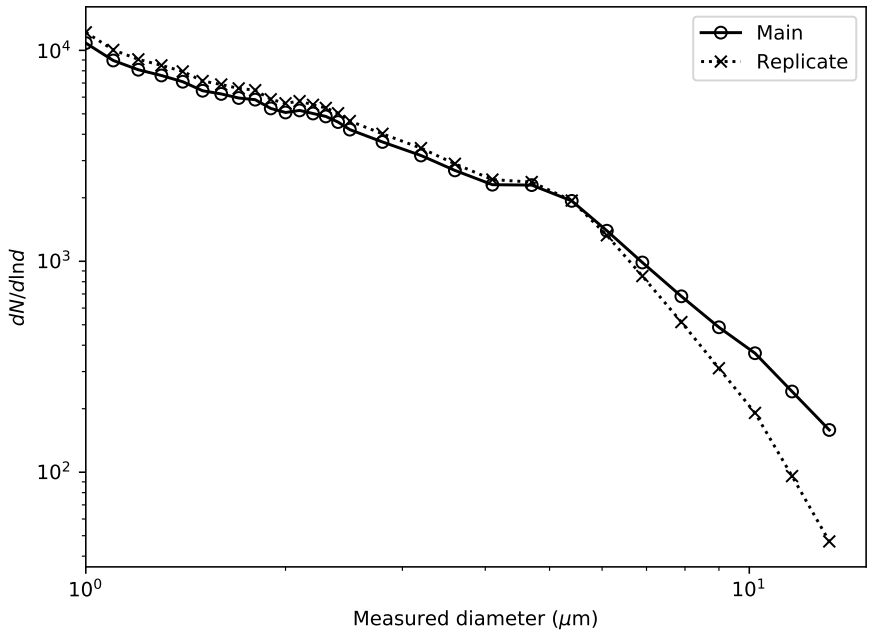

Figure 10. The upper 93 m of the RECAP ice core measured twice with the Abakus.

between small and large particle concentrations for different total dust concentration. In the glacial, for dust concentrations over 200 ppb, there is no correlation between the relative large particle concentration and the total concentration (figure 11). For concentrations smaller than 200, the relative large particle concentration is slightly larger. This could be a climatic signal. We find no significant trend with respect to concentration, suggesting no significant coincidence effect for our measured ice core samples.

Appendix G: Prolate particles

The RECAP samples consist primarily of oblate particles, so the analysis of sections 3.3 and 3.4 have not included prolate particles. The extension to prolate particles is however straight forward, and we show it here for possible future samples dominated by prolates. The aspect ratio of the RECAP samples will now be derived by comparing real Abakus data and modelled Abakus data derived from Coulter Counter data under the assumption that the particles are prolate. Prolate particles are free to rotate in a plane of constant velocity, but cannot rotate out of the plane (Jeffery, 1922). To describe their orientation, define a cartesian coordinate system with z in the flow direction, x in the laser light direction, and origin at the center of the rectangle (Figure 12). If a prolate particle is located at $y = 0$ and $x \neq 0$, its long side will always face the light beam, since its rotation is in the plane orthogonal to the light beam. In the 2D rectangle model (Figure 9), this corresponds to the side a always

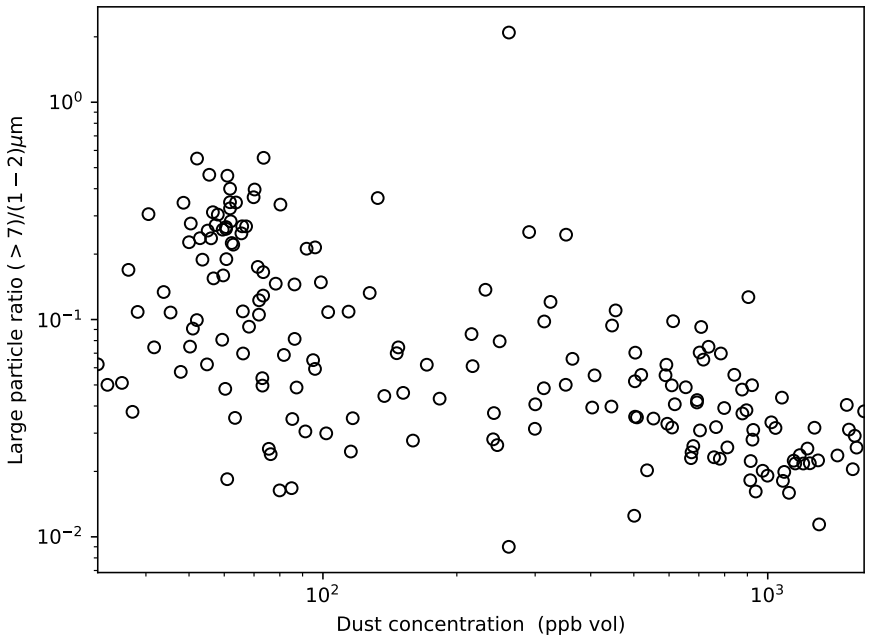

Figure 11. The ratio between small and large particle concentration by volume as a function of total dust concentration. The points are 10 cm sections from 533-554 m depth.

facing the light. This gives a unique d_{ext} for each d_{vol}, and Equation 1 is replaced by

$$\frac{dP(d_{\text{ext}}|d_{\text{vol}})}{d\ln d_{\text{ext}}} = \delta(\ln d_{\text{ext}} - \ln(\alpha d_{\text{vol}})), \tag{G1}$$

where δ is the Dirac delta function and

$$\alpha = \sqrt{\frac{\pi}{4c}}. \tag{G2}$$

This value of α is calculated by letting c be the aspect ratio of the rectangle, d_{ext} the long side and d_{vol} the diameter of a circle with the same radius as the rectangle. In effect, Equation G1 means that the distribution of d_{ext} is equal to the distribution of d_{vol}, just with $d_{\text{ext}} = \alpha d_{\text{vol}}$. If a prolate particle is located at $x = 0$ and $y \neq 0$, all rotation angles relative to the light are equally likely. It can therefore be modelled like the oblates. We assume that all positions in the x, y plane are equally likely. For $x \neq 0$ and $y \neq 0$, $\frac{dP(d_{\text{ext}}|d_{\text{vol}})}{d\ln d_{\text{ext}}}$ is a combination of Equation 1 and G1. The combination of the equations depend on x and y in a non-trivial manner. However, we assume that the aspect ratio derived from the combination will lie between the aspect ratios derived from Equation 1 and G1. To approximate the exact combination, we take the mean of the two distributions. Using Equation 3, modelled Abakus data can be generated from the Coulter Counter data, similar to what we did for the oblate particles. The best correspondence between modelled and real Abakus data is for $c = 0.34 \pm 0.04$ for the glacial and $c = 0.43 \pm 0.08$ for the Holocene. As the correct relative weight of Equation 1 and G1 in $\frac{dP(d_{\text{ext}}|d_{\text{vol}})}{d\ln d_{\text{ext}}}$ is uncertain, an upper bound on the aspect ratio

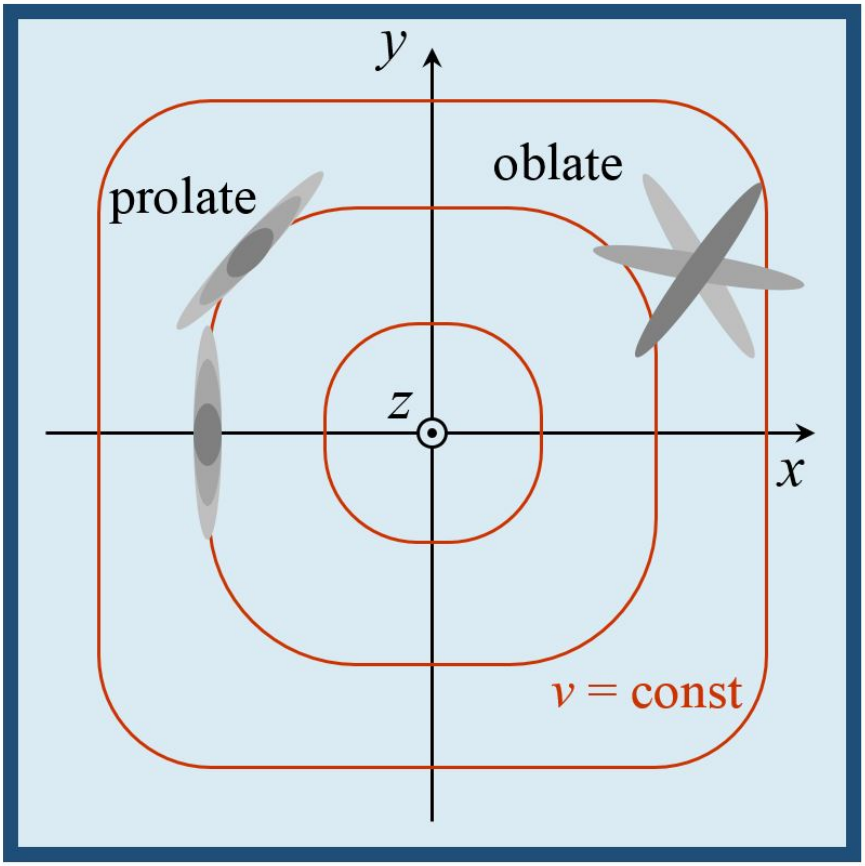

Figure 12. The Abakus flow cell. The flow is in the z direction and the laser beam is in the x direction. The red curves are contours of constant flow velocity. Oblate particles are free to rotate in the x, y plane, while prolates can rotate in a plane of constant flow.

can be calculated by using only Equation G1. This gives $c = 0.37 \pm 0.03$ for the glacial and $c = 0.45 \pm 0.06$ for the Holocene. The uncertainty on c arising from a wrong relative weight of Equation 1 and G1 is therefore smaller than the uncertainty from other sources, and can be neglected. In conclusion, the aspect ratio derived from comparing Abakus to Coulter Counter data is less extreme when prolate rather than oblate particles are assumed.

ADDA simulations of prolate particles can also be used to extract an aspect ratio from the SPES data. This is rather artificial, as the SPES data shows that the particles are oblate. However, we do it to show that adding a fraction of prolates does not change the fitted aspect ratio significantly. As described in section 3.3, the mean optical thickness ρ is calculated as function of extinction cross section σ_{ext} for different aspect ratios c (Figure 13). These curves are interpolated to generate a contour plot of c in $\rho, \sigma_{\text{ext}}$ space. The mean ρ curve is then calculated for the aspect ratios 0.25, 0.33 and 0.50 for prolate particles. By fitting these mean ρ curves to the oblate aspect ratio contour, it is found that they correspond to oblate particles of aspect ratio 0.23, 0.28 and 0.41 respectively. The fit is only performed for σ_{ext} values between the 0.25 and 0.75 quantiles of the SPES data, ie.

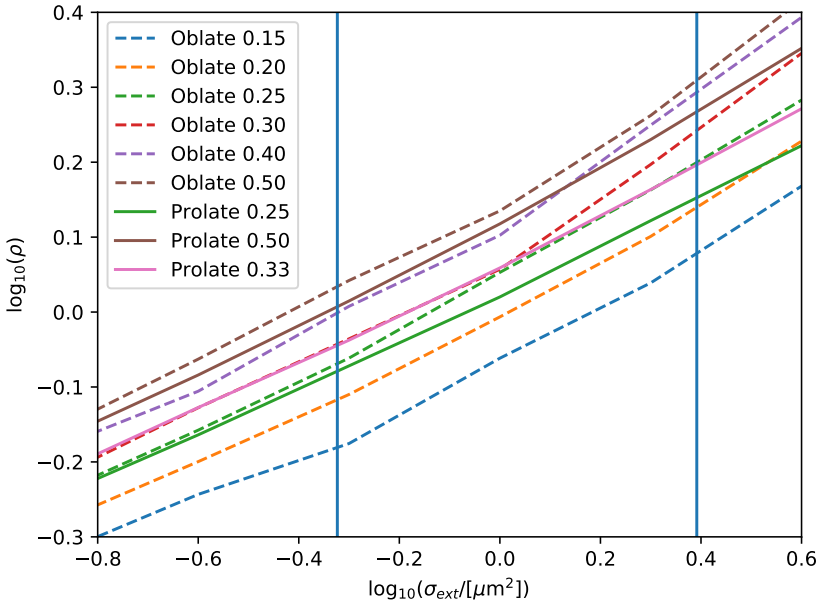

Figure 13. Mean optical thickness curves for oblate and prolate particles for different aspect ratios indicated in the legend.

between the blue lines of Figure 6. By interpolating between the prolate/oblate aspect ratio pairs, it is found that the prolate aspect ratios corresponding to the oblate aspect ratios of 0.33 and 0.39 of the RECAP glacial and Holocene samples are 0.39 and 0.47 respectively (Figure 14). The ADDA simulations therefore predict less extreme aspect ratios for prolates than for oblates, similarly to the Abakus/Coulter Counter comparison. This analysis is however artificial in the sense that the RECAP samples are dominated by oblates and not prolates.

Competing interests. The authors declare that they have no conflict of interest.

Acknowledgements. The RECAP ice coring effort was financed by the Danish Research Council through a Sapere Aude grant, the NSF through the Division of Polar Programs, the Alfred Wegener Institute, and the European Research Council under the European Community's Seventh Framework Programme (FP7/2007-2013) / ERC grant agreement 610055 through the Ice2Ice project. The Centre for Ice and Climate is funded by the Danish National Research Foundation.

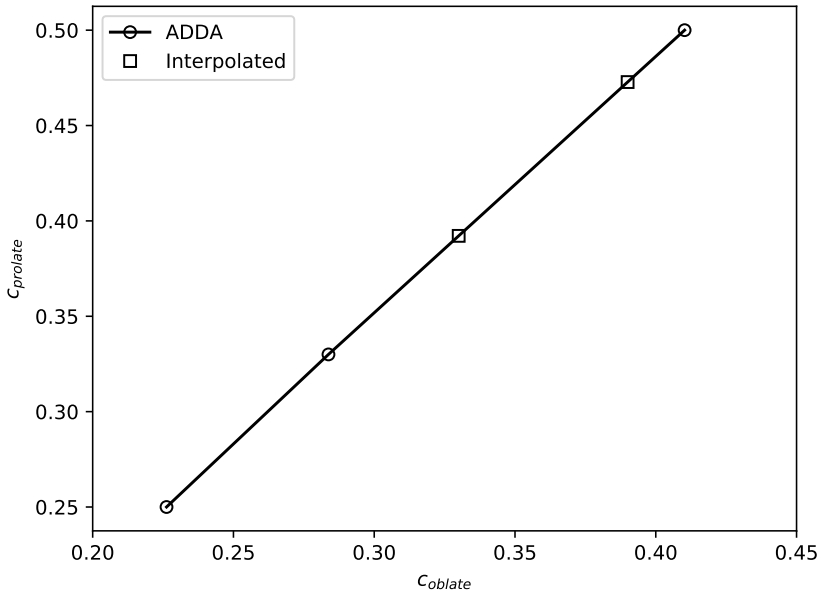

Figure 14. ADDA simulated prolate aspect ratios for the corresponding oblate aspect ratios, derived from Figure 13. The squares are at c_{oblate} values of 0.33 and 0.39, interpolated between the simulated values.

References

Bigler, M., Svensson, A., Kettner, E., Vallelonga, P., Nielsen, M. E., and Steffensen, J. P.: Optimization of high-resolution continuous flow analysis for transient climate signals in ice cores, Environmental Science & Technology, 45, 4483–4489, 2011.

Biscaye, P., Grousset, F., Revel, M., Van der Gaast, S., Zielinski, G., Vaars, A., and Kukla, G.: Asian provenance of glacial dust (stage 2) in the Greenland Ice Sheet Project 2 ice core, Summit, Greenland, Journal of Geophysical Research: Oceans, 102, 26 765–26 781, 1997.

Bory, A. J.-M., Biscaye, P. E., Piotrowski, A. M., and Steffensen, J. P.: Regional variability of ice core dust composition and provenance in Greenland, Geochemistry, Geophysics, Geosystems, 4, doi:10.1029/2003GC000627, 1107, 2003.

Brazitikos, S., Giannopoulos, A., Valettas, P., and Vritsiou, B.: Geometry of Isotropic Convex Bodies:, Mathematical Surveys and Monographs, American Mathematical Society, 2014.

Chỳlek, P. and Klett, J. D.: Extinction cross sections of nonspherical particles in the anomalous diffraction approximation, JOSA A, 8, 274–281, 1991.

Delmonte, B., Petit, J., Andersen, K. K., Basile-Doelsch, I., Maggi, V., and Lipenkov, V. Y.: Dust size evidence for opposite regional atmospheric circulation changes over east Antarctica during the last climatic transition, Climate Dynamics, 23, 427–438, 2004.

Draine, B. T. and Flatau, P. J.: Discrete-dipole approximation for scattering calculations, JOSA A, 11, 1491–1499, 1994.

Grams, G., Blifford Jr, I. H., Gillette, D., and Russell, P.: Complex index of refraction of airborne soil particles, Journal of Applied Meteorology, 13, 459–471, 1974.

Hansson, M. E.: The Renland ice core. A Northern Hemisphere record of aerosol composition over 120,000 years, Tellus B, 46, 390–418, 1994.

Jeffery, G. B.: The motion of ellipsoidal particles immersed in a viscous fluid, in: Proceedings of the royal society of London A: Mathematical, physical and engineering sciences, 715, pp. 161–179, The Royal Society, 1922.

Kaufmann, P. R., Federer, U., Hutterli, M. A., Bigler, M., Schüpbach, S., Ruth, U., Schmitt, J., and Stocker, T. F.: An improved continuous flow analysis system for high-resolution field measurements on ice cores, Environmental science & technology, 42, 8044–8050, 2008.

Knippertz, P. and Stuut, J.-B. W.: On Composition, Morphology, and Size Distribution of Airborn Mineral Dust, in: Mineral Dust, pp. 15–50, Springer, 2014.

Koffman, B. G., Kreutz, K., Breton, D., Kane, E., Winski, D., Birkel, S., Kurbatov, A., and Handley, M.: Centennial-scale variability of the Southern Hemisphere westerly wind belt in the eastern Pacific over the past two millennia, Climate of the Past, 10, 1125–1144, 2014.

Lambert, F., Delmonte, B., Petit, J. R., Bigler, M., Kaufmann, P. R., Hutterli, M. A., Stocker, T. F., Ruth, U., Steffensen, J. P., and Maggi, V.: Dust-climate couplings over the past 800,000 years from the EPICA Dome C ice core, Nature, 452, 616–619, 2008.

Lambert, F., Bigler, M., Steffensen, J. P., Hutterli, M., and Fischer, H.: Centennial mineral dust variability in high-resolution ice core data from Dome C, Antarctica, Climate of the Past, 8, 609–623, doi:10.5194/cp-8-609-2012, 2012.

Lambert, F., Tagliabue, A., Shaffer, G., Lamy, F., Winckler, G., Farias, L., Gallardo, L., Pol-Holz, D., et al.: Dust fluxes and iron fertilization in Holocene and Last Glacial Maximum climates, Geophysical Research Letters, 42, 6014–6023, 2015.

Mahowald, N., Kohfeld, K., Hansson, M., Balkanski, Y., Harrison, S. P., Prentice, I. C., Schulz, M., and Rodhe, H.: Dust sources and deposition during the last glacial maximum and current climate: A comparison of model results with paleodata from ice cores and marine sediments, Journal of Geophysical Research: Atmospheres, 104, 15 895–15 916, 1999.

Potenza, M. A. C., Albani, S., Delmonte, B., Villa, S., Sanvito, T., Paroli, B., Pullia, A., Baccolo, G., Mahowald, N., and Maggi, V.: Shape and size constraints on dust optical properties from the Dome C ice core, Antarctica, Scientific Reports, 6, 28 162 EP –, http://dx.doi.org/10.1038/srep28162, 2016.

Röthlisberger, R., Bigler, M., Hutterli, M., Sommer, S., Stauffer, B., Junghans, H. G., and Wagenbach, D.: Technique for continuous high-resolution analysis of trace substances in firn and ice cores, Environmental Science & Technology, 34, 338–342, 2000.

Royer, A., De Angelis, M., and Petit, J.: A 30000 year record of physical and optical properties of microparticles from an East Antarctic ice core and implications for paleoclimate reconstruction models, Climatic Change, 5, 381–412, 1983.

Ruth, U.: Concentration and size distribution of microparticles in the NGRIP ice core (Central Greenland) during the last glacial period, Ph.D. thesis, University of Bremen, 2002.

Ruth, U., Wagenbach, D., Steffensen, J. P., and Bigler, M.: Continuous record of microparticle concentration and size distribution in the central Greenland NGRIP ice core during the last glacial period, Journal of Geophysical Research: Atmospheres, 108, 2003.

Ruth, U., Barbante, C., Bigler, M., Delmonte, B., Fischer, H., Gabrielli, P., Gaspari, V., Kaufmann, P., Lambert, F., Maggi, V., et al.: Proxies and measurement techniques for mineral dust in Antarctic ice cores, Environmental science & technology, 42, 5675–5681, 2008.

Saey, P.: Diplomarbeit im Studiengang Physik, Master's thesis, Fakultät für Physik und Astronomie, Ruprecht-Karls-Universität Heidelberg, 1998.

Shettle, E. P. and Fenn, R. W.: Models for the aerosols of the lower atmosphere and the effects of humidity variations on their optical properties, Tech. rep., Air Force Geophysics Laboratory Hanscom Air Force Base, Mass.,, USA, 1979.

Sokolik, I., Andronova, A., and Johnson, T. C.: Complex refractive index of atmospheric dust aerosols, Atmospheric Environment. Part A. General Topics, 27, 2495–2502, 1993.

Steffensen, J. P.: The size distribution of microparticles from selected segments of the Greenland Ice Core Project ice core representing different climatic periods, Journal of Geophysical Research: Oceans, 102, 26 755–26 763, 1997.

van de Hulst, H. C.: Light scattering by small particles, Courier Corporation, 1957.

Villa, S., Sanvito, T., Paroli, B., Pullia, A., Delmonte, B., and Potenza, M. A. C.: Measuring shape and size of micrometric particles from the analysis of the forward scattered field, Journal of Applied Physics, 119, 224 901, doi:10.1063/1.4953332, 2016.

Yurkin, M. A. and Hoekstra, A. G.: The discrete-dipole-approximation code ADDA: capabilities and known limitations, Journal of Quantitative Spectroscopy and Radiative Transfer, 112, 2234–2247, 2011.

Chapter 4

Local ice core dust reveals past glacier extent in East Greenland

Renland is a peninsula in the Scoresby Sund area of eastern Greenland (Figure 2.7) with a 600 m thick ice cap that has a surface elevation of 2.3 km. The neighbouring glaciers have large outwash plains, from where large dust storms rise. During the glacial, the Greenland ice sheet and local glaciers advanced and covered almost all land area in the Scoresby Sund area On the Renland ice cap, the 120,000 year long RECAP ice core was drilled in 2015.

The RECAP dust record is almost identical to the central Greenlandic NGRIP core during the glacial (Ruth et al., 2003), where the dust concentration is almost perfectly inversely correlated with temperature. This similarity is broken during the Holocene, where the 700 mg dust per kg ice is more than 10 times larger than in NGRIP. Furthermore, while the particle size distribution has a mode of around 2 μm during glacial, the Holocene mode is around 20 μm. This larger mode together with radiogenic isotope measurements suggest that the Holocene dust particles come from the local Scoresby Sund area, as opposed to the Asian source of glacial dust, similarly to the old Renland ice core from 1988 (Bory et al., 2003a). The large particles appeared after the glacial because the glaciers retreated and exposed the sources. This process happened from from 12.1 ± 0.1 to 9.0 ± 0.1 ka b2k. Similarly, the Eemian had a high large particle concentration that dropped from 116.6 ± 0.7 to 111.1 ± 0.5 ka b2k during the glacier advance.

The timing of the early Holocene dust increase agrees with glacier retreat measurements based on rock exposure dating and radiocarbon dating of sea shells on raised beaches (Sinclair et al., 2016). Even though the large particle concentration is more than 90% lower during the glacial than during the Holocene, the non-zero concentration implies that some ice free area existed during the glacial. It is debated whether Jameson Land east of Renland was ice covered or not during the glacial (Håkansson et al., 2009; Funder et al., 2011), while strong evidence shows that the rest of the Scoresby Sund area was completely ice covered during the glacial (Funder et al., 2011). The local RECAP dust signal prevailing through the glacial supports an ice free Jameson Land.

This is further discussed in the following manuscript, which is intended for submission

to Nature Geoscience.

Local ice core dust reveals past glacier extent in East Greenland

Marius Folden Simonsen[1], Giovanni Baccolo[2], Thomas Blunier[1], Alejandra Borunda[3,4], Barbara Delmonte[2], Aslak Grinsted[1], Helle Astrid Kjær[1], Todd Sowers[6], Anders Svensson[1], Bo Vinther[1], Diana Vladimirova[1], Mai Winstrup[5], and Paul Vallelonga[1]

[1]Centre for Ice and Climate, Niels Bohr Institute, University of Copenhagen, Copenhagen, Denmark
[2]Department of Earth and Environmental Sciences, University Milano-Bicocca, Piazza della Scienza 1, I20126 Milan, Italy
[3]Lamont-Doherty Earth Observatory, Columbia University, Palisades, NY, USA
[4]Department of Earth and Environmental Sciences, Columbia University, New York, NY, USA
[5]Danish Meteorological Institute, Copenhagen, Denmark
[6]Earth and Environmental Systems Institute, Pennsylvania State University, University Park, Pennsylvania 16802, USA

March 22, 2018

Mapping the paleo extent of Greenland glaciers provides tie points for ice sheet models and is important for constraining Greenland's response to climate forcing and contribution to future sea level rise. Here we present a continuous ice core dust record from the Renland ice cap on the east coast of Greenland. During both the Holocene and the previous interglacial period (the Eemian), the ice core dust record is dominated by coarse particles from local East Greenlandic sources, whereas the dust from the last glacial period consists mainly of smaller particles from remote sources. The fraction of coarse particles in the record is a proxy for glacier extent in the Scoresbysund area, as the reduction of coarse particles during the glacial indicates that most local dust sources were ice covered. At the onset of the last glacial period, local glaciers advanced from 116.6 ± 0.7 to 111.1 ± 0.5 ka before present whereas they retreated from 12.1 ± 0.1 to 9.0 ± 0.1 ka before present. The constant low concentration of large particles during the glacial shows that some local dust sources remained and were unaffected by stadial/interstadial climate variations.

[1] Understanding the relationship between Greenland ice sheet evolution and climate forcing is necessary to accurately forecast the future of the Greenland ice sheet. The climate history of Greenland has been accurately determined from ice cores using temperature proxies based on borehole temperatures, isotopes of water molecules and atmospheric gases [1–3]. Even though ice cores are geographical point measurements, they are representative of the area of provenance of the air, water and aerosols in the ice, which can have regional or even hemispheric extent.

In contrast, measurements of past ice sheet extent are typically limited to the location of the measurement [4, 5]. The extent of past ice sheets are constrained by dating of moraines and subglacial rocks by cosmogenic surface-exposure methods and by radiocarbon dating of sea shells on raised beaches [6]. Since Eastern Greenland is large and inaccessible, few measurements are available for this area.

The most important sources of mineral dust in Central Greenland ice cores are Central Asian deserts [7–9]. The dust flux at the Central Greenlandic GRIP site is around 7-11 mg m^{-2} yr^{-1} during the Holocene [10, 11]. During the last glacial period, the ice core dust concentration was 10-100 times larger than in the Holocene due to enhanced continental aridity, increased wind strength and higher atmospheric particle lifetime [10, 12, 13].

Here we study the RECAP ice core from the Renland ice cap in the Scoresby Sund area of East Greenland which has a surface elevation of 2,300 m. The core is drilled to bedrock, and contains a stratified climate record back to 120,000 years before present (see Methods for time scale). During the Holocene and the previous interglacial, the Eemian, we find a strong contribution to the dust record from local sources in the Scoresby Sund region, while the glacial is dominated by Central Asian sources. The reduction of local dust during the glacial is due to the sources being covered by glaciers. We determined the timing of glacial advance at the onset of the last glacial period to be from 116.6±0.7 to 111.1 ± 0.5 ka before present and the retreat at the end of the glacial from 12.1±0.1 to 9.0±0.1 ka before present. This agrees with other geological reconstructions of glacier extent for both the Holocene [14, 15] and the Eemian [4, 16].

1 Dust record

During the last glacial period, the RECAP dust concentration varies by a factor 10-100 between mild interstadial and cold stadial periods (Figure 1). These variations are a general feature of Greenlandic dust profiles and are also present and almost identical in the NGRIP ice core from central Greenland [12] (Figure 1). This can be quantified by the 95% correlation between the RECAP and NGRIP glacial dust records that we observe for the log-scaled 100 year averaged data sets. The NGRIP dust concentration is 1.72 ± 0.03 times larger than the RECAP dust concentration. If the ratio between accumulation rates at NGRIP and RECAP was the same during the glacial as it is today, 19 [17] versus 45 cm ice equivalent annually, partial dry deposition could explain the difference between NGRIP and RECAP dust concentration without assuming different atmospheric dust concentrations at the two sites. The volume mode of the glacial dust size distribution is 2.21 ± 0.02 μm for RECAP and 1.73 μm

[1] FiXme Note: Use b2k instead of BP

for NGRIP (Figure 2) [12]. The close similarity between both concentration time series and size distributions indicate that the dust deposition at the two sites are governed by the same physical mechanisms. Based on minerology and geochemical fingerprinting, Central Greenlandic glacial GRIP and GISP2 dust was found to originate from the East Asian deserts [7, 8]. Bory (2003) has identified similar geochemical signatures for 17th-18th century dust from Central and South Greenland (Figure 3), which combined with the strong concentration time series correlation, points to a common source of dust during the glacial for the Greenland ice sheet.

Interglacial dust concentrations at RECAP are disproportionately greater than at central Greenland ice cores sites, suggesting a significant local dust input that is absent both during stadial and interstadial parts of the glacial. In the Holocene, the RECAP dust concentration is 750 μg dust per kg ice, as compared to 66 μg/kg in early Holocene NGRIP. This contrasts the glacial, where there is 63% more dust in NGRIP than in RECAP. During the Holocene there must therefore be an additional dust source for RECAP that does not contribute to Central Greenland. The volume mode of the Holocene size distribution is 18.9 $\pm$ 0.6 μm for RECAP and 1.47 μm for NGRIP (Figure 2). The larger mode of the RECAP Holocene dust suggests that the source of the particles is local, as particles of this size only reside in the atmosphere for a few hours [18].

While the RECAP glacial dust size distribution is concave with power law tails, the Holocene size distribution is bimodal, indicating contributions from two distinct sources. The small mode distribution has a mode of 1.88 $\pm$ 0.04 μm (see Methods for details on separating the two distributions), suggesting a remote origin. In the GRIP ice core [10], where both the Holocene and glacial dust has a remote origin, the ratio between the Holocene and glacial dust concentrations range between 33 and 230. In RECAP, the concentration ratio between the glacial and small mode Holocene dust is 87$\pm$4. The mode and concentration of the small mode Holocene dust suggest that it has a remote origin similar to the glacial RECAP dust and Holocene dust from Central Greenlandic ice cores.

In the Eemian, the large particle concentration (8.13 to 10.5 μm diameter) in RECAP is 136 μg/kg, as compared to 72 μg/kg and 10 μg/kg in the Holocene and glacial, respectively (Figure 4). This suggests that the local Holocene source was also active and maybe even stronger during the previous interglacial.

In the glacial, the total dust concentration anticorrelates with temperature with a factor 28 difference in concentration between NGRIP temperatures of -50°C and -35‰ (Figure 8). The large particle concentration only varies by a factor 2.2 over this interval. Assuming dry deposition [18] of the large particles, this small variability can be explained by an accumulation difference between stadials and interstadials of a factor 2 like in the NEEM [19] and NGRIP [20] ice cores. As particles of this size has an atmospheric lifetime of around a day [18], they must be of local origin like the interglacial large particles. Since the large particle flux is constant over stadial/interstadial cycles, the strength of the local dust sources does not vary significantly from stadials to interstadials.

2 Source regions

To determine the provenance of coarse RECAP dust, we have measured the strontium and neodymium isotopes of particles larger than 5 μm for three

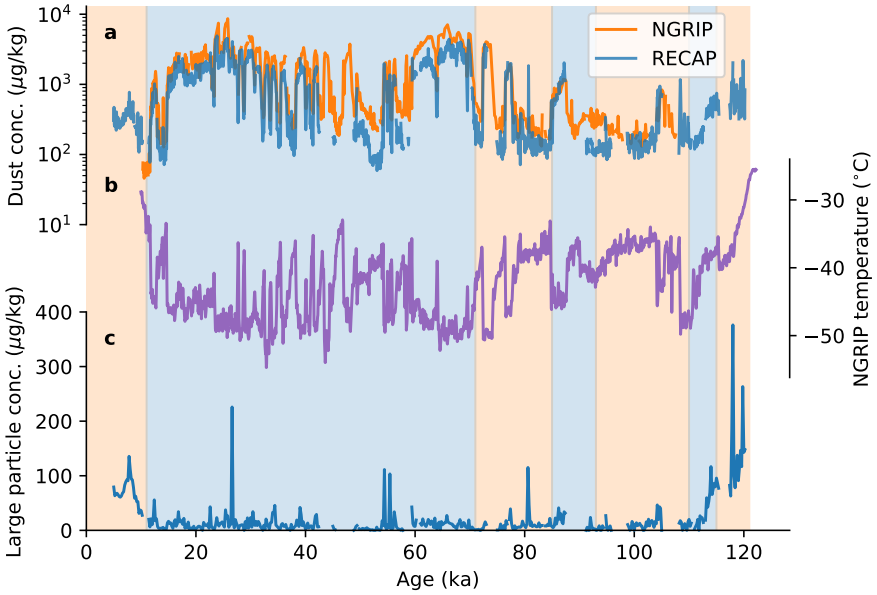

Figure 1: **Dust concentration.** a: The total concentration of dust particles in the size range 1.25 to 10.5 μm in the RECAP and NGRIP ice cores over a full glacial cycle on 50 year resolution. b: NGRIP temperature [25]. c: The ratio between the small (1.25-2.9 μm) and large (8.13-10.5 μm) particle concentrations on 200 year resolution. The background shows warm periods or periods of glacier retreat (orange) and cold periods or periods of glacier advance (blue) in the Scoresby Sund region [5, 16].

Holocene time periods (Figure 3). Their $^{87}Sr/^{86}Sr$ values are similar to those of the old Renland core, and support the proposal of a radiogenic signature for Greenlandic source rock typical of ice-free coastal regions [9]. In comparison, dust from Central Greenlandic ice cores are consistent with central Asian dust sources [9, 21]. Present day atmospheric dust models disagree on the amount of Icelandic dust deposited on the Greenland ice sheet. The FLEXPART model apportioned up to 1,000 mg m^{-2} yr^{-}1 of Icelandic dust deposited on the eastern part of the Greenland ice sheet [22], which would completely dominate the Asian dust flux found in the GRIP ice core. On the contrary, Baddock et al. (2017) [23] finds that Icelandic dust is limited to the low-altitude coastal regions of Greenland. Icelandic dust has low $^{87}Sr/^{86}Sr$ and high ϵNd values [24], and can therefore not contribute significantly in RECAP, consistent with the findings of Baddock et al. [23]. With an average annual snow accumulation rate of 437 kg m^{-2} yr^{-1} over the last 4,000 years, the average RECAP Holocene dust flux is 330 mg m^{-2} yr^{-1}. The 1,000 mg m^{-2} yr^{-1} of Icelandic dust proposed by the FLEXPART model [22] is therefore not observed in RECAP.

We exclude West Greenland as a plausible dust source for RECAP ice, as the atmospheric lifetime of only a few hours for large dust particles [18] does not

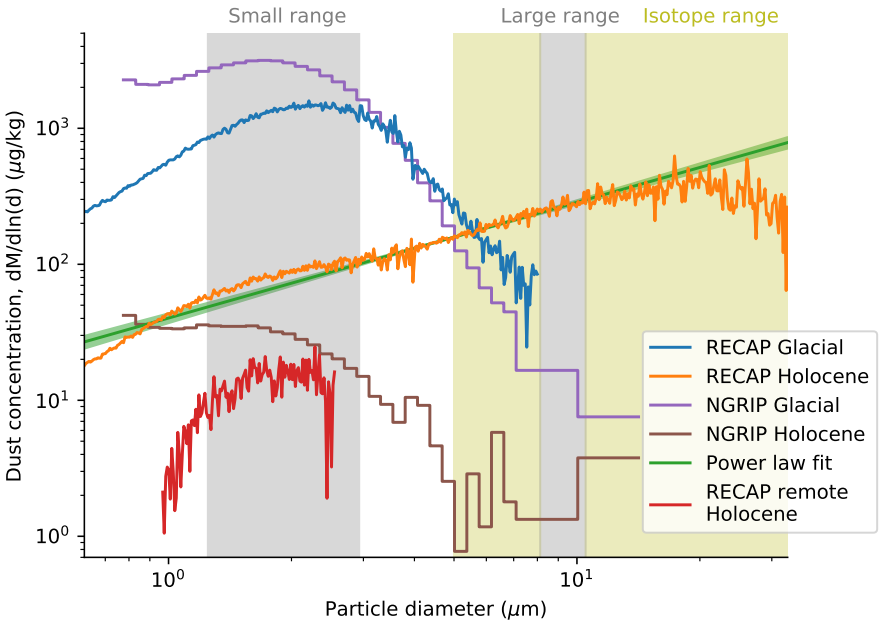

Figure 2: **Dust size distribution.** RECAP dust size distribution measured by Coulter Counter. The probability density function for particle mass, $\frac{dM}{d\ln(d)}$, is defined such that $\int_{d_1}^{d_2} \frac{dM}{d\ln(d)} d\ln(d)$ gives the total dust mass of particles in the diameter range $[d_1, d_2]$. The glacial data cover the time period $(12,800 - 33,900) \pm 500$ years before present, while the Holocene covers selected samples from the period $(356 \pm 2 - 4,010 \pm 50)$ years before present. A power law is fitted to the Holocene data from 4 to 6 μm, and the excess of Holocene dust relative to the power law fit is in red. It is interpreted as the size distribution of the remote Holocene dust. The grey bars show the size ranges used for the small and large particle time series in Figure 4. The yellow area shows the size range of particles used for the Sr and Nd isotope measurements.

allow them to be transported such long distances and there is no evidence of such dust in central and southern Greenland ice cores. The only possible source is therefore East Greenland. Many of the glaciers around Renland form outwash plains between their termination and the sea (Figure 3). Generally, outwash plains are strong dust sources in the high latitudes [27]. The Worldview satellite has captured a dust storm rising from the glacial outwash plain in Schuchert Dal, proving that sources of atmospheric dust exist closer than 100 km to the RECAP drill site (Figure 9). Satellite reanalysis data (Figure 3) shows that the local dust plumes originating from the Scoresby Sund area extend several hundred kilometers away from the source.

Even though there are other dust sources on the east coast of Greenland, the proximity and strength of the sources in the Scoresby Sund area suggest that they are the main contributors to the RECAP dust today. East Greenland has not previously been recognised as a significant high latitude dust source [27].

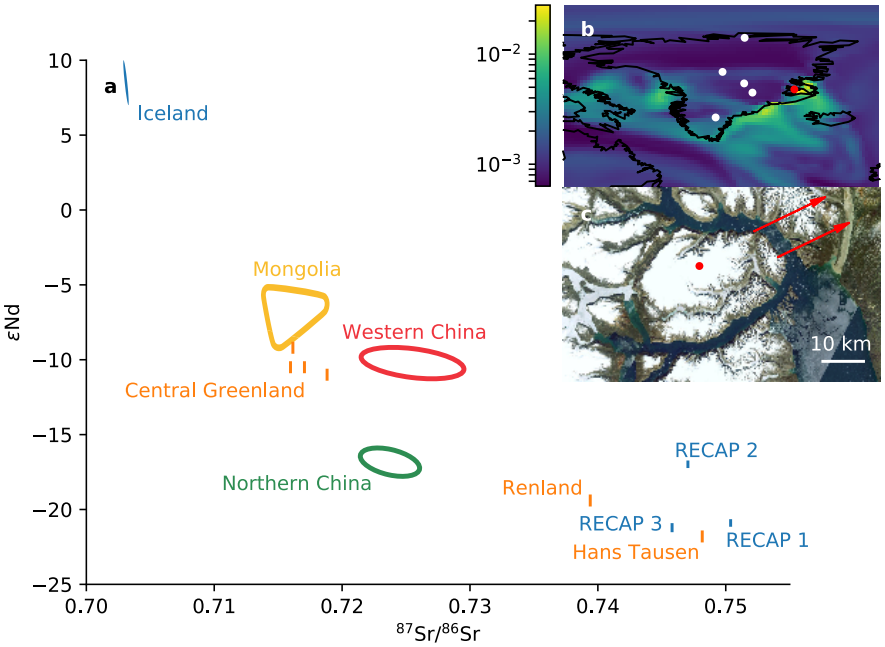

Figure 3: **Dust sources.** a: Strontium and neodymium isotope ratios from RECAP compared to possible source regions in Iceland [24] and Asia, the coastal Renland and Hans Tausen ice cores and the four Central Greenlandic ice cores DYE-3, NGRIP, GRIP and Site A (orange bars) [9]. The samples 1,2,3 cover approximately 4-5, 5-6 and 6-7 ka before present (Supplement D), while Bory et al.'s dust is from the 17th-18th century. b: CAMS reanalysis map of total aerosol optical depth from April 27 2016 [26]. See Methods for more details. The white dots are the locations of ice core drill sites, from north to south, Hans Tausen, NGRIP, GRIP, Site A and DYE-3. c: Renland. the arrows point to, from north to south, Schuchert Dal and Gurreholm Dal. The red dot is the RECAP drill site in both b and c. The Renland core was drilled 2 km from the RECAP site.

However, our results show that it is the dominating source for dust on the Renland Ice Cap and probably contributes significantly to the dust concentration in the East Greenlandic cryosphere. A Holocene dust concentration of 750 μg/kg as found in RECAP is equivalent to an albedo reduction of around 1% [28, 29]. As the surface of the Renland Ice Cap lies 2,300 m above sea level, only a small fraction of the dust that is uplifted from the surrounding outwash plains reaches it. It is therefore likely that the lower lying glaciers in the area receive more dust than the Renland Ice Cap, significantly lowering their albedo.

3 Past glacier extent of the Scoresby Sund area

A ramp fit to the ratio between small and large particles at the glacial-Holocene transition shows that the increase in local dust sources in the Scoresby Sund

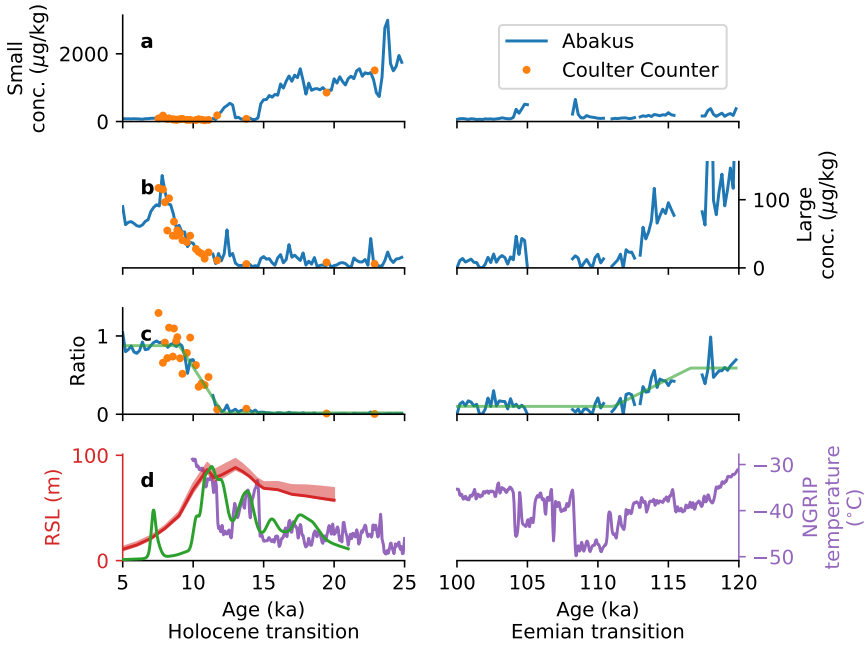

Figure 4: **Glacial-interglacial transitions.** The small (1.25-2.9 μm) (a) and large (8.13-10.5 μm) (b) particle concentration and the ratio (c) between them. The blue line is measured a 200 year average of the Abakus data, the orange dots are Coulter Counter data, and the green line is a ramp fit to the Abakus data (see Methods for instrument description). (d): The purple line is NGRIP temperature, the red is relative sea level in Scoresby Sund adapted from [15]. The green is a glacier retreat index for the Scoresby Sund region based on ^{10}Be measurements adapted from [14]. It shows the density of measurements of when rocks where exposed for the first time.

area occured from 12.1 ± 0.2 to 9.0 ± 0.1 years before present (Figure 4). This change is almost two orders of magnitude slower than the 40-100 year transitions between stadial and interstadial dust concentrations [30], supporting that the RECAP post glacial large particle increase is governed by a different physical mechanism than the stadial-interstadial transitions. The timing of exposure of coarse dust sources agrees with Scoresby Sund region glacier retreat estimates based on radiocarbon dating of marine shells on raised beaches and cosmogenic surface-exposure dating of rocks [6, 14]. The glacier retreat index (Figure 4) [14] starts increasing around 20 ka before present which is 8 ka earlier than our measurements indicate. However, exposure dates are typically measured on the valley sides which were exposed before the outwash plain [31]. The maximum glacier retreat index around 11 ka before present coincides well with our measurements. Gurreholm Dal glacier retreated from 13.0 to 10.6 years before present [31], and Schuchert Dal reached its present day extent around 9.6 years before present (Figure 9) [32]. Exposure of outwash plains was further enhanced by decreasing relative sea level from 80 ± 10 to 40 ± 5 m above the

present level from 11.0 to 9.0 ka before present [15]. As most of Schuchert Dal is less than 50 m above sea level, the relative sea level lowering during the deglaciation must have had a significant effect on the area of the outwash plain.

After the Eemian, the glaciers around Scoresby Sund advanced and covered most of the dust source areas. The RECAP dust record shows that most local dust sources became extinct from 116.6 ± 0.7 to 111.1 ± 0.5 ka before present. This coincides with the glacier advance from 115 ka in Scoresby Sund (Figure 1). However, the glacier retreats that followed over the next 35 ka did not give rise to an increased large particle concentration in RECAP. Their magnitude can therefore not have been large enough to expose the outwash plains of the Holocene and Eemian.

Even though the large particle concentration dropped by more than 90% after the Eemian, the remaining 10 μg/kg indicates that some local dust sources existed throughout the glacial. While almost all of East Greenland was covered by ice during the last glacial maximum [4], it is still disputed whether Jameson Land 50 km east of Renland was ice free or not. Young ^{10}Be ages indicate that it was ice covered [33], while lack of glacial erosion younger than the previous glacial (Saalian) indicates that it was ice free [4,34,35]. As all other dust sources were most likely covered by ice, the RECAP dust record supports that at least parts of Jameson Land were ice free. The lack of variability from stadials to interstadials shows that rapid climate oscillations did not have a significant impact on the activity of local dust sources.

4 Methods

The RECAP dust record was measured using an Abakus laser particle sensor (Klotz GmbH, Germany) connected to an ice core melting continuous flow analysis system [36]. The Abakus measures particle concentration as a function of size. The size bins are calibrated by comparing to Coulter Counter data [37], and cover the range 0.64 - 9.6 μm. The depth resolution of the Abakus measurements is 0.5 cm. With an annual snow accumulation rate of 40 cm, this gives sub annual resolution down to 4,000 years before present. However, due to extreme ice sheet thinning the layer thickness diminishes down through the core, so in the glacial ice, 1 cm corresponds to 100 years. The two categories "small" and "large" are used for particles in the range 1.25-2.9 μm and 8.13-10.5 μm. These ranges give the best separation between small and large particles, since the Abakus measures particles between 1.25 and 10.5 μm.

All ages are measured relative to 2000 CE, and the conversion from depth to age follows the RECAP time scale.

To separate the local and remote contributions to the Holocene size distributions, we assume that the size distribution of the local dust has power law tails like the glacial dust. The lower tail is determined by fitting a power law to the Holocene size distribution between 4 and 6 μm. The difference between the data and the power law tail is interpreted as the long-range dust size distribution. The ratio between the small mode Holocene dust concentration and the glacial dust concentration is calculated as a ratio between the maximum values of the two distributions. First a parabola was fitted to the two distributions, and then the ratio between the maxima of the two fitted parabolas was used as the concentration ratio.

To calibrate the Abakus data, parallel ice sticks 55 cm long were measured Coulter Counter at the University of Milano-Biccocca Ice lab. The samples were decontaminated by washing the outer surfaces three times with ultra pure water. They were measured both with a 100 μm and a 30 μm aperture for accurate size determination of both large and small particles.

The Strontium and Neodymium isotopes were measured on XX μg samples with blanks of XX [2] by TIMS.

Figure 3 c and Figure 9 are from Google Earth Pro V 7.3.0.3832. Figure 3 c is centered on 71 ° 15' 11.62"N, 26 ° 26 08' 28.86"W with an eye altitude of 156.85 km. It is a composite of summer pictures from 2015. Copyright: The US Geological Survey. Figure 9 is centered on 71 ° 16' 57.18"N, 24 ° 38' 19.25"W, with an eye altitude of 8.95 km, taken August 12 2012. Copyright: DigitalGlobe.

The reanalysis data (Figure 3 b) is from the Copernicus Atmosphere Monitoring Service Near Real Time model [26]. We have used the 3 hour prediction of the 'Dust Aerosol Optical Depth at 550 nm' product. The data is from April 27 2016, 00:00 + the 3 hour prediction.

5 References

References

[1] Dorte Dahl-Jensen, Klaus Mosegaard, Niels Gundestrup, Gary D Clow, Sigfus J Johnsen, Aksel W Hansen, and Niels Balling. Past temperatures directly from the greenland ice sheet. *Science*, 282(5387):268–271, 1998.

[2] Christo Buizert, Vasileios Gkinis, Jeffrey P Severinghaus, Feng He, Benoit S Lecavalier, Philippe Kindler, Markus Leuenberger, Anders E Carlson, Bo Vinther, Valérie Masson-Delmotte, et al. Greenland temperature response to climate forcing during the last deglaciation. *Science*, 345(6201):1177–1180, 2014.

[3] Bo Møllesøe Vinther, Susanne Lilja Buchardt, Henrik Brink Clausen, Dorthe Dahl-Jensen, Sigfus Johann Johnsen, DA Fisher, RM Koerner, D Raynaud, V Lipenkov, KK Andersen, et al. Holocene thinning of the Greenland ice sheet. *Nature*, 461(7262):385–388, 2009.

[4] Svend Funder, K Kjellerup Kjeldsen, Kurt Henrik Kjær, and CÓ Cofaigh. The Greenland ice sheet during the past 300,000 years: A review. *Developments in Quaternary Science*, 15:699–713, 2011.

[5] Richard B Alley, John Thomas Andrews, Julia Brigham-Grette, GKC Clarke, Kurt M Cuffey, JJ Fitzpatrick, S Funder, SJ Marshall, GH Miller, JX Mitrovica, et al. History of the greenland ice sheet: paleoclimatic insights. *Quaternary Science Reviews*, 29(15):1728–1756, 2010.

[6] Meredith A Kelly and Thomas V Lowell. Fluctuations of local glaciers in Greenland during latest Pleistocene and Holocene time. *Quaternary Science Reviews*, 28(21):2088–2106, 2009.

[2] FiXme Note: Ale?

[7] PE Biscaye, FE Grousset, M Revel, S Van der Gaast, GA Zielinski, A Vaars, and G Kukla. Asian provenance of glacial dust (stage 2) in the Greenland Ice Sheet Project 2 ice core, Summit, Greenland. *Journal of Geophysical Research: Oceans*, 102(C12):26765–26781, 1997.

[8] Anders Svensson, Pierre E Biscaye, and Francis E Grousset. Characterization of late glacial continental dust in the Greenland Ice Core Project ice core. *Journal of Geophysical Research: Atmospheres*, 105(D4):4637–4656, 2000.

[9] A. J.-M. Bory, P. E. Biscaye, A. M. Piotrowski, and J. P. Steffensen. Regional variability of ice core dust composition and provenance in Greenland. *Geochemistry, Geophysics, Geosystems*, 4(12), 2003. 1107.

[10] Jørgen Peder Steffensen. The size distribution of microparticles from selected segments of the Greenland Ice Core Project ice core representing different climatic periods. *Journal of Geophysical Research: Oceans*, 102(C12):26755–26763, 1997.

[11] SJ Johnsen, Henrik B Clausen, Willi Dansgaard, K Fuhrer, N Gundestrup, Claus Uffe Hammer, Pl Iversen, J Jouzel, B Stauffer, et al. Irregular glacial interstadials recorded in a new Greenland ice core. *Nature*, 359(6393):311–313, 1992.

[12] Urs Ruth, Dietmar Wagenbach, Jørgen P Steffensen, and Matthias Bigler. Continuous record of microparticle concentration and size distribution in the central Greenland NGRIP ice core during the last glacial period. *Journal of Geophysical Research: Atmospheres*, 108(D3), 2003.

[13] Natalie Mahowald, Karen Kohfeld, Margaret Hansson, Yves Balkanski, Sandy P Harrison, I Colin Prentice, Michael Schulz, and Henning Rodhe. Dust sources and deposition during the last glacial maximum and current climate: A comparison of model results with paleodata from ice cores and marine sediments. *Journal of Geophysical Research: Atmospheres*, 104(D13):15895–15916, 1999.

[14] G Sinclair, AE Carlson, AC Mix, BS Lecavalier, G Milne, A Mathias, C Buizert, and R DeConto. Diachronous retreat of the Greenland ice sheet during the last deglaciation. *Quaternary Science Reviews*, 145:243–258, 2016.

[15] Benoit S Lecavalier, Glenn A Milne, Matthew JR Simpson, Leanne Wake, Philippe Huybrechts, Lev Tarasov, Kristian K Kjeldsen, Svend Funder, Antony J Long, Sarah Woodroffe, et al. A model of Greenland ice sheet deglaciation constrained by observations of relative sea level and ice extent. *Quaternary Science Reviews*, 102:54–84, 2014.

[16] Svend Funder, Christian Hjort, Jon Y Landvik, Seung-Il Nam, Niels Reeh, and Ruediger Stein. History of a stable ice margin—East Greenland during the middle and upper Pleistocene. *Quaternary Science Reviews*, 17(1-3):77–123, 1998.

[17] Katrine K Andersen, N Azuma, J-M Barnola, Matthias Bigler, P Biscaye, N Caillon, J Chappellaz, Henrik Brink Clausen, Dorthe Dahl-Jensen, Hubertus Fischer, et al. High-resolution record of northern hemisphere climate extending into the last interglacial period. *Nature*, 431(7005):147–151, 2004.

[18] Ina Tegen and Inez Fung. Modeling of mineral dust in the atmosphere: Sources, transport, and optical thickness. *Journal of Geophysical Research: Atmospheres*, 99(D11):22897–22914, 1994.

[19] Sune Olander Rasmussen, PM Abbott, Thomas Blunier, AJ Bourne, E Brook, Susanne Lilja Buchardt, Christo Buizert, J Chappellaz, Henrik Brink Clausen, E Cook, et al. A first chronology for the north greenland eemian ice drilling (neem) ice core. *Climate of the Past*, 9(6):2713–2730, 2013.

[20] M Guillevic, L Bazin, A Landais, Philippe Kindler, A Orsi, V Masson-Delmotte, T Blunier, SL Buchardt, E Capron, Markus Leuenberger, et al. Spatial gradients of temperature, accumulation and [delta] 18o-ice in greenland over a series of dansgaard-oeschger events. *Climate of the Past*, 9(3):1029, 2013.

[21] AJ-M Bory, Pierre E Biscaye, Anders Svensson, and Francis E Grousset. Seasonal variability in the origin of recent atmospheric mineral dust at NorthGRIP, Greenland. *Earth and Planetary Science Letters*, 196(3):123–134, 2002.

[22] Christine D Groot Zwaaftink, Ólafur Arnalds, Pavla Dagsson-Waldhauserova, Sabine Eckhardt, Joseph M Prospero, and Andreas Stohl. Temporal and spatial variability of Icelandic dust emissions and atmospheric transport. *Atmospheric Chemistry and Physics*, 17(17):10865–10878, 2017.

[23] Matthew C. Baddock, Tom Mockford, Joanna E. Bullard, and Throstur Thorsteinsson. Pathways of high-latitude dust in the North Atlantic. *Earth and Planetary Science Letters*, 459:170 – 182, 2017.

[24] Oliver Shorttle, John Maclennan, and Alexander M Piotrowski. Geochemical provincialism in the Iceland plume. *Geochimica et Cosmochimica Acta*, 122:363–397, 2013.

[25] Philippe Kindler, M Guillevic, M Baumgartner, Jakob Schwander, A Landais, and Markus Leuenberger. Temperature reconstruction from 10 to 120 kyr b2k from the ngrip ice core. *Climate of the Past*, 10(2):887–902, 2014.

[26] V. Huijnen, H.J. Eskes, A. Wagner, M. Schulz, Y. Christophe, M. Ramonet, S. Basart, A. Benedictow, A.-M. Blechschmidt, S. Chabrillat, H. Clark, E. Cuevas, H. Flentje, K.M. Hansen, U. Im, J. Kapsomenakis, B. Langerock, A. Richter, N. Sudarchikova, V. Thouret, T. Warneke, and C. Zerefos. Validation report of the cams near-real-time global atmospheric composition service. system evolution and performance statistics; status up to 1 june 2016. Technical Report CAMS84_2015SC1_D.84.1.4_2016Q3_201609, Copernicus Atmosphere Monitoring Service (CAMS), September 2016.

[27] Joanna E Bullard, Matthew Baddock, Tom Bradwell, John Crusius, Eleanor Darlington, Diego Gaiero, Santiago Gasso, Gudrun Gisladottir, Richard Hodgkins, Robert McCulloch, et al. High-latitude dust in the Earth system. *Reviews of Geophysics*, 54(2):447–485, 2016.

[28] Cheng Dang, Richard E Brandt, and Stephen G Warren. Parameterizations for narrowband and broadband albedo of pure snow and snow containing mineral dust and black carbon. *Journal of Geophysical Research: Atmospheres*, 120(11):5446–5468, 2015.

[29] Matteo Willeit and Andrey Ganopolski. The importance of snow albedo for ice sheet evolution over the last glacial cycle. In *Climate of the Past Discussions*, 2017.

[30] Jørgen Peder Steffensen, Katrine K Andersen, Matthias Bigler, Henrik B Clausen, Dorthe Dahl-Jensen, Hubertus Fischer, Kumiko Goto-Azuma, Margareta Hansson, Sigfús J Johnsen, Jean Jouzel, et al. High-resolution Greenland ice core data show abrupt climate change happens in few years. *Science*, 321(5889):680–684, 2008.

[31] Meredith A Kelly, Thomas V Lowell, Brenda L Hall, Joerg M Schaefer, Robert C Finkel, Brent M Goehring, Richard B Alley, and George H Denton. A 10 Be chronology of lateglacial and Holocene mountain glaciation in the Scoresby Sund Region, East Greenland: implications for seasonality during lateglacial time. *Quaternary Science Reviews*, 27(25):2273–2282, 2008.

[32] Brenda L Hall, Carlo Baroni, and George H Denton. The most extensive Holocene advance in the Stauning Alper, East Greenland, occurred in the little ice age. *Polar Research*, 27(2):128–134, 2008.

[33] Lena Håkansson, Helena Alexanderson, Christian Hjort, Per Möller, Jason P Briner, Ala Aldahan, and Göran Possnert. Late pleistocene glacial history of jameson land, central east greenland, derived from cosmogenic 10be and 26al exposure dating. *Boreas*, 38(2):244–260, 2009.

[34] Per Möller, Christian Hjort, Lena Adrielsson, and Otto Salvigsen. Glacial history of interior jameson land, east greenland. *Boreas*, 23(4):320–348, 1994.

[35] S Funder. Ice-age plant refugia in east greenland. *Palaeogeography, Palaeoclimatology, Palaeoecology*, 28:279–295, 1979.

[36] Matthias Bigler, Anders Svensson, Ernesto Kettner, Paul Vallelonga, Maibritt E Nielsen, and Jørgen Peder Steffensen. Optimization of high-resolution continuous flow analysis for transient climate signals in ice cores. *Environmental Science & Technology*, 45(10):4483–4489, 2011.

[37] M. F. Simonsen, L. Cremonesi, G. Baccolo, S. Bosch, B. Delmonte, T. Erhardt, H. A. Kjær, M. Potenza, A. Svensson, and P. Vallelonga. Particle shape accounts for instrumental discrepancy in ice core dust size distributions. *Climate of the Past Discussions*, 2017:1–19, 2017.

[38] Mai Winstrup, AM Svensson, Sune Olander Rasmussen, Ole Winther, EJ Steig, and AE Axelrod. An automated approach for annual layer counting in ice cores. *Climate of the Past*, 8(6):1881–1895, 2012.

[39] Mai Winstrup. A hidden markov model approach to infer timescales for high-resolution climate archives. In *AAAI*, pages 4053–4061, 2016.

[40] Bo Møllesøe Vinther, Henrik Brink Clausen, DA Fisher, RM Koerner, Sigfus Johann Johnsen, Katrine Krogh Andersen, Dorthe Dahl-Jensen, Sune Olander Rasmussen, Jørgen Peder Steffensen, and AM Svensson. Synchronizing ice cores from the renland and agassiz ice caps to the greenland ice core chronology. *Journal of Geophysical Research: Atmospheres*, 113(D8), 2008.

[41] Sune O Rasmussen, Matthias Bigler, Simon P Blockley, Thomas Blunier, Susanne L Buchardt, Henrik B Clausen, Ivana Cvijanovic, Dorthe Dahl-Jensen, Sigfus J Johnsen, Hubertus Fischer, et al. A stratigraphic framework for abrupt climatic changes during the last glacial period based on three synchronized greenland ice-core records: refining and extending the intimate event stratigraphy. *Quaternary Science Reviews*, 106:14–28, 2014.

[42] Matthias Baumgartner, Philippe Kindler, Olivier Eicher, G Floch, Adrian Schilt, Jakob Schwander, Renato Spahni, E Capron, J Chappellaz, Markus Leuenberger, et al. Ngrip ch 4 concentration from 120 to 10 kyr before present and its relation to a δ 15 n temperature reconstruction from the same ice core. *Climate of the Past*, 10(2):903–920, 2014.

[43] E Capron, A Landais, B Lemieux-Dudon, A Schilt, Valérie Masson-Delmotte, D Buiron, J Chappellaz, Dorthe Dahl-Jensen, S Johnsen, M Leuenberger, et al. Synchronising edml and northgrip ice cores using δ 18 o of atmospheric oxygen (δ 18 o atm) and ch 4 measurements over mis5 (80–123 kyr). *Quaternary Science Reviews*, 29(1):222–234, 2010.

6 Acknowledgements

The RECAP ice coring effort was financed by the Danish Research Council through a Sapere Aude grant, the NSF through the Division of Polar Programs, the Alfred Wegener Institute, and the European Research Council under the European Community's Seventh Framework Programme (FP7/2007-2013) / ERC grant agreement 610055 through the Ice2Ice project. The Centre for Ice and Climate is funded by the Danish National Research Foundation.

7 Author contributions

8 Additional information

9 Competing financial interests

A Time scale

A.1 The RECAP annual-layer counted timescale

The RECAP timescale down to [3] was produced using the StratiCounter software (https://github.com/maiwinstrup/StratiCounter) [38], extended to include multiple chemistry series in parallel with annual signal [39]. StratiCounter was here constrained to fit volcanic [4] marker horizons dated in other Greenland ice cores (DYE-3, GRIP, NGRIP and NEEMS1), thereby tying the RECAP timescale to the Greenland Ice Core Chronology 2005 [5]. The upper 10.9m was manually counted. Below this topmost section, the timescale was derived fully automatically between volcanic markers. The upper 100 m [6] of the core has been measured twice by continuous flow analysis, and both measurements have been used with even weight in StratiCounter.

A.2 Volcanic match

The synchronization to the GICC05 time scale was carried below the annual layer counting down to the 8.2k cold event by continuing the match of volcanic reference horizons between RECAP and the central Greenland cores using ECM data. The synchronization procedure followed the methodology used for the Renland core drilled in 1988 outlined in Vinther et al. 2008 [40], i.e. shape-preserving piecewise cubic Hermite interpolation was used between reference horizons.

A.3 Synchronization to the Rasmussen et al. 2014 stratigraphy

In Rasmussen et al. 2014 [41] a common stratigraphic framework was developed for the GRIP, GISP2 and NGRIP cores, identifying climatic transitions common to all three cores from the 8.2 ka cold event down through the entire Glacial period. All climatic transitions that were identifiable in the RECAP core were used to create the RECAP time scale for the period from 8.2 ka to 110.6 ka BP. Given the extreme thinning of the RECAP glacial ice, the highly resolved dust measurement was the main parameter used for this synchronization. An example of the impressive resolution provided by the dust as well as the synchronization itself can be seen in Figure 5. As there is no systematic flow related thinning of the glacial layers with depth in the RECAP core, the age-depth scale is linearly interpolated between climatic transitions in the glacial

[3] FiXme Note: X meters
[4] FiXme Note: are they only volcanic?
[5] FiXme Note: GICC05 reference
[6] FiXme Note: Check precise depth

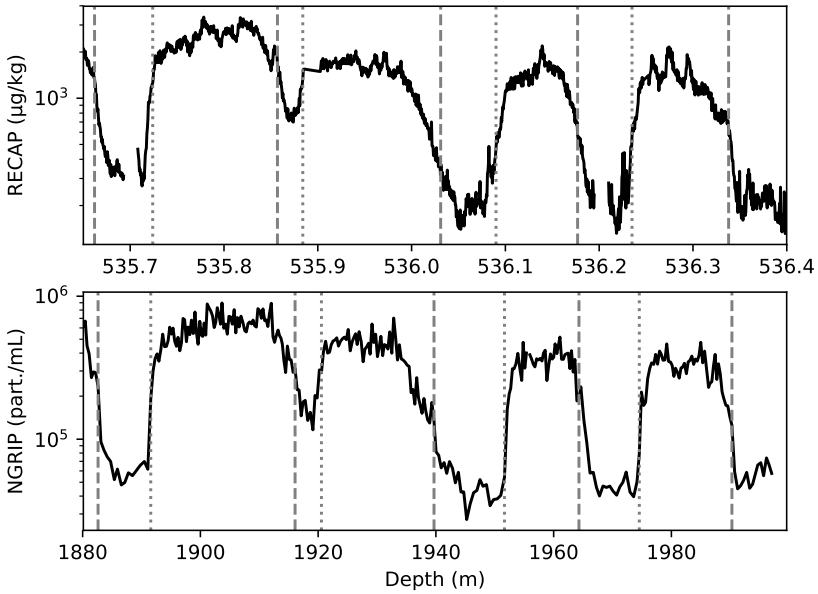

Figure 5: **Dust record match.** Dust concentration of RECAP and NGRIP. The grey dashed and dotted lines are the tie points used for synchronising the RECAP core with the GICC05 time scale of NGRIP.

period. The Holocene section (8.2 ka to 11.7 ka BP) is systematically thinning with depth, hence the shape-preserving piecewise cubic Hermite interpolation used in between Holocene volcanic reference horizons was also used here.

A.4 Gas Synchronization to NGRIP by CH_4 and $\delta^{18}O_{atm}$ records

The transition from GI25 to GS25 dated to 110,640 kyr b2k in GICC05modelext [41] is the deepest transition clearly identifiable in the RECAP dust record. Hence, below this transition a different dating methodology relying on globally well mixed atmospheric gasses has been used. Three tie-points constrain the deepest part of the RECAP time scale: (1) the peak in NGRIP CH_4 [42] observed during GI25 (see figure x), (2) and (3) the sharp change in NGRIP $\delta^{18}O_{atm}$ values [43] observed approximately 120 ka ago (see figures x and y). The RECAP time scale has been linearly interpolated between the three tie points; hereby the difference between gas ages and ice ages has been ignored for the RECAP gas data. The latter decision is justified by the small delta age during warm climatic periods at Renland. Under present day conditions, the Δage is less than 100 years due to high accumulation rates and melt. The number of $\delta^{18}O_{atm}$ values suitable to serve as tie points is limited in RECAP. They assure that the linear trend in the RECAP $\delta^{18}O_{atm}$ data set exactly matches the linear trend in the NGRIP $\delta^{18}O_{atm}$ data. It should be noted, however, that a number of RECAP $\delta^{18}O_{atm}$ measurements were left out of the RECAP age

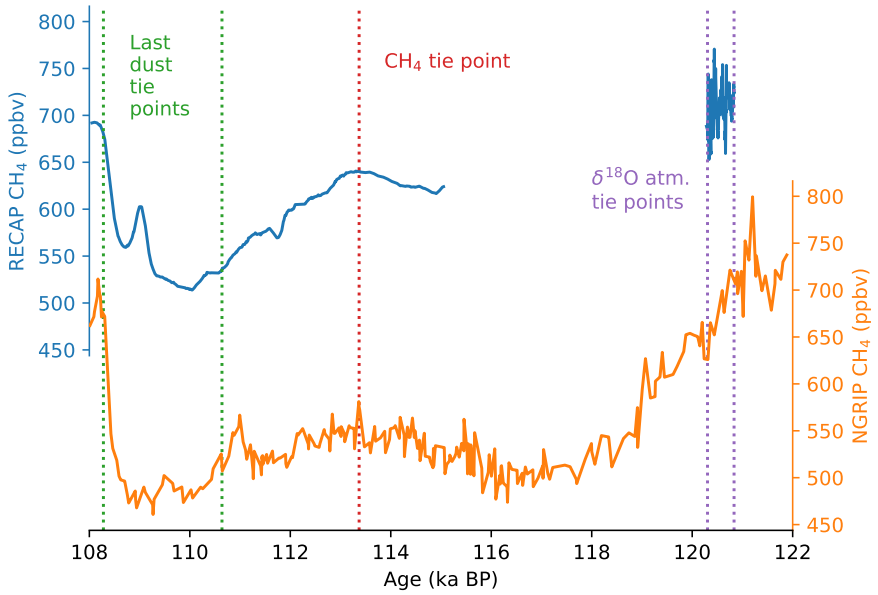

Figure 6: **CH_4 age match.** RECAP (blue) and NGRIP (orange) CH_4 data on the GICC05modelext time scale. The 5 ka data gap in the RECAP CH_4 record corresponds to a 25 cm section of poor core quality. The two last dust transition tie points as well as the GI25 peak CH_4 tie point and the two tie points inferred from $\delta^{18}O_{atm}$ measurements used to constrain the RECAP time scale are indicated by dashed lines.

model as the $\delta^{15}N$ values (measured on the same samples) were too low (less than 0.1‰) t be consistent with a normal firn column. It is speculated that significant melt during the Eemian warm period took place at Renland causing these low $\delta^{15}N$ values due to melt layers prematurely sealing off the firn column. $\delta^{15}N$ measurements are used to correct for mass dependent fractionation effects (gravitation) in the firn column. Applying the correction to $\delta^{18}O_{atm}$ data with anomalous $\delta^{15}N$ in RECAP leads to inconsistencies. Consequently the values are excluded from further analysis.

It should be stressed that the oldest part of the RECAP time scale is less precisely constrained than the part of the time scale that is based on the dust tie points. This is both due to data gaps caused by small sections of poor core quality (i.e. the gap in the RECAP CH_4 record seen in figure x) and the large scatter in both RECAP $\delta^{15}N$ and $\delta^{18}O_{atm}$ data. Hence, it cannot be ruled out that the part of the time scale constrained by the RECAP trend in $\delta^{18}O_{atm}$ could contain stratigraphic disturbances both due to excessive melt and possible folds. Despite these uncertainties the RECAP $\delta^{18}O_{atm}$ values do seem to be entirely inconsistent with a younger age for this section of the RECAP core (see figure y).

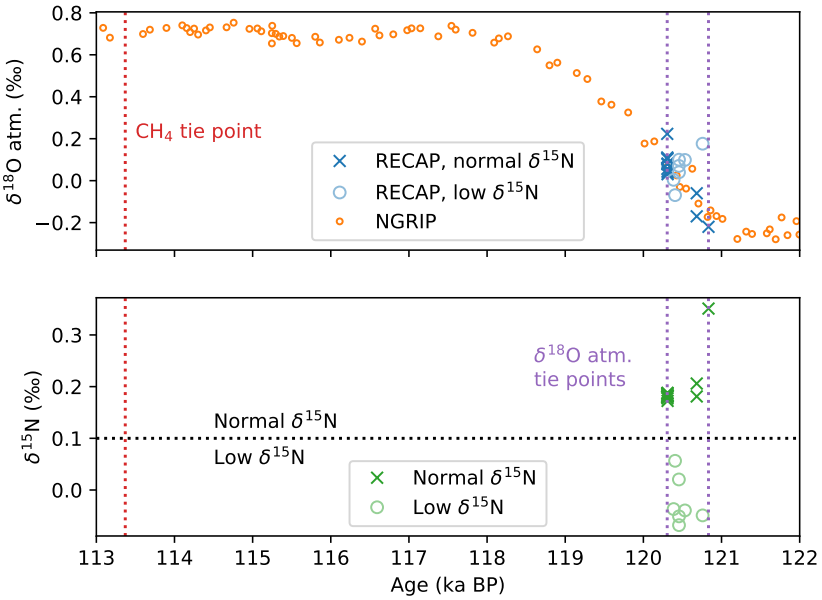

Figure 7: **$\delta^{18}O_{atm}$ age match.** Top panel shows NGRIP (orange) and RECAP (blue) $\delta^{18}O_{atm}$ values on the GICC05modelext time scale. Values of RECAP $\delta^{18}O_{atm}$ that are associated with normal $delta^{15}N$ values observed in firn columns are indicated with x, while RECAP $\delta^{18}O_{atm}$ values associated with abnormally low $\delta^{15}N$ values are indicated with an o. The corresponding RECAP $\delta^{15}N$ values are shown in the lower panel. The RECAP time scale has been constructed so the trend in the RECAP $\delta^{18}O_{atm}$ values associated with normal $\delta^{15}N$ values corresponds to the trend in the NGRIP $\delta^{18}O_{atm}$ data. The three tie points derived from $\delta^{18}O_{atm}$ and CH_4 measurements are indicated by dashed lines.

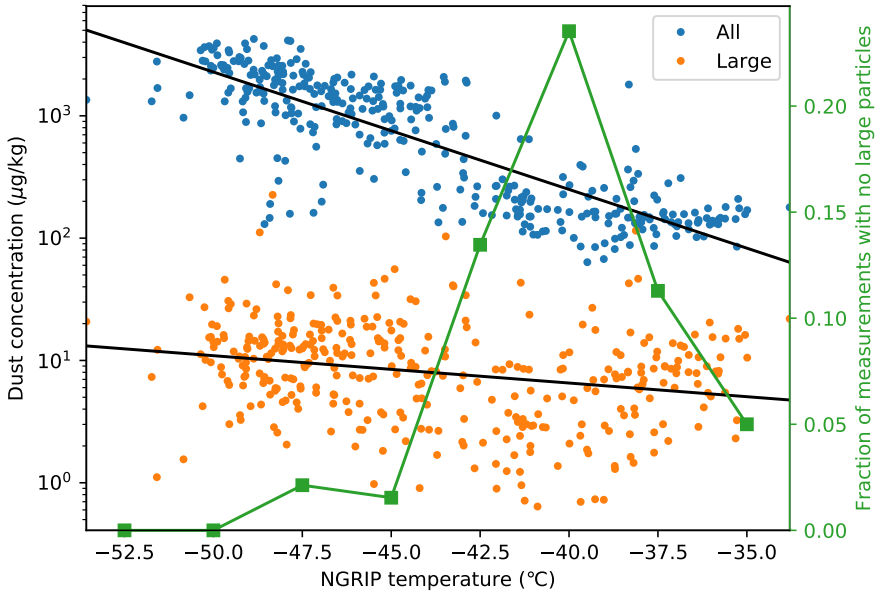

Figure 8: **Large glacial particles.** The orange and blue points are the large particles (> 8.13 μm) and full measured size range (1.25-10.5 μm) for the glacial (111.1 - 12.1 ka before present) as a function of temperature at NGRIP. The black lines are linear fits to the logarithm of the dust concentration. The green line shows the fraction of data points with no large particles in 2.5 °C intervals. The data is down sampled to 200 year intervals.

B Large glacial particles

During the glacial, the logarithm of the total dust concentration has a -84% pearson correlation with the temperature at NGRIP (Figure 8). A linear fit for the logarithm of the dust concentration as a function of NGRIP temperature gives that the dust concentration drops by a factor 28 over 15 °C. The large particles correlate only by -25% with NGRIP temperature, and drop by a factor 2.2 over 15 °C . For the fit, only data points with non zero large particles was used. This gives a resolution dependent bias, as lower resolution would have averaged the zeros with the non zero data points, and thereby given a lower value for data points used for the fit. To correct for this bias, the fraction p of zero valued data points for each 2.5 °C interval was calculated (Figure 8). All non zero concentrations in each interval were then multiplied by $(1 - p)$ for the interval. The linear fit was then reapplied to this zero corrected data set, giving a factor 2.6 per 15 °C instead of 2.2 for the uncorrected data. The effect of of neglecting the zero valued data points is therefore small compared to both the δ^{18}O correlation with large particles and especially the difference between the δ^{18}O correlation with total dust concentration and large particles.

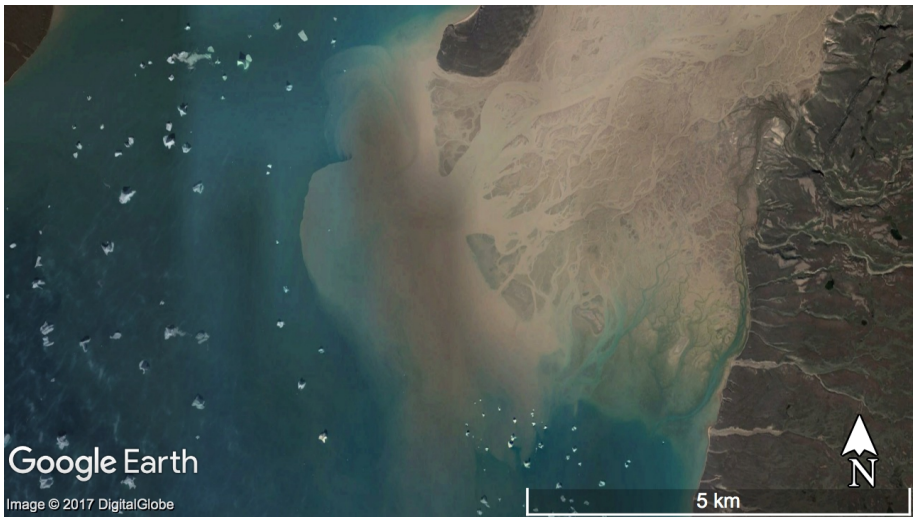

Figure 9: **Dust storm from Gurreholm Dal.** See Methods for details.

C Dust storm

D Dust isotope ages

Strontium and Neodymium isotope values for the three samples (Figure 3):

Sample	$^{87}Sr/^{86}Sr$	$^{87}Sr/^{86}Sr$ error	ϵNd	ϵNd error
1	0.750382	0.000028	-20.900469	0.252463
2	0.747042	0.000027	-16.981157	0.251486
3	0.745803	0.000032	-21.214295	0.302566

Depth and age intervals of the bags used for the three dust isotope samples:

Sample 1

Bag	Top depth (m)	Bottom depth (m)	Top age (years before present)	Bottom age (years before present)
846	464.75	465.30	4281	4301
850	466.95	467.50	4364	4385
855	469.70	470.25	4471	4492
857	470.80	471.35	4514	4536
861	473.00	473.55	4604	4627
866	475.75	476.30	4721	4744
869	477.40	477.95	4792	4816
875	480.70	481.25	4942	4969
877	481.80	482.35	4997	5025
880	483.45	484.00	5082	5112

Sample 2

Bag	Top depth (m)	Bottom depth (m)	Top age (years before present)	Bottom age (years before present)
883	485.10	485.65	5170	5200
886	486.75	487.30	5259	5289
890	488.95	489.50	5379	5409
896	492.25	492.80	5567	5600
897	492.80	493.35	5600	5635
900	494.45	495.00	5707	5745
901	495.00	495.55	5745	5784
902	495.55	496.10	5784	5824
903	496.10	496.65	5824	5864
906	497.75	498.30	5943	5983

Sample 3

Bag	Top depth (m)	Bottom depth (m)	Top age (years before present)	Bottom age (years before present)
910	499.95	500.50	6100	6140
913	501.60	502.15	6219	6258
916	503.25	503.80	6338	6379
919	504.90	505.45	6460	6501
921	506.00	506.55	6543	6586
923	507.10	507.65	6629	6672
926	508.75	509.30	6762	6808
928	509.85	510.40	6855	6904
931	511.50	512.05	7004	7056
933	512.60	513.15	7109	7163

E Coulter Counter ages

Depth and age intervals of the bags used for the Coulter Counter measurements. The size distributions shown in Figure 2, are a mean of the Holocene and glacial samples.

Holocene

Bag	Top depth (m)	Bottom depth (m)	Top age (years before present)	Bottom age (years before present)
300	164.45	165.00	356	358
304	166.65	167.20	363	365
305	167.20	167.75	365	367
321	176.00	176.55	395	397
335	183.70	184.25	423	425
714	392.15	392.70	1980	1989
716	393.25	393.80	1998	2006
746	409.75	410.30	2282	2293
747	410.30	410.85	2293	2303
755	414.70	415.25	2379	2390
759	416.90	417.45	2423	2434
760	417.45	418.00	2434	2446
762	418.55	419.10	2457	2469
788	432.85	433.40	2785	2799
795	436.70	437.25	2884	2899
797	437.80	438.35	2914	2928
799	438.90	439.45	2943	2958
800	439.45	440.00	2958	2974
836	459.25	459.80	3588	3608
837	459.80	460.35	3608	3629
838	460.35	460.90	3629	3650
840	461.45	462.00	3671	3692
842	462.55	463.10	3713	3734
847	465.30	465.85	3822	3845
848	465.85	466.40	3845	3868
850	466.95	467.50	3890	3914
851	467.50	468.05	3914	3937
852	468.05	468.60	3937	3961
854	469.15	469.70	3984	4008

Transition

Bag	Top depth (m)	Bottom depth (m)	Top age (years before present)	Bottom age (years before present)
940	516.45	517.00	7509	7571
945	519.20	519.75	7822	7888
947	520.30	520.85	7956	8030
949	521.40	521.95	8115	8226
950	521.95	522.50	8226	8341
953	523.60	524.15	8519	8598
954	524.15	524.70	8598	8676
956	525.25	525.80	8754	8834
957	525.80	526.35	8834	8920
959	526.90	527.45	9017	9140
960	527.45	528.00	9140	9414
961	528.00	528.55	9414	9676
962	528.55	529.10	9676	9894
964	529.65	530.20	10095	10290
965	530.20	530.75	10290	10488
966	530.75	531.30	10488	10699
967	531.30	531.85	10699	10940
968	531.85	532.40	10940	11283
969	532.40	532.95	11283	12800
970	532.95	533.50	12800	14560

Glacial

Bag	Top depth (m)	Bottom depth (m)	Top age (years before present)	Bottom age (years before present)
972	534.05	534.60	17760	21170
973	534.60	535.15	21170	24745
974	535.15	535.70	24745	28783
975	535.70	536.25	28783	33885

Chapter 5

Interglacial dust in interior Greenland

5.1 Introduction

Atmospheric dust concentrations depend strongly on climate, as seen by the 30 times increase in Greenland dust deposition flux during the last glacial maximum (Ruth et al., 2003). Dust is not only a climate proxy, it also plays an active role through its fertilisation of the ocean and radiation balance effects (Tegen et al., 1996). Human agriculture has increased the total dust source area significantly due to the large areas of exposed soil (Mahowald, 2011). Atmospheric dust is therefore an important variable in models predicting the future climate. Paleo record and model comparisons have been used (Albani et al., 2015) to constrain dust climate models. However, no continuous Holocene insoluble particle record from Greenland has yet been published. This is most likely due to the very low detection limit and hence high accuracy required in combination with the huge amount of labour needed for measuring kilometres of ice core. While the labour has been greatly reduced by continuous flow analysis systems and Abakus laser sensors, these systems have accuracy issues for very low concentrations and measurement campaigns spanning months or years. Furthermore, a large section of the mid Holocene has not been measured continuously in the NEEM and other deep ice cores due to low sample quality in the brittle zone, which covers from 600 to 1,300 m depth.

As soluble calcium correlates strongly with insoluble dust (Steffensen, 1997), the GISP2 calcium record from the summit of the Greenland ice sheet (Mayewski et al., 1997) has been used as a Greenland Holocene dust proxy (Albani et al., 2015). The dust/calcium ratio varies however by a factor 3 between climatic periods and across geographical locations (Steffensen, 1997; Ruth et al., 2002). A robust Greenland Holocene dust record therefore requires replicate measurements, different locations, and both calcium and insoluble particles.

Here we compare the GISP2 calcium record to the GRIP, NEEM and NGRIP dust and calcium records. We show that the calcium flux is the same at NEEM and GISP2, which disagrees with the 10 times higher modelled dust flux at NEEM than at GISP2 (Albani

et al., 2015). There is no trend in the dust and calcium records over the Holocene. The NEEM Eemian has comparable dust concentration to the early Holocene.

5.2 Data sets and methods

The GRIP and GISP2 records are from the summit of the Greenland ice sheet, drilled only 30 km apart. The GRIP soluble calcium (Fuhrer et al., 1999) has been measured by continuous flow analysis from 1,300 m down, which corresponds to older than 7.9 ka b2k. The GRIP insoluble dust record (Steffensen, 1997) has been sparsely measured by Coulter Counter. It contains one early and one late Holocene non-continuously sampled millenium, and two continuously sampled decades during the late Holocene. The GISP2 soluble calcium record has been measured by ion chromatography for the complete 1.7 km of Holocene ice in 1.1 m resolution.

NGRIP is located 300 km north-northwest of summit. The NGRIP1 core was drilled to 1372 m, where the drill got stuck, and the NGRIP2 core was subsequently drilled to bedrock (Rasmussen et al., 2006). The unpublished NGRIP1 soluble calcium samples have been measured by ion chromatography in 5 cm resolution over the top 350 m, which corresponds to the last 1.8 ka. Below this depth, selected samples have been measured, primarily around sulphate peaks. The NGRIP2 soluble calcium record (Seierstad et al., 2014; Rasmussen et al., 2014) has been measured by continuous flow analysis. It covers the early Holocene up to 10.3 ka b2k. The NGRIP2 insoluble dust record (Ruth et al., 2003) has been measured by Abakus on a continuous flow analysis system. It covers the early Holocene until 9.7 ka b2k.

The NEEM ice core was drilled 650 km north-northwest of summit. Its Holocene and Eemian insoluble dust concentration has been measured by both Coulter Counter and Abakus laser sensor, and the soluble calcium record has been measured by continuous flow analysis (CFA) fluorescence spectroscopy (Röthlisberger et al., 2000). The NEEM CFA system operated in the field at NEEM during the 2009, 2010 and 2011 field seasons. While the Abakus and calcium were measured directly on the CFA system, discrete samples were collected from the melt water sample stream and sent to Jean-Robert Petit at LGGE, Grenoble, for Coulter Counter measurements. The Abakus record is discussed in detail in Erhardt (2013). The top 602.25 m were measured in 2009, from 1282.5 to 2200.55 m in 2010, and the brittle ice from 602.25 to 1282.5 m in 2011. The brittle section has not been measured continuously due to drill fluid contamination of the fractured samples. While the contamination risk in CFA systems is normally small but non-negligible, the clean air at NEEM means that the risk of contamination by airborne particles is very small. The Coulter Counter samples are 1.1 m long, and the resolution of calcium and Abakus data are on the order of a centimetre. For all comparisons between the data sets, the Abakus and calcium records have been down sampled to the Coulter Counter resolution.

To compare the different records, the concentrations have been converted to flux by multiplying by density of ice (913 kg/m^3) and the local annual accumulation. The annual accumulation is given by Alley (2000) for GISP2 and GRIP, Andersen et al. (2006) for NGRIP1, Kindler et al. (2014) for NGRIP2 and Rasmussen et al. (2013) for NEEM. For

the recent GIP accumulation, 24 cm/year of ice equivalent has been used (Alley et al., 1993).

All uncertainties are calculated using bootstrap resampling (Mudelsee, 2014).

5.3 NEEM data quality

5.3.1 Folded Eemian

The Eemian ice is folded (Dahl-Jensen et al., 2013). The ice core age is therefore neither continuous nor monotonously increasing with depth. It has been divided into zones, each with a continuous stratigraphy. Three different zones overlap in the period $120.5 - 119.5$ ka b2k and two in $119.5 - 118.5$ ka b2k. They can be used as replicate measurements for investigating measurement uncertainty. The ice in the different zones has been deposited at different locations. Radio echo sounding images show that fold structures are typically around 25 km long (Dahl-Jensen et al., 2013, Fig. 3f). This is therefore roughly the distance between the zones before the folding. The distance between the original deposition locations is approximately the prefolding distances multiplied by the strain factor. As the strain factor at the bottom of the unfolded ice is 0.07 (Rasmussen et al., 2013), the deposition distance between the zones is on the order of kilometres. The different zones have therefore experienced the same deposition conditions. This means that they show not only instrument uncertainty, but also also local deposition variability, similar to what was investigated by Gfeller et al. (2014).

Results

The correlation between the data series of different zones for dust is of the same magnitude as the δ^{18}O correlation (Figure 5.1). The relative difference between the zones is independent of concentration. The first data point of Zone 2 is very different from the corresponding Zone 3 data both for dust and δ^{18}O. It is therefore more likely caused by wrong alignment of the zones than by deposition or measurement variablility, and will be discarded for the following analysis.

We assume that the dust concentration at a certain location can be expressed as a sum of a climate dependent mean dust concentration, representing a larger area, and som noise. Since the ice of Zone 2-4 have the same deposition conditions, it can be used to estimate both the mean dust concentration and the noise. The noise can then be extended outside the range of overlapping zones and used as measurement uncertainty.

To estimate the dust concentration noise, the data is first down sampled to 100 year resolution, since even sampling is necessary for comparing different zones. Then the standard deviation, σ, of the logarithm of the data is calculated for each time point, using

$$\sigma(t) = \sqrt{\frac{\sum_i^{N(t)} (x_i(t) - \overline{x}(t))^2}{N(t) - 1}}, \tag{5.1}$$

where $N(t)$ is the number of zones that have data, $x_i(t)$ is the data, $\overline{x}(t)$ is the mean of

$x_i(t)$. The median of the standard deviation is 17±3%, 15±4% and 18±4% for the Coulter Counter, Abakus and soluble calcium.

We would like to test the null hypothesis that the climatic signal of the Coulter Counter, Abakus and soluble calcium is the same. If this is not true, the total noise derived from the variance of all measurements is larger than the noise from each instrument. To determine the total noise, the measurements of the different instruments have to be scaled, so they are comparable, and the standard deviation of all measurements is then calculated in the same way as for the individual instruments. This gives a median standard deviation of 17±2%, which is within the uncertainty of the median standard deviations of the individual instruments, so there is no indication that the three instruments measure different climatic signals. The best estimate of the dust concentration time series is obtained by scaling the Abakus and soluble calcium time series to the Coulter Counter and taking the mean of the three (Figure 5.1). The scaling factors are 0.93±0.04 and 7.1±0.1 for the Abakus and soluble calcium respectively.

5.3.2 Holocene

The mean Abakus and soluble calcium concentrations during the Holocene are 1.11±0.04 and 7.8±0.3 times smaller than the Coulter Counter concentration, differing slightly from the Eemian instrument ratios. After scaling the Abakus and soluble calcium to the Coulter Counter, their median standard deviation is 22±2%, which is significantly greater than during the Eemian. We will show below that this greater difference is due to systematic error in the calcium and Abakus data.

There is a systematic bias between the Abakus data of different measurement seasons (Fig. 5.2). To investigate the significance of this bias, we have calculated the difference between the mean of the logarithm of the 50 m of data above and below the new year transitions (Table 5.1). To examine whether this step difference is significant for the two Holocene transitions, a similar step difference has been calculated for every metre through the Holocene (Figure 5.3). This gives a probability distribution for step differences through the Holocene, to which the new year transitions can be compared. We will now test the null hypothesis that the step difference of the transitions are not outliers in the Holocene distribution of step differences. This means that we want to find the probability that at least one of two random step differences from the Holocene distribution is as large as the largest of the two new year step differences. The new year step differences are located at some quantile q of the Holocene step difference distribution. The probability of selecting randomly a larger step difference than the new year from the Holocene distribution is $1-q$. The probability of selecting at least one step difference larger than the new year out of two is $1 - q^2$. As this is large for the Coulter Counter but small for the Abakus (Table 5.1), there is no difference between the new year transition and the rest of the Holocene for the Coulter Counter, while the Abakus data have a significant jump at the transition. The Abakus therefore has a systematic bias between different measurement years, while the Coulter Counter appears to be consistent between years. We will therefore not use the Abakus for reconstructing the Holocene dust concentration. While the the calcium record does not have jumps from one year to the next, it has increased values between 2 and 3

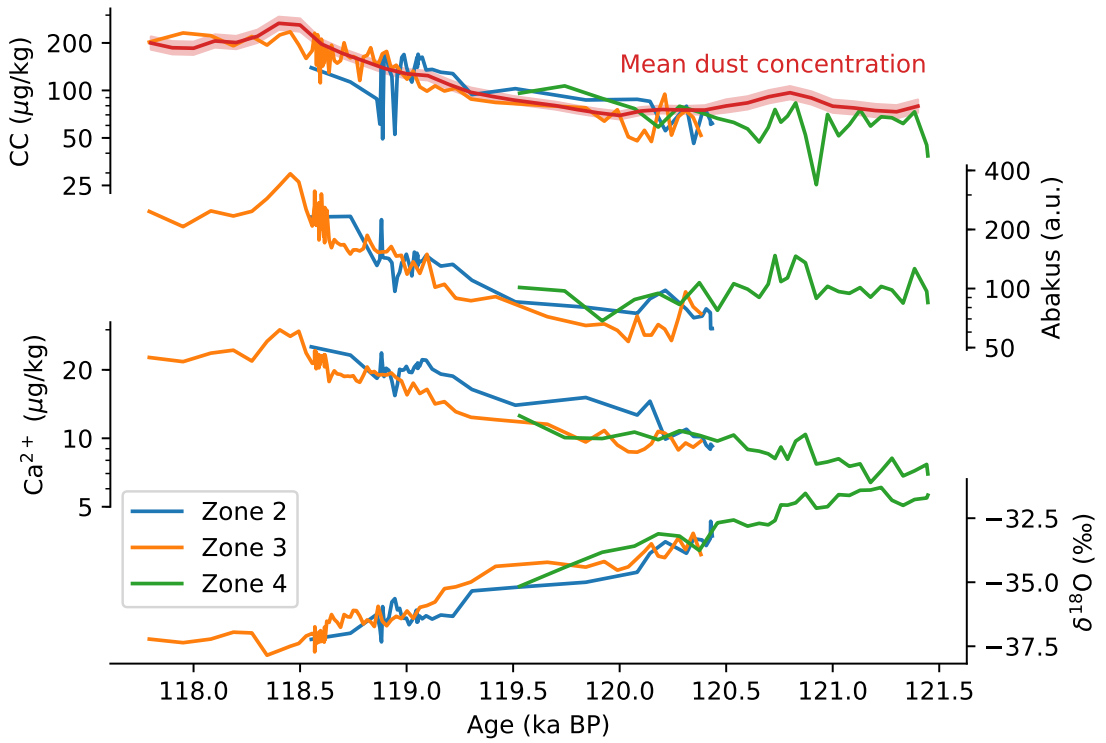

Figure 5.1: Coulter Counter (CC), Abakus, soluble Ca^{2+} and ice $\delta^{18}O$ from Zones 2, 3 and 4 of the NEEM ice core. The best estimate of the Eemian dust concentration (red curve) is the mean of the Coulter Counter data and the Abakus and calcium data scaled to the Coulter Counter data. Its uncertainty (red shaded area) is the median standard deviation of all curves of 17% divided by the square root of the number of data sets.

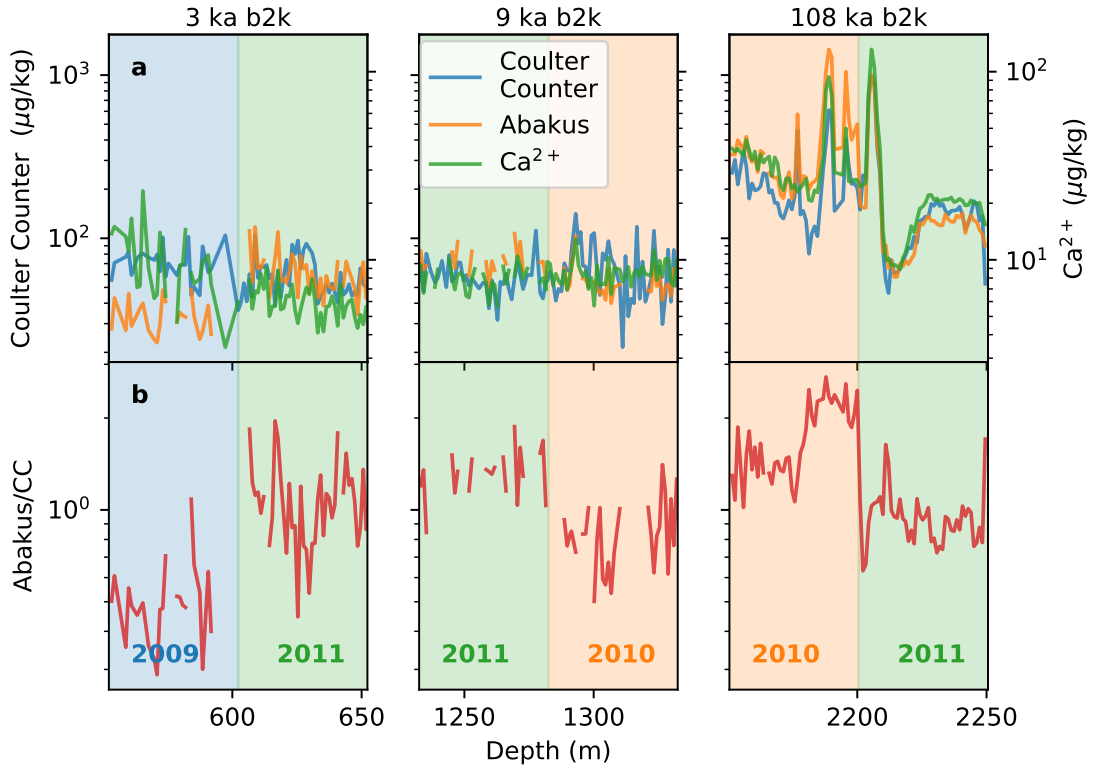

Figure 5.2: **a**: Coulter Counter, Abakus and soluble Ca^{2+} concentrations on 1.1 m resolution. **b**: Ratio between Abakus and Coulter Counter concentrations. The background colors are the depth ranges measured each season, where blue is 2009, orange is 2010 and green is 2011.

ka b2k, that are neither present in the NEEM dust record nor the other ice core calcium records (Figure 5.5). As calcium is easily contaminated by drill fluid (Vallelonga, 2018), this might explain these excessive values.

The systematic bias in Abakus data from one season to the next is a low frequency effect, that should not influence the relative concentration measurement difference between consecutive bags. The short scale variability between bags could therefore reflect a true variability in the dust concentration. We find the same short scale (decadal) variability in Coulter Counter, Abakus and calcium, which shows that the variability is not due to noise in the instrument (Figure 5.4, Table 5.2).

5.4 Results

The dust and calcium fluxes in the early Holocene are similar in all cores (Figure 5.6). The dust flux is between 10 and 15 mg/m^2/year, and the calcium flux is around 1.5

Instrument	Transition	step difference	Quantile, q	$1 - q^2$
Coulter Counter	602.25 m	0.19 ± 0.26	81%	34%
Coulter Counter	1282.50 m	-0.09 ± 0.30	39%	85%
Abakus	602.25 m	-0.58 ± 0.24	99.3%	1.4%
Abakus	1282.50 m	0.31 ± 0.23	91%	17%

Table 5.1: The step difference is the difference between the mean of the logartihm of the 50 m of data before and after the transition. For each metre of the Holocene, the absolute value of the step difference was calculated. The step difference for the transitions correspond to the some quantile of the Holocene step difference distribution, which is shown in the last column.

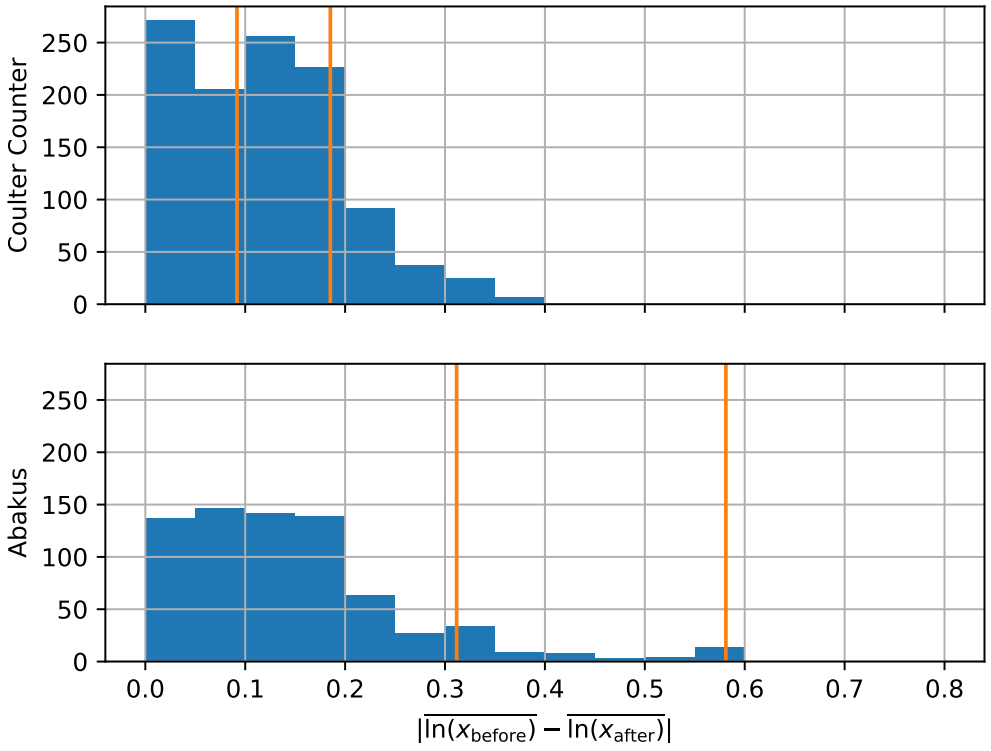

Figure 5.3: Step differences from Table 5.1 (orange lines) together with a histogram of step differences for every metre of the Holocene.

	Abakus	Ca^{2+}
Coulter Counter	0.32 ± 0.05	0.19 ± 0.05
Abakus		0.40 ± 0.06

Table 5.2: Pearson correlation during the Holocene for data minus 5 data point (5.5 m) rolling mean.

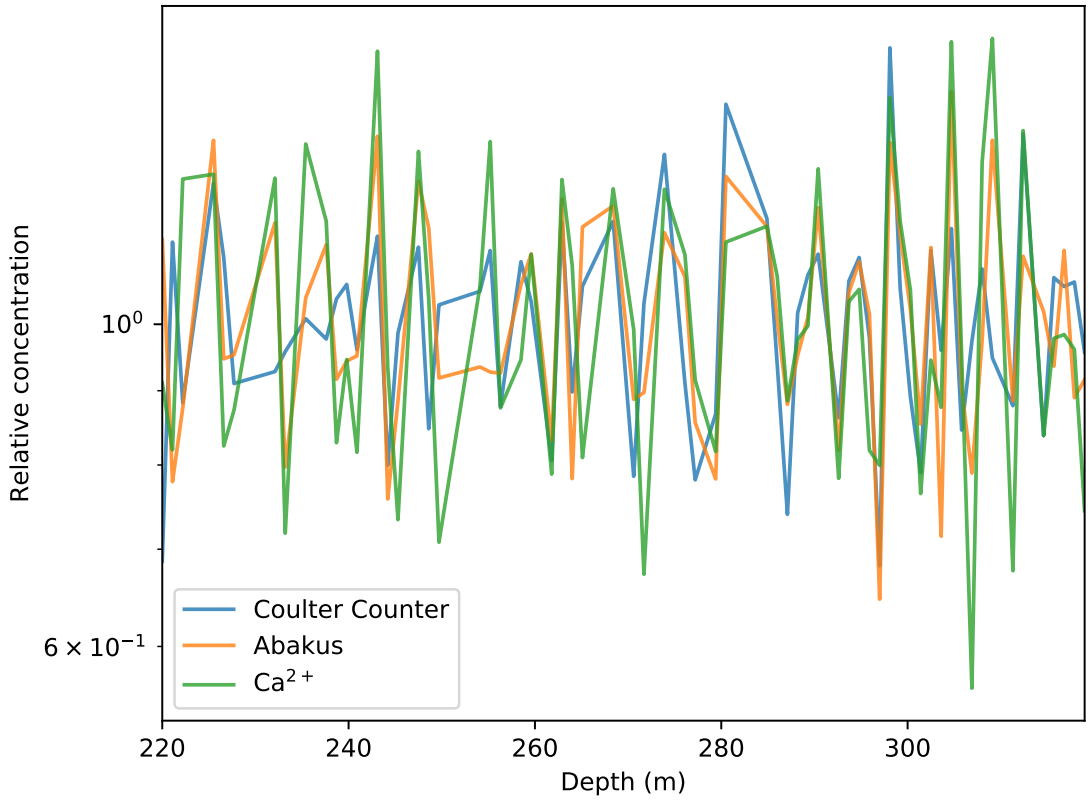

Figure 5.4: A Holocene section of data minus 5 data point (5.5 m) rolling mean. Each data point corresponds to 6 years.

	Dust (μg/kg)	Ca^{2+} (μg/kg)	Dust flux (mg/m^2/year)
0-4 ka b2k	69 ± 2	7.1 ± 0.3	14.3 ± 0.7
7-11 ka b2k	62 ± 2	9.2 ± 0.3	10.5 ± 0.7
120.5-121.5 ka b2k	61 ± 3	8.3 ± 0.3	

Table 5.3: Mean dust and calcium concentration of the NEEM ice core during the late and early Holocene and the Eemian.

mg/m^2/year. There is therefore no spatial variability in the dust and calcium fluxes from summit to NGRIP and NEEM. The NEEM late Holocene dust flux is 40 % higher than the early Holocene dust flux (Figure 5.7), while the calcium records are constant over the Holocene (Figure 5.7). The calcium level is 40 % higher during the last 500 years than during the previous 500 years, but is not high compared to the general variability over the last 4 ka (Figure 5.5). This is not seen in the dust concentration. Even though NEEM and GRIP calcium records have been measured by continuous flow analysis while GISP2 and NGRIP1 have been measured by ion chromatography (IC) on discrete samples, there are no systematic shifts between the measurements. The NEEM calcium/dust ratio is between 0.10 and 0.15, which is only half of the GRIP (Steffensen, 1997) and NGRIP (Ruth et al., 2002) calcium/dust ratios (Table 2.2). The Eemian has the same dust concentration as the early Holocene in NEEM (Table 5.3).

5.5 Discussion, data/model comparison and conclusions

The NEEM record has a Holocene dust flux between 10 and 15 mg/m^2/year. This is much lower than the around 200 mg/m^2/year and 40 mg/m^2/year modelled by Albani et al. (2015), and (Mahowald et al., 1999) respectively. There is therefore a discrepancy of an order of magnitude between the modelled and measured dust fluxes. Lambert et al. (2015) uses dust fluxes at GRIP (Steffensen, 1997) and NGRIP (Ruth et al., 2003) of 9 and 8 mg/m^2/year respectively to estimate 70-110 mg/m^2/year of dust flux at summit, NGRIP and NEEM. They compare this value to four different models, and find that the models predict around 3 times as much dust as their data interpolated dust map.

The difference in dust and calcium flux between the records does not show any systematic geographical trend. The GISP2 average calcium concentration is not more similar to GRIP that was drilled only 30 km away than to NEEM that was drilled 650 km away. Furthermore, even though NGRIP is halfway between NEEM and summit, the NGRIP dust and calcium concentrations are not between the NEEM and summit values. This contrasts Albani et al. (2015) and Mahowald et al. (1999), who model 10 and 3 times more dust at NEEM than at summit. The strong spatial gradient seen in the models is not seen in the data, suggesting that the atmospheric dust concentration is constant over central and northern Greenland.

When all dust and calcium records are compared, there is no general trend in dust flux over the Holocene. The trend of the GISP2 calcium record, which has a clear maximum between 5 and 6 ka b2k, is therefore not generally representative of Greenland.

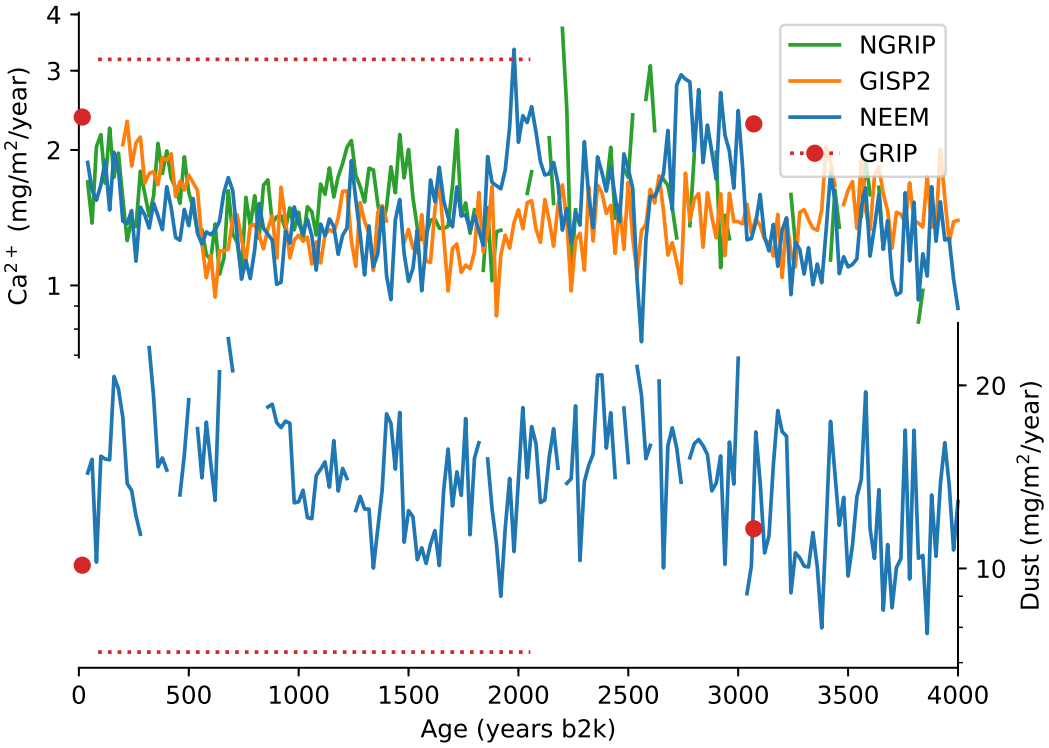

Figure 5.5: Dust and calcium flux over the last 4 ka. GRIP has been discretely measured at two known depths (red circles) and for selected samples within a range (dotted line). Both the GRIP and NEEM dust data have been measured by Coulter Counter.

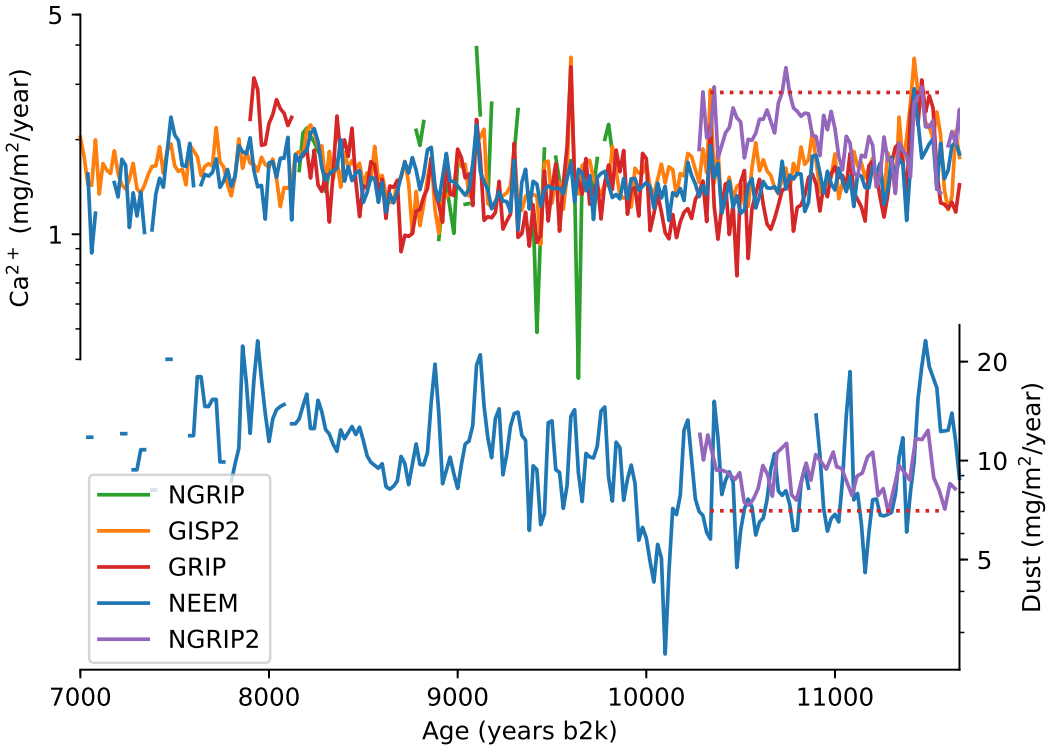

Figure 5.6: Early Holocene dust and calcium flux. GRIP has been both continously measured (continuous line) and discretely measured for selected samples within a range (dotted line). The GRIP and NEEM dust data have been measured by Coulter Counter, while NGRIP2 has been measured by Abakus.

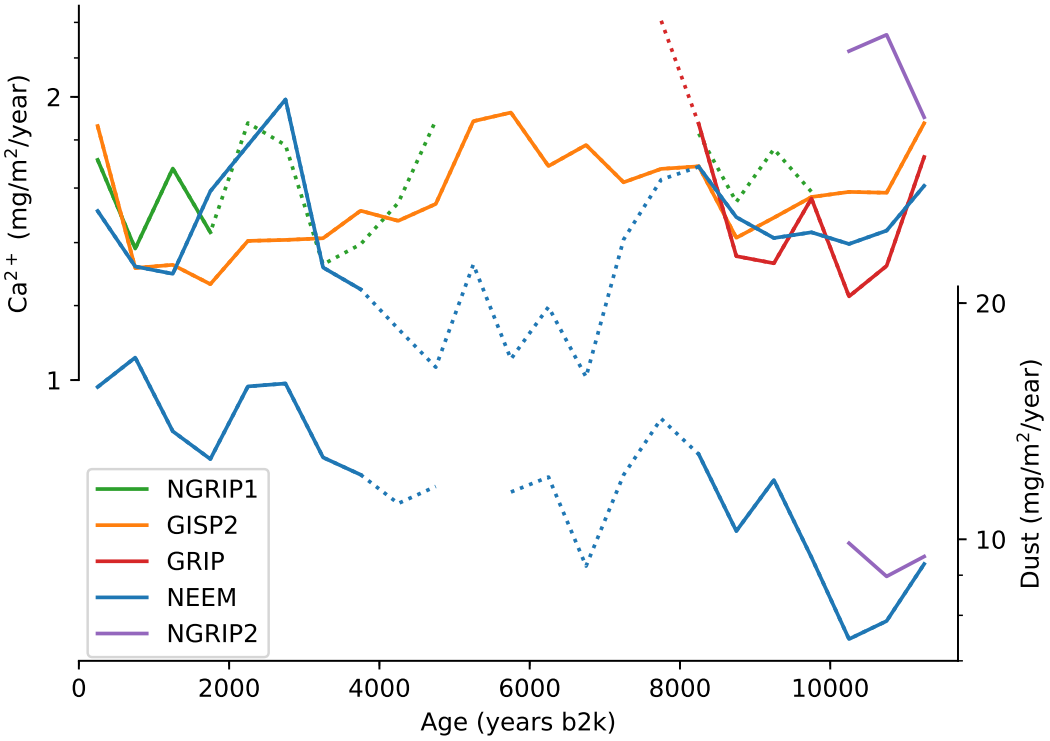

Figure 5.7: Calcium and dust flux on 500 year resolution. The dotted lines are where only selected samples in the section have been measured.

The GRIP dust measurements are systematically lower than the continuous measurements, while the GRIP IC calcium measurements are higher, giving twice as large calcium/dust ratio as at NEEM. Both the calcium and dust records of NEEM are consistent with all other continuous records. The NEEM calcium/dust ratio of 0.10 to 0.15 is therefore most likely more representative of interior Greenland than the GRIP calcium/dust ratio. Albani et al. (2015) use a calcium/dust ratio of 0.36 ± 0.10 based on selected GRIP (Steffensen, 1997) and NGRIP (Ruth et al., 2002) samples for comparing model results to the GISP2 data set. This gives a magnitude of model/data discrepancy that is 3 times too high, based on the NEEM calcium/dust ratio.

Chapter 6

Conclusion and outlook

We have shown that the discrepancy between the Coulter Counter and Abakus dust concentration and size distribution instruments arises because dust particles are non-spherical. The difference between the two instruments can be used to determine the shape of the particles. We have shown that remote Asian dust is more elongated than local east Greenlandic dust, and thereby that particle shape can help distinguish dust provenance. Furthermore, if the shape is known, the Abakus can be calibrated to the Coulter Counter. This enables accurate measurements of absolute concentrations and size distributions with the Abakus in the future, for example for the EastGRIP ice core.

We have used the Abakus to measure the concentration and size distribution of dust in the RECAP ice core. The particles are 10 times larger in the Holocene and Eemian than in the glacial, pointing to a local east Greenlandic Holocene dust source as opposed to the Asian source during the glacial. This has been confirmed by geochemical analysis of the Holocene dust. The local sources were absent during the glacial, as they were covered by ice. The large particle dust concentration is therefore a proxy for glacier extent in the Scoresby Sund area, and its time series shows the exact timing of the advance and retreat at the beginning and end of the glacial. If more coastal ice cores are drilled in Greenland, this could be used to map paleo ice sheet extent around the coast line. It could also be applied in Antarctica, where it might give new insights into the evolution of the west Antarctic ice sheet during the deglaciation.

While the RECAP ice core gives a Holocene dust record, it is very different from central Greenlandic cores. Their dust comes from Asia in spring, and they are therefore a proxy for climate variability on a hemispheric scale. We present the NEEM dust record, which covers most of the Holocene, and compare it to all available dust records from interior Greenland. It has an average dust concentration between 10 and 15 mg/m^2/year, which is an order of magnitude smaller than model predictions. The compilation of all Greenland dust records shows no systematic trend over the Holocene. This is due to a combination of measurement uncertainty and lack of data, especially in the brittle zone covering the mid-Holocene. The main question is whether the mid Holocene maximum of the GISP2 calcium record or the steady increase of the NEEM dust record is most respresentative of the general trend in Greenland. A new dust record covering the complete Holocene could

solve this problem. Hopefully the EastGRIP ice core will have brittle zone ice of sufficient quality for continuous measurements. In addition to the lack of any detectable trend, there is also no geographical variability between the fluxes, even though the models predict up to 10 times more dust at NEEM than at summit. The large discrepancy between data and dust transport models highlights the need for continued development of more accurate models.

Bibliography

S Albani, NM Mahowald, AT Perry, RA Scanza, CS Zender, NG Heavens, V Maggi, JF Kok, and BL Otto-Bliesner. Improved dust representation in the community atmosphere model. *Journal of Advances in Modeling Earth Systems*, 6(3):541–570, 2014.

S Albani, NM Mahowald, G Winckler, RF Anderson, LI Bradtmiller, B Delmonte, R François, M Goman, NG Heavens, PP Hesse, et al. Twelve thousand years of dust: the holocene global dust cycle constrained by natural archives. *Climate of the Past*, 2015.

S Albani, NM Mahowald, LN Murphy, R Raiswell, JK Moore, RF Anderson, D McGee, LI Bradtmiller, B Delmonte, PP Hesse, et al. Paleodust variability since the last glacial maximum and implications for iron inputs to the ocean. *Geophysical Research Letters*, 43(8):3944–3954, 2016.

Richard B Alley. The younger dryas cold interval as viewed from central greenland. *Quaternary science reviews*, 19(1-5):213–226, 2000.

Richard B Alley, DA Meese, CA Shuman, AJ Gow, Kendrick C Taylor, PM Grootes, JWC White, M Ram, ED Waddington, PA Mayewski, et al. Abrupt increase in greenland snow accumulation at the end of the younger dryas event. *Nature*, 362(6420):527, 1993.

Katrine Krogh Andersen, Peter D Ditlevsen, Sune Olander Rasmussen, Henrik Brink Clausen, Bo Møllesøe Vinther, Sigfus Johann Johnsen, and Jørgen Peder Steffensen. Retrieving a common accumulation record from greenland ice cores for the past 1800 years. *Journal of Geophysical Research: Atmospheres*, 111(D15), 2006.

J. Ryan Banta, Joseph R. McConnell, Ross Edwards, and Johann P. Engelbrecht. Delineation of carbonate dust, aluminous dust, and sea salt deposition in a greenland glaciochemical array using positive matrix factorization. *Geochemistry, Geophysics, Geosystems*, 9(7):n/a–n/a, 2008. ISSN 1525-2027. doi: 10.1029/2007GC001908. URL `http://dx.doi.org/10.1029/2007GC001908`. Q07013.

Jean-Marc Barnola, DYSN Raynaud, Ye S Korotkevich, and Cl Lorius. Vostok ice core provides 160,000-year record of atmospheric co2. *Nature*, 329(6138):408, 1987.

Isabelle Basile, Francis E Grousset, Marie Revel, Jean Robert Petit, Pierre E Biscaye, and Nartssis I Barkov. Patagonian origin of glacial dust deposited in east antarctica (vostok

and dome c) during glacial stages 2, 4 and 6. *Earth and Planetary Science Letters*, 146 (3-4):573–589, 1997.

Matthias Bigler, Anders Svensson, Ernesto Kettner, Paul Vallelonga, Maibritt E Nielsen, and Jørgen Peder Steffensen. Optimization of high-resolution continuous flow analysis for transient climate signals in ice cores. *Environmental Science & Technology*, 45(10): 4483–4489, 2011.

PE Biscaye, FE Grousset, M Revel, S Van der Gaast, GA Zielinski, A Vaars, and G Kukla. Asian provenance of glacial dust (stage 2) in the Greenland Ice Sheet Project 2 ice core, Summit, Greenland. *Journal of Geophysical Research: Oceans*, 102(C12):26765–26781, 1997.

A. J.-M. Bory, P. E. Biscaye, A. M. Piotrowski, and J. P. Steffensen. Regional variability of ice core dust composition and provenance in Greenland. *Geochemistry, Geophysics, Geosystems*, 4(12), 2003a. ISSN 1525-2027. doi: 10.1029/2003GC000627. 1107.

AJ-M Bory, Pierre E Biscaye, Anders Svensson, and Francis E Grousset. Seasonal variability in the origin of recent atmospheric mineral dust at NorthGRIP, Greenland. *Earth and Planetary Science Letters*, 196(3):123–134, 2002.

Aloys J-M Bory, Pierre E Biscaye, and Francis E Grousset. Two distinct seasonal asian source regions for mineral dust deposited in greenland (northgrip). *Geophysical research letters*, 30(4), 2003b.

Joanna E Bullard, Matthew Baddock, Tom Bradwell, John Crusius, Eleanor Darlington, Diego Gaiero, Santiago Gasso, Gudrun Gisladottir, Richard Hodgkins, Robert McCulloch, et al. High-latitude dust in the Earth system. *Reviews of Geophysics*, 54(2): 447–485, 2016.

Coulter-Electronics-Limited. Fine particle application notes for coulter counter instruments. Technical Report Issue E, Coulter Electronics Limited, Nortwell Drive, Luton, England, 1988.

JH Cragin, MM Herron, CC Langway Jr, and G Klouda. Interhemispheric comparison of changes in the composition of atmospheric precipitation during the late cenozoic era. *Polar Oceans*, pages 617–631, 1977.

John Crusius, Andrew W Schroth, Santiago Gasso, Christopher M Moy, Robert C Levy, and Myrna Gatica. Glacial flour dust storms in the gulf of alaska: Hydrologic and meteorological controls and their importance as a source of bioavailable iron. *Geophysical Research Letters*, 38(6), 2011.

Dorthe Dahl-Jensen, MR Albert, Ala Aldahan, N Azuma, D Balslev-Clausen, Matthias Baumgartner, A-M Berggren, Matthias Bigler, Thomas Binder, Thomas Blunier, et al. Eemian interglacial reconstructed from a greenland folded ice core. *Nature*, 493(7433): 489–494, 2013.

Remi Dallmayr, Kumiko Goto-Azuma, Helle Astrid Kjær, Nobuhiko Azuma, Morimasa Takata, Simon Schüpbach, and Motohiro Hirabayashi. A high-resolution continuous flow analysis system for polar ice cores. *Bulletin of Glaciological Research*, 34:11–20, 2016.

M De Angelis, Jørgen Peder Steffensen, M Legrand, H Clausen, and C Hammer. Primary aerosol (sea salt and soil dust) deposited in greenland ice during the last climatic cycle: Comparison with east antarctic records. *Journal of Geophysical Research: Oceans*, 102 (C12):26681–26698, 1997.

B Delmonte, J Petit, and V Maggi. Glacial to holocene implications of the new 27000-year dust record from the epica dome c (east antarctica) ice core. *Climate Dynamics*, 18(8): 647–660, 2002.

B Delmonte, I Basile-Doelsch, J-R Petit, V Maggi, Marie Revel-Rolland, A Michard, E Jagoutz, and F Grousset. Comparing the epica and vostok dust records during the last 220,000 years: stratigraphical correlation and provenance in glacial periods. *Earth-Science Reviews*, 66(1-2):63–87, 2004.

Barbara Delmonte, Jean Robert Petit, Isabelle Basile-Doelsch, Emil Jagoutz, and Valter Maggi. 6. late quaternary interglacials in east antarctica from ice-core dust records. In *Developments in Quaternary Sciences*, volume 7, pages 53–73. Elsevier, 2007.

Barbara Delmonte, Carlo Baroni, Per S Andersson, Hans Schoberg, Margareta Hansson, Sarah Aciego, Jean-Robert Petit, Samuel Albani, Claudia Mazzola, Valter Maggi, et al. Aeolian dust in the talos dome ice core (east antarctica, pacific/ross sea sector): Victoria land versus remote sources over the last two climate cycles. *Journal of Quaternary Science*, 25(8):1327–1337, 2010.

Andrea Dutton and Kurt Lambeck. Ice volume and sea level during the last interglacial. *Science*, 337(6091):216–219, 2012.

Tobias Erhardt. A 3000 year high resolution dust record from the neem ice core. Master's thesis, Institute of Climate and Environmental Physics, Oeschger Centre for Climate Change Research, University of Bern, 2013.

Katrin Fuhrer, Eric W Wolff, and Sigfus J Johnsen. Timescales for dust variability in the greenland ice core project (grip) ice core in the last 100,000 years. *Journal of Geophysical Research: Atmospheres*, 104(D24):31043–31052, 1999.

Svend Funder, Christian Hjort, Jon Y Landvik, Seung-Il Nam, Niels Reeh, and Ruediger Stein. History of a stable ice margin—East Greenland during the middle and upper Pleistocene. *Quaternary Science Reviews*, 17(1-3):77–123, 1998.

Svend Funder, K Kjellerup Kjeldsen, Kurt Henrik Kjær, and CÓ Cofaigh. The Greenland ice sheet during the past 300,000 years: A review. *Developments in Quaternary Science*, 15:699–713, 2011.

GEUS, 2018a. URL http://www.geus.dk/DK/data-maps/greenland/Sider/anhstart-dk.aspx.

GEUS, 2018b. URL http://www.geus.dk/DK/data-maps/greenland/Documents/map_e_gree_70_82_1-1mill.pdf.

Gideon Gfeller, Hubertus Fischer, Matthias Bigler, Simon Schüpbach, Daiana Leuenberger, and Olivia Mini. Representativeness and seasonality of major ion records derived from neem firn cores. *The Cryosphere*, 8(5):1855–1870, 2014.

Francis E Grousset, Pierre E Biscaye, Marie Revel, Jean-Robert Petit, Kenneth Pye, Sylvie Joussaume, and Jean Jouzel. Antarctic (dome c) ice-core dust at 18 ky bp: Isotopic constraints on origins. *Earth and Planetary Science Letters*, 111(1):175–182, 1992.

Lena Håkansson, Helena Alexanderson, Christian Hjort, Per Möller, Jason P Briner, Ala Aldahan, and Göran Possnert. Late pleistocene glacial history of jameson land, central east greenland, derived from cosmogenic 10be and 26al exposure dating. *Boreas*, 38(2): 244–260, 2009.

James E Hansen and Makiko Sato. Paleoclimate implications for human-made climate change. In *Climate change*, pages 21–47. Springer, 2012.

Sigfus J Johnsen, Henrik B Clausen, Willi Dansgaard, Niels S Gundestrup, Margareta Hansson, Peter Jonsson, Jørgen P Steffensen, and Arny E Sveinbjørnsdottir. A" deep" ice core from east greenland. *MoG Geoscience*, 29, 1992.

Jung-Ho Kang, Heejin Hwang, Sang Bum Hong, Soon Do Hur, Sung-Deuk Choi, Jeonghoon Lee, and Sungmin Hong. Mineral dust and major ion concentrations in snowpit samples from the neem site, greenland. *Atmospheric Environment*, 120:137–143, 2015.

Frank Kaspar, Norbert Kühl, Ulrich Cubasch, and Thomas Litt. A model-data comparison of european temperatures in the eemian interglacial. *Geophysical Research Letters*, 32 (11), 2005.

Philippe Kindler, M Guillevic, M Baumgartner, Jakob Schwander, A Landais, and Markus Leuenberger. Temperature reconstruction from 10 to 120 kyr b2k from the ngrip ice core. *Climate of the Past*, 10(2):887–902, 2014.

Robert E Kopp, Frederik J Simons, Jerry X Mitrovica, Adam C Maloof, and Michael Oppenheimer. Probabilistic assessment of sea level during the last interglacial stage. *Nature*, 462(7275):863, 2009.

F. Lambert, B. Delmonte, J. R. Petit, M. Bigler, P. R. Kaufmann, M. A. Hutterli, T. F. Stocker, U. Ruth, J. P. Steffensen, and V. Maggi. Dust-climate couplings over the past 800,000 years from the epica dome c ice core. *Nature*, 452(7187):616–619, 04 2008.

F. Lambert, M. Bigler, J. P. Steffensen, M. Hutterli, and H. Fischer. Centennial mineral dust variability in high-resolution ice core data from dome c, antarctica. *Climate of the Past*, 8(2):609–623, 2012. doi: 10.5194/cp-8-609-2012.

Fabrice Lambert, Alessandro Tagliabue, Gary Shaffer, Frank Lamy, Gisela Winckler, Laura Farias, Laura Gallardo, De Pol-Holz, et al. Dust fluxes and iron fertilization in holocene and last glacial maximum climates. *Geophysical Research Letters*, 42(14): 6014–6023, 2015.

M Lupker, SM Aciego, B Bourdon, J Schwander, and TF Stocker. Isotopic tracing (sr, nd, u and hf) of continental and marine aerosols in an 18th century section of the dye-3 ice core (greenland). *Earth and Planetary Science Letters*, 295(1):277–286, 2010.

Natalie Mahowald. Aerosol indirect effect on biogeochemical cycles and climate. *Science*, 334(6057):794–796, 2011.

Natalie Mahowald, Karen Kohfeld, Margaret Hansson, Yves Balkanski, Sandy P Harrison, I Colin Prentice, Michael Schulz, and Henning Rodhe. Dust sources and deposition during the last glacial maximum and current climate: A comparison of model results with paleodata from ice cores and marine sediments. *Journal of Geophysical Research: Atmospheres*, 104(D13):15895–15916, 1999.

Natalie M Mahowald, Daniel R Muhs, Samuel Levis, Philip J Rasch, Masaru Yoshioka, Charles S Zender, and Chao Luo. Change in atmospheric mineral aerosols in response to climate: Last glacial period, preindustrial, modern, and doubled carbon dioxide climates. *Journal of Geophysical Research: Atmospheres*, 111(D10), 2006.

Paul A Mayewski, Loren D Meeker, Mark S Twickler, Sallie Whitlow, Qinzhao Yang, W Berry Lyons, and Michael Prentice. Major features and forcing of high-latitude northern hemisphere atmospheric circulation using a 110,000-year-long glaciochemical series. *Journal of Geophysical Research: Oceans*, 102(C12):26345–26366, 1997.

M. Mudelsee. *Climate Time Series Analysis: Classical Statistical and Bootstrap Methods*. Atmospheric and Oceanographic Sciences Library. Springer International Publishing, 2014. ISBN 9783319044507. URL `https://books.google.dk/books?id=C5gpBAAAQBAJ`.

M. A. C. Potenza, S. Albani, B. Delmonte, S. Villa, T. Sanvito, B. Paroli, A. Pullia, G. Baccolo, N. Mahowald, and V. Maggi. Shape and size constraints on dust optical properties from the dome c ice core, antarctica. *Scientific Reports*, 6:28162 EP –, 06 2016. URL `http://dx.doi.org/10.1038/srep28162`.

Sune O Rasmussen, Matthias Bigler, Simon P Blockley, Thomas Blunier, Susanne L Buchardt, Henrik B Clausen, Ivana Cvijanovic, Dorthe Dahl-Jensen, Sigfus J Johnsen, Hubertus Fischer, et al. A stratigraphic framework for abrupt climatic changes during the last glacial period based on three synchronized greenland ice-core records: refining and extending the intimate event stratigraphy. *Quaternary Science Reviews*, 106:14–28, 2014.

Sune Olander Rasmussen, Katrine K Andersen, AM Svensson, Jørgen Peder Steffensen, Bo Møllesøe Vinther, Henrik Brink Clausen, M-L Siggaard-Andersen, Sigfus Johann Johnsen, Lars Berg Larsen, Dorthe Dahl-Jensen, et al. A new greenland ice core chronology for the last glacial termination. *Journal of Geophysical Research: Atmospheres*, 111 (D6), 2006.

Sune Olander Rasmussen, PM Abbott, Thomas Blunier, AJ Bourne, E Brook, Susanne Lilja Buchardt, Christo Buizert, J Chappellaz, Henrik Brink Clausen, E Cook, et al. A first chronology for the north greenland eemian ice drilling (neem) ice core. *Climate of the Past*, 9(6):2713–2730, 2013.

RECAP, 2018. URL `http://recap.nbi.ku.dk/`.

Regine Röthlisberger, Matthias Bigler, Manuel Hutterli, Stefan Sommer, Bernhard Stauffer, Hans G Junghans, and Dietmar Wagenbach. Technique for continuous high-resolution analysis of trace substances in firn and ice cores. *Environmental Science & Technology*, 34(2):338–342, 2000.

Urs Ruth. *Concentration and size distribution of microparticles in the NGRIP ice core (Central Greenland) during the last glacial period.* PhD thesis, University of Bremen, 2002.

Urs Ruth, Dietmar Wagenbach, Matthias Bigler, Jørgen P Steffensen, Regine Röthlisberger, and Heinz Miller. High-resolution microparticle profiles at northgrip, greenland: case studies of the calcium-dust relationship. *Annals of Glaciology*, 35(1): 237–242, 2002.

Urs Ruth, Dietmar Wagenbach, Jørgen P Steffensen, and Matthias Bigler. Continuous record of microparticle concentration and size distribution in the central Greenland NGRIP ice core during the last glacial period. *Journal of Geophysical Research: Atmospheres*, 108(D3), 2003.

Urs Ruth, Carlo Barbante, Matthias Bigler, Barbara Delmonte, Hubertus Fischer, Paolo Gabrielli, Vania Gaspari, Patrik Kaufmann, Fabrice Lambert, Valter Maggi, et al. Proxies and measurement techniques for mineral dust in antarctic ice cores. *Environmental science & technology*, 42(15):5675–5681, 2008.

Paul Saey. Diplomarbeit im studiengang physik. Master's thesis, Fakultät für Physik und Astronomie, Ruprecht-Karls-Universität Heidelberg, 1998.

Inger K Seierstad, Peter M Abbott, Matthias Bigler, Thomas Blunier, Anna J Bourne, Edward Brook, Susanne L Buchardt, Christo Buizert, Henrik B Clausen, Eliza Cook, et al. Consistently dated records from the greenland grip, gisp2 and ngrip ice cores for the past 104 ka reveal regional millennial-scale δ18o gradients with possible heinrich event imprint. *Quaternary Science Reviews*, 106:29–46, 2014.

Oliver Shorttle, John Maclennan, and Alexander M Piotrowski. Geochemical provincialism in the Iceland plume. *Geochimica et Cosmochimica Acta*, 122:363–397, 2013.

M. F. Simonsen, L. Cremonesi, G. Baccolo, S. Bosch, B. Delmonte, T. Erhardt, H. A. Kjær, M. Potenza, A. Svensson, and P. Vallelonga. Particle shape accounts for instrumental discrepancy in ice core dust size distributions. *Climate of the Past Discussions*, 2017: 1–19, 2017. doi: 10.5194/cp-2017-149. URL `https://www.clim-past-discuss.net/cp-2017-149/`.

G Sinclair, AE Carlson, AC Mix, BS Lecavalier, G Milne, A Mathias, C Buizert, and R DeConto. Diachronous retreat of the Greenland ice sheet during the last deglaciation. *Quaternary Science Reviews*, 145:243–258, 2016.

Konrad Steffen and Jason Box. Surface climatology of the greenland ice sheet: Greenland climate network 1995–1999. *Journal of Geophysical Research: Atmospheres*, 106(D24): 33951–33964, 2001.

Jørgen Peder Steffensen. The size distribution of microparticles from selected segments of the Greenland Ice Core Project ice core representing different climatic periods. *Journal of Geophysical Research: Oceans*, 102(C12):26755–26763, 1997.

Jørgen Peder Steffensen, Katrine K Andersen, Matthias Bigler, Henrik B Clausen, Dorthe Dahl-Jensen, Hubertus Fischer, Kumiko Goto-Azuma, Margareta Hansson, Sigfús J Johnsen, Jean Jouzel, et al. High-resolution Greenland ice core data show abrupt climate change happens in few years. *Science*, 321(5889):680–684, 2008.

David E Sugden, Robert D McCulloch, Aloys J-M Bory, and Andrew S Hein. Influence of patagonian glaciers on antarctic dust deposition during the last glacial period. *Nature Geoscience*, 2(4):281, 2009.

Anders Svensson. *Characterization of continental dust in the Greenland GRIP ice core back to 44 kyr BP*. University of Copenhagen. Department of Geophysics, 1998.

Anders Svensson, Pierre E Biscaye, and Francis E Grousset. Characterization of late glacial continental dust in the Greenland Ice Core Project ice core. *Journal of Geophysical Research: Atmospheres*, 105(D4):4637–4656, 2000.

Anders Svensson, Katrine Krogh Andersen, Matthias Bigler, Henrik Brink Clausen, Dorthe Dahl-Jensen, SM Davies, Sigfus Johann Johnsen, Raimund Muscheler, F Parrenin, Sune Olander Rasmussen, et al. A 60 000 year greenland stratigraphic ice core chronology. *Climate of the Past*, 4(1):47–57, 2008.

Ina Tegen and Inez Fung. Modeling of mineral dust in the atmosphere: Sources, transport, and optical thickness. *Journal of Geophysical Research: Atmospheres*, 99(D11):22897–22914, 1994.

Ina Tegen, Andrew A Lacis, and Inez Fung. The influence on climate forcing of mineral aerosols from disturbed soils. *Nature*, 380(6573):419, 1996.

Paul Vallelonga. Personal communication, 2018.

Paul Vallelonga and Anders Svensson. Ice core archives of mineral dust. In Peter Knippertz and jen Berend W. Stuut, editors, *Mineral Dust*, chapter 18, pages 463–485. Springer, 2014.

Richard A VanCuren, Thomas Cahill, John Burkhart, David Barnes, Yongjing Zhao, Kevin Perry, Steven Cliff, and Joe McConnell. Aerosols and their sources at summit greenland–first results of continuous size-and time-resolved sampling. *Atmospheric environment*, 52:82–97, 2012.

S. Villa, T. Sanvito, B. Paroli, A. Pullia, B. Delmonte, and M. A. C. Potenza. Measuring shape and size of micrometric particles from the analysis of the forward scattered field. *Journal of Applied Physics*, 119(22):224901, 2016. doi: 10.1063/1.4953332.

Bo Møllesøe Vinther, Susanne Lilja Buchardt, Henrik Brink Clausen, Dorthe Dahl-Jensen, Sigfus Johann Johnsen, DA Fisher, RM Koerner, D Raynaud, V Lipenkov, KK Andersen, et al. Holocene thinning of the Greenland ice sheet. *Nature*, 461(7262):385–388, 2009.

Eric W Wolff, Jérôme Chappellaz, Thomas Blunier, Sune Olander Rasmussen, and Anders Svensson. Millennial-scale variability during the last glacial: The ice core record. *Quaternary Science Reviews*, 29(21-22):2828–2838, 2010.